Special polynomials associated with rational solutions of Painlevé equations

Sanjida Piuli Islam

A thesis submitted for the degree of

Doctor of Philosophy in Mathematics

University of Kent

September 2022

Abstract

In this thesis, I investigate properties of special polynomials associated with rational solutions of the Painlevé equations. The Painlevé equations are second order non-linear differential equations. The Painlevé equations have a plethora of interesting mathematical properties and arise in a variety of applications such as plasma physics, random matrix theory, linear waves, and quantum gravity. The generalised Okamoto polynomials are special polynomials associated with rational solutions of the fourth Painlevé equation. The main focus of this thesis are the generalised Okamoto polynomials and polynomials that are defined in this thesis called the 4-Okamoto polynomials. Both the generalised Okamoto and the 4-Okamoto polynomials depend on several parameters. In this thesis, we investigate properties such as the structures formed by the roots of these polynomials in the complex plane and the discriminant of the polynomials. We find that various properties of the generalised Okamoto and the 4-Okamoto polynomials depend on the relative size of the parameters of each polynomial. The generalised Okamoto polynomials and the 4-Okamoto polynomials are naturally associated with families of partitions. The partitions associated with the generalised Okamoto polynomials are so-called 3-core partitions and the partitions associated with the 4-Okamoto polynomials are so-called 4-core partitions. In this thesis, we explore how aspects of partitions associated with polynomials play a role in the properties of the polynomials.

Acknowledgements

Thank you to my supervisors, Dr Clare Dunning and Professor Peter A. Clarkson, for their guidance, support and unwavering patience throughout the years. I will forever be grateful for their supervision. I also owe many thanks to the University of Kent. I thankfully acknowledge the Engineering and Physical Sciences Research Council for my PhD studentship. It has been a pleasure to be a part of the School of Mathematics, Statistics and Actuarial Science. A special thanks to my friends and colleagues at the university for all the cherished memories.

To my mum, dad and family, thank you for your continued support in all my endeavours.

Declaration

I declare that this thesis was composed by myself and that the work contained in this thesis is my own, except where explicitly stated otherwise.

List of Figures

Contents

Chapter 1

Introduction and background

In this chapter, we discuss the history and application of the Painlevé equations and special polynomials associated with rational solutions of the Painlevé equations. We then define partitions and diagrams that we will use to investigate properties of special polynomials. This chapter ends with an outline of this thesis.

1.1 Painlevé equations

The Painlevé equations are second order non-linear differential equations. Iwasaki, Kimura, Shimomura and Yoshida [42] consider the Painlevé equations to be "the most important non-linear ordinary differential equations" and state that "many specialists believe that during the twenty-first century the Painlevé functions will become new members of the community of special functions". The Painlevé equations have arisen in a variety of applications such as non-linear waves, plasma physics, random matrix theory, the asymptotic theory of orthogonal polynomials, fibre optics, topological field theory, non-linear waves (e.g. resonant oscillations in shallow water), quantum gravity, statistical mechanics (correlation functions of the XY model and the Ising model) and Bose-Einstein condensation [21]. The Painlevé equations have attracted a lot of interest since they also arise in many physical situations and as reductions of the soliton equations which are solvable by inverse scattering [1]. The Painlevé equations are named after the French mathematician and politician, Paul Painlevé, who served as the Prime Minister of France twice, and as the French minister of War during the First World War. The Painlevé equations were discovered by Painlevé, Gambier, Fuchs and their colleagues (1893-1906) whilst studying a problem posed by Picard in 1887 [73]. Picard asked which second order differential equations of the form

$$\frac{\mathrm{d}^2 w}{\mathrm{d}z^2} = F\left(z, w, \frac{\mathrm{d}w}{\mathrm{d}z}\right), \tag{1.1}$$

where F is rational in $\frac{\mathrm{d}w}{\mathrm{d}z}$ and w, and analytic in z, have the property that the solutions have no movable critical points, i.e. the location of critical points are independent of the particular solution chosen and only dependent on the equation; this property is now known as the *Painlevé property.* The critical points of (1.1) are the points $\left(z, w, \frac{\mathrm{d}w}{\mathrm{d}z}\right)$ such that (1.1) is equal to zero. Painlevé, Gambier and colleagues showed that there are fifty canonical equations that have the *Painlevé property*, up to a Möbius (bilinear rational) transformation

$$W(\zeta) = \frac{a(z)w + b(z)}{c(z)w + d(z)}, \quad \zeta = \phi(z),$$

where $a(z)$, $b(z)$, $c(z)$, $d(z)$ and $\phi(z)$ are locally analytic functions. Out of the fifty equations that satisfy the *Painlevé property*, forty four are either integrable i.e. solvable, in terms of previously known functions, such as elliptic functions and linear equations, or are reducible to one of six non-linear ordinary differential equations known as the Painlevé equations. The six Painlevé equations are

$$\mathrm{P_I}: \ \frac{\mathrm{d}^2 w}{\mathrm{d}z^2} = 6w^2 + z,$$

$$\mathrm{P_{II}}: \ \frac{\mathrm{d}^2 w}{\mathrm{d}z^2} = 2w^3 + zw + \alpha,$$

$$\mathrm{P_{III}}: \ \frac{\mathrm{d}^2 w}{\mathrm{d}z^2} = \frac{1}{w}\left(\frac{\mathrm{d}w}{\mathrm{d}z}\right)^2 - \frac{1}{z}\frac{\mathrm{d}w}{\mathrm{d}z} + \frac{\alpha w^2 + \beta}{z} + \gamma w^3 + \frac{\delta}{w},$$

$$\mathrm{P_{IV}}: \frac{\mathrm{d}^2w}{\mathrm{d}z^2} = \frac{1}{2w}\left(\frac{\mathrm{d}w}{\mathrm{d}z}\right)^2 + \frac{3}{2}w^3 + 4zw^2 + 2(z^2-\alpha)w + \frac{\beta}{w},$$

$$\mathrm{P_{V}}: \frac{\mathrm{d}^2w}{\mathrm{d}z^2} = \left(\frac{1}{2w}+\frac{1}{w-1}\right)\left(\frac{\mathrm{d}w}{\mathrm{d}z}\right)^2 - \frac{1}{z}\frac{\mathrm{d}w}{\mathrm{d}z} + \frac{(w-1)^2}{z^2}\left(\alpha w + \frac{\beta}{w}\right) + \frac{\gamma w}{z} + \frac{\delta w(w+1)}{w-1},$$

$$\mathrm{P_{VI}}: \frac{\mathrm{d}^2w}{\mathrm{d}z^2} = \frac{1}{2}\left(\frac{1}{w}+\frac{1}{w-1}+\frac{1}{w-z}\right)\left(\frac{\mathrm{d}w}{\mathrm{d}z}\right)^2 - \left(\frac{1}{z}+\frac{1}{z-1}+\frac{1}{w-z}\right)\frac{\mathrm{d}w}{\mathrm{d}z} + \frac{w(w-1)(w-z)}{z^2(z-1)^2}\left(\alpha + \frac{\beta z}{w^2} + \frac{\gamma(z-1)}{(w-1)^2} + \frac{\delta z(z-1)}{(w-z)^2}\right),$$

where α, β, γ and δ are arbitrary constants. The Painlevé equations have a plethora of interesting properties. For example, all six Painlevé equations can be written as (non-autonomous) Hamiltonian systems [44, 69, 70]. Another property of Painlevé equations is that $\mathrm{P_{II}}$-$\mathrm{P_{VI}}$ have Bäcklund transformations which map solutions of a given Painlevé equation to solutions of the same Painlevé equation, with different values of α, β, γ and δ. We discuss Bäcklund transformations of Painlevé equations later in this chapter.

The solutions of Painlevé equations are called the *Painlevé transcendents*. The general solutions of the Painlevé equations are transcendental, i.e. irreducible, in the sense that they cannot be expressed in terms of previously known functions such as elliptic functions, rational functions or the classical special functions. However, for certain values of α, β, γ and δ, the Painlevé equations $\mathrm{P_{II}}$-$\mathrm{P_{VI}}$ have rational solutions, and $\mathrm{P_{III}}$, $\mathrm{P_{V}}$ and $\mathrm{P_{VI}}$ also have algebraic solutions. The Painlevé equations $\mathrm{P_{II}}$-$\mathrm{P_{VI}}$ have special function solutions for certain values of α, β, γ and δ. The special function solutions (also known as one parameter solutions) of $\mathrm{P_{II}}$-$\mathrm{P_{VI}}$ are expressed in terms of classical special functions; Airy, Bessel, parabolic cylinder, Kummer and hypergeometric functions, respectively (see, e.g. [25, 34, 39] and the references therein). The rational, algebraic and special function solutions of $\mathrm{P_{II}}$-$\mathrm{P_{VI}}$ are often written in a determinantal form, for example, as Wronskians of polynomials. In this thesis, our interest is in rational solutions of Painlevé equations. In particular, we are interested in special polynomials associated with rational solutions of Painlevé equations. A *special polynomial* is a polynomial that has particular use in mathematical physics or other branches of mathematics. Special polynomials are often named after an early investigator of its properties.

1.2 Rational solutions of Painlevé equations

We now discuss rational solutions of Painlevé equations. In 1910, Gambier [36] proved that for every $\alpha \in \mathbb{Z}$ there exists a unique rational solution $w_n(z)$ of $\mathrm{P_{II}}$. Given a solution $w(z;\alpha)$ of $\mathrm{P_{II}}$ with $\alpha \in \mathbb{Z}$, the Bäcklund transformations in Theorem 1 can be used to find solutions of $\mathrm{P_{II}}$. The Bäcklund transformations for $\mathrm{P_{III}}$, $\mathrm{P_{IV}}$, $\mathrm{P_{V}}$ and $\mathrm{P_{VI}}$ can be found in [34], [51], [37] and [72], respectively.

Theorem 1. *Suppose $w(z;\alpha)$ is a solution of $\mathrm{P_{II}}$ then the transformations*

$$\begin{aligned} \mathcal{S} \quad &: \quad w(z;-\alpha) = -w(z;\alpha), \\ \mathcal{T}_{\pm} \quad &: \quad w(z;\alpha \pm 1) = -w(z;\alpha) - \frac{2\alpha \pm 1}{2w^2(z;\alpha) \pm 2w'(z;\alpha) + z}, \end{aligned}$$

where $' \equiv d/dz$, gives solutions of $\mathrm{P_{II}}$ provided that $\alpha \neq \mp\frac{1}{2}$.

The proof of this theorem can be found in [36] and [52]. Theorem 1 tells us that given a solution $w_\alpha(z) = w(z;\alpha)$ with $\alpha = n \in \mathbb{Z}$, the Bäcklund transformation

$$w_{n+1}(z) = -w_n(z) - \frac{2n+1}{2w_n(z)^2 + w_n(z)' + z}, \tag{1.2}$$

can be used to generate the hierarchy of rational solutions of $\mathrm{P_{II}}$ from the "seed solution" $w_0(z) = 0$. Table 1.1 gives examples of rational solutions of $\mathrm{P_{II}}$ obtained from (1.2) with $w_0(z) = 0$.

$$w_1(z) = -\frac{1}{z},$$

$$w_2(z) = \frac{1}{z} - \frac{3z^2}{z^3+4},$$

$$w_3(z) = \frac{3z^2}{z^3+4} - \frac{6z^5+60z^2}{z^6+20z^3-80},$$

$$w_4(z) = \frac{6z^5+60z^2}{z^6+20z^3-80} - \frac{1}{z} - \frac{9z^8+360z^5}{z^9+60z^6+11200},$$

$$w_5(z) = \frac{1}{z} + \frac{9z^8+360z^5}{z^9+60z^6+11200} - \frac{15z^{14}+1680z^{11}+25200z^8+470400z^5-9408000z^2}{z^{15}+140z^{12}+2800z^9+78400z^6-3136000z^3-627200},$$

TABLE 1.1: Rational solutions $w_\alpha(z) = w(z;\alpha)$ of $\mathrm{P_{II}}$ obtained from (1.2) with $w_0(z) = 0$.

The result $w_1(z)$ in Table 1.1 can be written as

$$\begin{aligned} w_1(z) &= -\frac{1}{z} \\ &= \frac{\mathrm{d}}{\mathrm{d}z}\ln\frac{1}{z}. \end{aligned}$$

Similarly, other rational solutions of $\mathrm{P_{II}}$ can be written as the following

$$\begin{aligned} w_2(z) &= \frac{1}{z} - \frac{3z^2}{z^4+4} \\ &= \frac{\mathrm{d}}{\mathrm{d}z}\ln\frac{z}{z^3+4}, \\ w_3(z) &= \frac{3z^2}{z^3+4} - \frac{6z^5+60z^2}{z^6+20z^3-80} \\ &= \frac{\mathrm{d}}{\mathrm{d}z}\ln\frac{z^3+4}{z^6+20z^3-80}, \\ w_4(z) &= \frac{6z^5+60z^2}{z^6+20z^3-80} - \frac{1}{z} - \frac{9z^8+360z^5}{z^9+60z^6+11200} \\ &= \frac{\mathrm{d}}{\mathrm{d}z}\ln\frac{z^6+20z^3-80}{z^{10}+60z^7+11200z}, \end{aligned}$$

and so on. In other words, rational solutions of $\mathrm{P_{II}}$ obtained from (1.2) with the seed solution $w_0(z) = 0$ can be written as

$$w_n(z) = \frac{\mathrm{d}}{\mathrm{d}z} \ln \left(\frac{P(z)}{Q(z)} \right)$$

where $P(z)$ and $Q(z)$ are polynomials. The rational solutions of $\mathrm{P_{II}}$ are summarised in the following theorem due to Vorob'ev [81] and Yablonskii [83].

Theorem 2. *Rational solutions of P_{II} exist if and only if $\alpha = n \in \mathbb{Z}$, that are unique, and have the form*

$$w_n(z) = w(z;n) = \frac{\mathrm{d}}{\mathrm{d}z} \ln \left(\frac{Q_{n-1}(z)}{Q_n(z)} \right)$$

for $n \geq 1$, where the polynomial $Q_n(z)$ satisfies the differential-difference equation

$$Q_{n+1}(z)Q_{n-1}(z) = zQ_n^2(z) - 4 \left(Q_n(z)\frac{\mathrm{d}^2 Q_n(z)}{\mathrm{d}z^2} - \left(\frac{\mathrm{d}Q_n(z)}{\mathrm{d}z} \right)^2 \right), \tag{1.3}$$

with $Q_0 = 1$ and $Q_1 = z$. Other rational solutions of P_{II} are given by $w_0 = 0$ and $w_{-n} = -w_n$.

The proof of this theorem can be found in [35, 76, 81, 83]. It is clear from the differential-difference equation (1.3) that $Q_n(z)$ are rational functions. However, remarkably $Q_n(z)$ are actually polynomials despite dividing by $Q_{n-1}(z)$ at every iteration. Taneda [76] used an algebraic method to prove that the $Q_n(z)$ are indeed polynomials. Another surprising aspect is that (1.3) gives polynomials that are monic and have integer coefficients. The polynomials $Q_n(z)$ are special polynomials known as the Yablonskii–Vorob'ev polynomials. Examples of Yablonskii–Vorob'ev polynomials can be found in Table 1.2. The polynomials $Q_n(z)$ are of degree $\frac{n(n+1)}{2}$.

Fukutani, Okamoto and Umemura [35] found that the Yablonskii–Vorob'ev polynomials $Q_n(z)$, where n is a positive integer, have $\frac{n(n+1)}{2}$ simple roots and that $Q_n(z)$ and $Q_{n+1}(z)$ have no roots in common. The plots in Figure 1.1 show the

$$
\begin{aligned}
Q_0(z) &= 1 \\
Q_1(z) &= z \\
Q_2(z) &= z^3 + 4 \\
Q_3(z) &= z^6 + 20z^3 - 80 \\
Q_4(z) &= z^{10} + 60z^7 + 11200z \\
Q_5(z) &= z^{15} + 140z^{12} + 2800z^9 + 78400z^6 - 313600z^3 - 6272000 \\
Q_6(z) &= z^{21} + 280z^{18} + 18480z^{15} + 627200z^{12} - 17248000z^9 + 1448832000z^6 \\
&\quad +19317760000z^3 - 38635520000
\end{aligned}
$$

TABLE 1.2: Yablonskii–Vorob'ev polynomials.

roots of some Yablonskii–Vorob'ev polynomials. Clarkson and Mansfield [28] investigated the locations of the roots of Yablonskii-Vorob'ev polynomials in the complex plane and found that surprisingly the roots of $Q_n(z)$ form very regular approximate equilateral triangle structures. The term "approximate" is used since the structures are not exact triangles as the roots do not lie on straight lines. Clarkson and Mansfield [28] used the numerical value of roots of $Q_n(z)$ to show that the roots lie in a triangular region bounded by curves. Many years later, Buckingham and Miller [15, 16] and Bertola and Bothner [7] analytically studied the Yablonskii-Vorob'ev polynomials and found that as $n \to \infty$ the roots of $Q_n(z)$ lie in a triangular shaped region with sides that meet with interior angle $\frac{2}{5}\pi$.

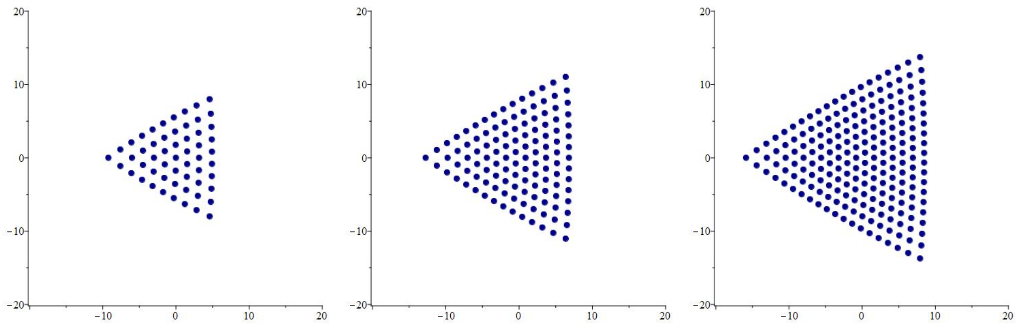

$Q_{10}(z)$ $Q_{15}(z)$ $Q_{20}(z)$

FIGURE 1.1: Plot of roots of Yablonskii–Vorob'ev polynomials $Q_n(z)$ for $n = 10, 15, 20$.

Another indication that the Yablonskii–Vorob'ev polynomials are special is given by their discriminant. The discriminant of monic polynomials is defined in Definition 1 and will be used throughout this thesis. If the discriminant of a polynomial is non-zero, it shows that the roots of the polynomial are simple.

Definition 1. The *discriminant* of a monic polynomial

$$f(z) = z^n + a_{n-1}z^{n-1} + \ldots + a_1 z + a_0,$$

with roots $\alpha_1, \alpha_2, \ldots, \alpha_n \in \mathbb{C}$ is given by

$$\mathrm{Dis}(f(z)) = \prod_{1\le j<k\le n} (\alpha_j - \alpha_k)^2.$$

The discriminant of the first few Yablonskii–Vorob'ev polynomials are given in Table 1.3. The results in Table 1.3 show that the discriminant of $Q_n(z)$ are expressed as products of small integers to large powers. The following theorem is due to Roberts [74].

$$\begin{aligned}
\mathrm{Dis}(Q_2) &= -(2)^4(3)^3\\
\mathrm{Dis}(Q_3) &= (2)^{20}(3)^{12}(5)^5\\
\mathrm{Dis}(Q_4) &= (2)^{60}(3)^{27}(5)^{20}(7)^7\\
\mathrm{Dis}(Q_5) &= (2)^{140}(3)^{66}(5)^{20}(7)^7\\
\mathrm{Dis}(Q_6) &= -(2)^{280}(3)^{147}(5)^{80}(7)^{63}(11)^{11}\\
\mathrm{Dis}(Q_7) &= (2)^{504}(3)^{270}(5)^{125}(7)^{112}(11)^{44}(13)^{13}\\
\mathrm{Dis}(Q_8) &= (2)^{840}(3)^{450}(5)^{195}(7)^{175}(11)^{99}(13)^{52}
\end{aligned}$$

TABLE 1.3: Discriminants of Yablonskii-Vorob'ev polynomials.

Theorem 3. *The discriminant of $Q_n(z)$ is given by*

$$|\operatorname{Dis}(Q_n)| = 2^{n(n^2-1)(n+2)/6} \prod_{j=1}^{n} (2j+1)^{(2j+1)(n-j)^2},$$

where $\operatorname{Dis}(Q_n) < 0$ *if and only if* $n \equiv 2 \bmod 4$.

Another remarkable property of the Yablonskii–Vorob'ev polynomials is that they can be written in a determinantal form as the Wronskian of polynomials. In Theorem 2, the Yablonskii–Vorob'ev polynomials are defined by the differential-difference equation (1.3). As a result, the first n Yablonskii–Vorob'ev polynomials are required in order to find the $n+1$ th polynomial. Kajiwara and Ohta [46] showed that the Yablonskii–Vorob'ev polynomials can be written as the Wronskian of polynomials $p_j(z)$ defined in Theorem 4. The Wronskian of polynomials is defined in Definition 2.

Definition 2. The *Wronskian* of polynomials $f_1(z)$, $f_2(z)$, ..., $f_n(z)$ is given by

$$\mathcal{W}(f_1, f_2, \ldots, f_n)(z) = \begin{vmatrix} f_1 & f_2 & \cdots & f_n \\ \frac{\mathrm{d}f_1}{\mathrm{d}z} & \frac{\mathrm{d}f_2}{\mathrm{d}z} & \cdots & \frac{\mathrm{d}f_n}{\mathrm{d}z} \\ \vdots & \vdots & & \vdots \\ \frac{\mathrm{d}^{n-1}f_1}{\mathrm{d}z^{n-1}} & \frac{\mathrm{d}^{n-1}f_2}{\mathrm{d}z^{n-1}} & \cdots & \frac{\mathrm{d}^{n-1}f_n}{\mathrm{d}z^{n-1}} \end{vmatrix}.$$

Theorem 4. *Let $p_j(z)$ be the polynomial defined as*

$$\sum_{j=0}^{\infty} p_j(z)\varepsilon^j = \exp\left(z\varepsilon - \frac{4}{3}\varepsilon^3\right). \tag{1.4}$$

Then the Yablonskii–Vorob'ev polynomial $Q_n(z)$ given by

$$Q_n(z) = c_n \mathcal{W}\big(p_1, p_3, \ldots, p_{2n-1}\big), \quad c_n = \prod_{j=1}^{n} (2j+1)^{n-j}$$

with

$$w(z;n) = \frac{\mathrm{d}}{\mathrm{d}z} \ln \left(\frac{Q_{n-1}(z)}{Q_n(z)} \right)$$

satisfies $\mathrm{P_{II}}$ *with* $\alpha = n \in \mathbb{Z}$ *and* $n \geq 1$.

Table 1.4 gives the first few $p_j(z)$ polynomials defined in (1.4). The Yablonskii–Vorob'ev polynomials arise in a multitude of areas, such as cold plasma physics [75] and boundary value problems [4]. In 2021, Yang and Yang [84] showed that Yablonskii–Vorob'ev polynomials can be used in the description of rogue wave patterns. Rogue waves, also known as freak waves, refer to waves that appear as extremely large, localized waves in the ocean, where the average height of a rogue waves is almost twice the height of the surrounding waves. Rogue waves were originally studied in oceanography due the potential threat rogue waves can have, for example, to large ships [31].

$$\begin{aligned}
p_0(z) &= 1 \\
p_1(z) &= z \\
p_2(z) &= \frac{z^2}{2!} \\
p_3(z) &= \frac{z^3 - 8}{3!} \\
p_4(z) &= \frac{z^4 - 32z}{4!} \\
p_5(z) &= \frac{z^5 - 80z^2}{5!}
\end{aligned}$$

TABLE 1.4: The first few polynomials $p_j(z)$ defined in (1.4).

So far, we have discussed the special polynomials $Q_n(z)$, associated with rational solutions of $\mathrm{P_{II}}$. We now discuss other special polynomials associated with rational solutions of Painlevé equations. Umemura [77] derived special polynomials $S_n(z;\tau)$ associated with rational solutions of $\mathrm{P_{III}}$. The polynomials $S_n(z;\tau)$ are known as the Umemura polynomials and are defined in Theorem 5. The proof of this theorem can be found in [23] and [45].

Theorem 5. *Suppose that $S_n(z;\tau)$ satisfies the differential-difference equation*

$$S_{n+1}S_{n-1} = -z\left(S_n\frac{\mathrm{d}^2 S_n}{\mathrm{d}z^2} - \left(\frac{\mathrm{d}S_n}{\mathrm{d}z}\right)^2\right) - S_n\frac{\mathrm{d}S_n}{\mathrm{d}z} + (z+\tau)S_n^2,$$

with $S_{-1}(z;\tau) = 1$ and $S_0(z;\tau) = 1$. Then

$$w_n(z,\tau) \equiv w(z;\alpha_n,\beta_n) = \frac{S_n(z;\tau-1)S_{n-1}(z;\tau)}{S_n(z;\tau)S_{n-1}(z,\tau-1)},$$

satisfies $\mathrm{P_{III}}$ *with $\gamma = 1$ and $\delta = -1$,*

$$\frac{\mathrm{d}^2 w}{\mathrm{d}z^2} = \frac{1}{w}\left(\frac{\mathrm{d}w}{\mathrm{d}z}\right)^2 - \frac{1}{z}\frac{\mathrm{d}w}{\mathrm{d}z} + \frac{\alpha w^2+\beta}{z} + w^3 - \frac{1}{w}, \tag{1.5}$$

with $\alpha_n = 2n + 2\tau - 1$ and $\beta_n = 2n - 2\tau + 1$ and

$$w_n(z,\tau) \equiv w(z;\widetilde{\alpha}_n,\widetilde{\beta}_n) = \frac{S_n(z;\tau)S_{n-1}(z;\tau-1)}{S_n(z;\tau-1)S_{n-1}(z,\tau)},$$

satisfies $\mathrm{P_{III}}$ *defined in (1.5), with $\widetilde{\alpha}_n = -2n + 2\tau - 1$ and $\widetilde{\beta}_n = -2n - 2\tau + 1$.*

The Umemura polynomials have applications in multivortex solutions of the complex sine-Gordon equation [8] and in MIMO wireless communication systems [20]. Examples of $S_n(z;\tau)$ and plots that show the roots $S_n(z;\tau)$ in the complex plane for various values of τ can be found in [23]. The general form of the discriminants of $S_n(z;\tau)$ can be found in [3]. Kajiwara and Masuda [48] derived the Wronskian representation of Umemura polynomials associated with rational solutions for $\mathrm{P_{III}}$ with $\gamma = 1$ and $\delta = -1$. The result and proof can be found in [48]. Recent work on rational and algebraic solutions of $\mathrm{P_{III}}$ can be found in [12, 13, 18].

Theorem 6. *The Painlevé equation* $\mathrm{P_{IV}}$

$$\frac{\mathrm{d}^2 w}{\mathrm{d}z^2} = \frac{1}{2w}\left(\frac{\mathrm{d}w}{\mathrm{d}z}\right)^2 + \frac{3}{2}w^3 + 4zw^2 + 2(z^2-\alpha)w + \frac{\beta}{w},$$

has rational solutions if and only if

$$\alpha = m, \quad \beta = -2(2n - m + 1)^2, \tag{1.6}$$

or

$$\alpha = m, \quad \beta = -2\left(-m + \frac{1}{3}\right)^2, \tag{1.7}$$

with $m, n \in \mathbb{Z}$*. Further, the rational solutions are unique.*

Rational solutions of $\mathrm{P_{IV}}$ are classified in Theorem 6. The proof of this theorem can be found in [5, 38, 51, 62]. Okamoto [71] derived special polynomials $R_n(z)$ and $S_n(z)$ associated with some rational solutions of $\mathrm{P_{IV}}$. The polynomials $R_n(z)$ and $S_n(z)$ are known as Okamoto polynomials. Noumi and Yamada [67] generalised the Okamoto polynomials so that all rational solutions of $\mathrm{P_{IV}}$ can be expressed in terms of special polynomials known as the generalized Hermite polynomials $H_{m,n}(z)$ and the generalized Okamoto polynomials $Q_{m,n}(z)$. Noumi and Yamada [67] obtained their results on rational solutions of $\mathrm{P_{IV}}$ by considering the symmetric representation of $\mathrm{P_{IV}}$. The symmetric representation of $\mathrm{P_{IV}}$ is discussed later in this chapter.

The generalized Okamoto polynomials associated with rational solutions of $\mathrm{P_{IV}}$ arise in supersymmetric quantum mechanics [54] and generate previously unknown rational-oscillatory solutions of the defocusing nonlinear Schrödinger (NLS) equation [26]. In Chapter 2, we discuss properties of the Okamoto polynomials and the generalised Okamoto polynomials in detail. The generalized Hermite polynomials associated with rational solutions of $\mathrm{P_{IV}}$ arise as multiple integrals in random matrix theory [9], in the description of vortex dynamics with quadrupole background flow [27] and in supersymmetric quantum mechanics [6]. For convenience, we will use the monic integer coefficient form of polynomials associated with rational solutions of $\mathrm{P_{IV}}$. The following definition is of the generalised Hermite polynomials $H_{m,n}(z)$. Examples of generalised Hermite polynomials can be found in Table 1.5.

Definition 3. The *generalised Hermite polynomial* $H_{m,n}(z)$, where m and n are integers, satisfy the differential-difference equations

$$mH_{m+1,n}H_{m-1,n} = H_{m,n}\frac{\mathrm{d}^2 H_{m,n}}{\mathrm{d}z^2} - \left(\frac{\mathrm{d}H_{m,n}}{\mathrm{d}z}\right)^2 + mH_{m,n}^2$$

$$-nH_{m,n+1}H_{m,n-1} = H_{m,n}\frac{\mathrm{d}^2 H_{m,n}}{\mathrm{d}z^2} - \left(\frac{\mathrm{d}H_{m,n}}{\mathrm{d}z}\right)^2 - nH_{m,n}^2$$

with $H_{0,0}(z) = H_{1,0}(z) = H_{0,1}(z) = 1$, and $H_{1,1}(z) = z$.

$$\begin{aligned}
H_{1,1}(z) &= z \\
H_{2,2}(z) &= z^4 + 3 \\
H_{3,4}(z) &= z^{12} + 6z^{10} + 45z^8 + 60z^6 - 225z^4 + 1350z^2 + 675 \\
H_{4,3}(z) &= z^{12} - 6z^{10} + 45z^8 - 60z^6 - 225z^4 - 1350z^2 + 675 \\
H_{5,3}(z) &= z^{15} - 15z^{13} + 135z^{11} - 525z^{11} - 525z^9 + 675z^7 - 4725z^5 - 7875z^3 \\
&\quad + 23625z
\end{aligned}$$

TABLE 1.5: Generalised Hermite polynomials $H_{m,n}(z)$.

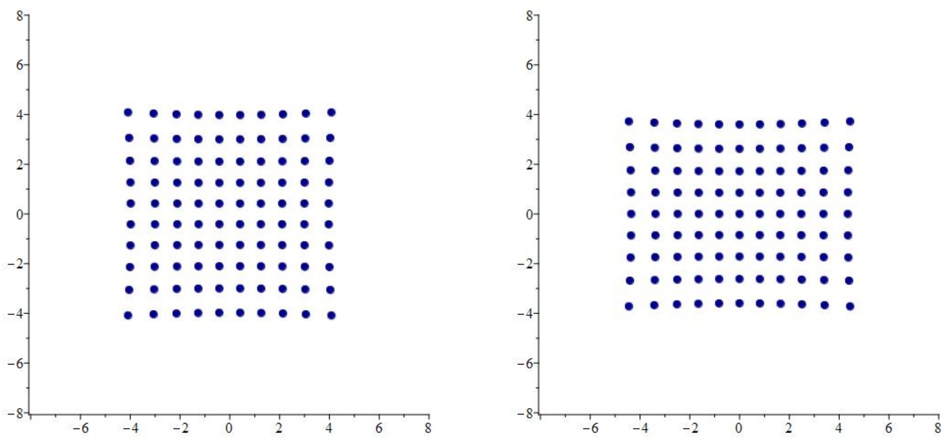

$H_{10,10}(z)$ $H_{9,11}(z)$

FIGURE 1.2: Plot of roots of generalised Hermite polynomials $H_{10,10}(z)$ and $H_{9,11}(z)$.

The plots in Figure 1.2 show the roots of some generalised Hermite polynomials. Clarkson [22] investigated the locations of the roots of $H_{m,n}(z)$ in the complex plane and surprisingly found that the roots of $H_{m,n}(z)$ form an approximate rectangle structure of size $m \times n$. Clarkson [22] used the numerical value of the roots of $H_{m,n}(z)$ to show that the roots lie in a rectangular region bounded by curves. Many years later, Masoero and Roffelsen [56] and Buckingham [14] analytically studied the roots of $H_{m,n}(z)$ as $m, n \to \infty$ and showed that roots lie in rectangles of size $m \times n$ bounded by curved lines. Recent studies on the asymptotic distribution of the roots of certain $H_{m,n}(z)$ can be found in [17, 55, 56].

The generalised Hermite polynomials and the generalised Okamoto polynomials can both be written in a determinantal form as the Wronskian of Hermite polynomials. The Hermite polynomials are defined in Definition 4. The n th Hermite polynomial denoted $H_n(z)$ is of degree n. The first few Hermite polynomials can be found in Table 1.6. The Wronskian representations in Theorems 7 and 8 are due to Noumi and Yamada [67]. For further details see Kajiwara and Ohta [47] and Noumi and Yamada [67].

Definition 4. The *Hermite polynomial* $H_n(z)$ is defined as

$$H_n(z) = (-1)^n \, \mathrm{e}^{z^2} \frac{\mathrm{d}^n}{\mathrm{d}z^n} \mathrm{e}^{-z^2},$$

and satisfies the recurrence relation

$$H_{n+1}(z) = 2zH_n(z) - 2nH_{n-1}(z).$$

Theorem 7. *The generalised Hermite polynomials $H_{m,n}(z)$, where m and n are positive integers, have the Wronskian representation*

$$\begin{aligned} H_{m,n}(z) &= \widetilde{c}_{m,n} \mathcal{W}\big(H_m(z), H_{m+1}(z), \ldots, H_{m+n-1}(z)\big) \\ &= \widetilde{c}_{m,n} \mathcal{W}\big(\{H_j(z)\}_{j=m}^{m+n-1}\big), \end{aligned}$$

where $\widetilde{c}_{m,n}$ is a constant that ensures the Wronskian is monic.

$$
\begin{aligned}
H_0(z) &= 1\\
H_1(z) &= 2z\\
H_2(z) &= 4z^2-2\\
H_3(z) &= 8z^3-12z\\
H_4(z) &= 16z^4-48z^2+12\\
H_5(z) &= 32z^5-160z^3+120z
\end{aligned}
$$

TABLE 1.6: The first few Hermite polynomials.

Theorem 8. *The generalised Okamoto polynomials $Q_{m,n}(z)$, where m and n are positive integers, have the Wronskian representation*

$$
\begin{aligned}
Q_{m,n}(z) &= c_{m,n}\mathcal{W}\big(H_1(z), H_4(z), \ldots, H_{3m-2}(z); H_2(z), H_5(z), \ldots, H_{3n-1}(z)\big)\\
&= c_{m,n}\mathcal{W}\big(\{H_{1+3j}(z)\}_{j=0}^{m-1}; \{H_{2+3j}(z)\}_{j=0}^{n-1}\big),
\end{aligned}
$$

where $c_{m,n}$ is a constant is a constant that ensures the Wronskian is monic.

The Wronskian of Hermite polynomials appear in the study of rational solutions of $\mathrm{P_{IV}}$ and in the theory of exceptional orthogonal polynomials (see, e.g. [30, 40, 68] and the references therein). Felder, Hemery and Veselov [32] conjectured that the roots of the Wronskian of Hermite polynomials are simple, except possibly at the origin. This conjecture is due to earlier work by Veselov [79]. This tells us that the discriminant of the Wronskian of Hermite polynomials with the exclusion of roots at the origin, is non-zero. The general form of the discriminant of $H_{m,n}(z)$ and $Q_{m,n}(z)$ was found by Roberts (see [74]).

We now continue our discussion on special polynomials associated with rational solutions of Painlevé equations. Kitaev, Law and McLeod [49] classified for which values of α, β, γ and δ rational solutions of $\mathrm{P_V}$ arise. Umemura [78] derived special polynomials associated with some rational solutions of $\mathrm{P_V}$ (also see [64]). Masuda, Ohta and Kajiwara [59] generalised the polynomials found by Umemura so that some rational solutions of $\mathrm{P_V}$ can be expressed in terms of special polynomials known as the generalised Umemura polynomials $U_{m,n}(z;\tau)$. Clarkson [24] investigated the location of the roots of $U_{m,n}(z;\tau)$ and found that when the parameter τ is large and negative, the roots $U_{m,n}(z;\tau)$ form two separate triangle structures, one with $\frac{1}{2}m(m+1)$ roots and another with $\frac{1}{2}n(n+1)$ roots. Examples of structures formed by the roots of $U_{m,n}(z;\tau)$ can be found in [24].

Masuda [57] found another set of special polynomials associated with rational solutions of $\mathrm{P_V}$. The rational solutions found by Masuda [57] are a special case of special function solutions of $\mathrm{P_V}$ expressible in terms of confluent hypergeometric functions ${}_1F_1(a;c:z)$, when the confluent hypergeometric function reduces to the associated Laguerre polynomial (see [57] for details).

Umemura [78] also derived special polynomials associated with some rational and algebraic solutions of $\mathrm{P_{VI}}$ (also see [63]). Mazzocco [61] classified for which values of α, β, γ and δ rational solutions of $\mathrm{P_{VI}}$ arise. Rational solutions of $\mathrm{P_{VI}}$ are still under investigation. A summary of some of the the special polynomials associated with rational solutions of $\mathrm{P_{II}}$–$\mathrm{P_V}$ can be found in Table 1.7.

Equation	Special polynomials
$\mathrm{P_{II}}$	Yablonskii–Vorob'ev polynomials $Q_n(z)$
$\mathrm{P_{III}}$	Umemura polynomials $S_n(z;\tau)$
$\mathrm{P_{IV}}$	Okamoto polynomials $R_n(z)$, $S_n(z)$
	Generalised Okamoto polynomials $Q_{m,n}(z)$
	Generalised Hermite polynomials $H_{m,n}(z)$
$\mathrm{P_V}$	Generalised Umemura polynomials $U_{m,n}(z;\tau)$

Table 1.7: Some of the special polynomials associated with rational solutions of $\mathrm{P_{II}}$–$\mathrm{P_V}$. The parameters m, n and τ are integers.

One of the ways to generalize the Painlevé equations was proposed by Veselov and Shabat [80] and Adler [2]. The idea is to write the Painlevé equations as a symmetric system of first order non-linear equations. The symmetric form of Painlevé equations are often used in the study of rational solutions of Painlevé equations. For example, Noumi and Yamada [67] obtained their results on rational solutions of $\mathrm{P_{IV}}$ by considering the symmetric representation of $\mathrm{P_{IV}}$. Noumi and Yamada [67] showed that the symmetric form of $\mathrm{P_{IV}}$ is the following system of equations

$$\begin{aligned} \frac{\mathrm{d}f_0}{\mathrm{d}z} + f_0(f_1 - f_2) &= \alpha_0, \qquad (1.8)\\ \frac{\mathrm{d}f_1}{\mathrm{d}z} + f_1(f_2 - f_0) &= \alpha_1, \qquad (1.9)\\ \frac{\mathrm{d}f_2}{\mathrm{d}z} + f_2(f_0 - f_1) &= \alpha_2, \qquad (1.10)\end{aligned}$$

where α_0, α_1 and α_2 are constants. By taking the sum of the three equations (1.8)-(1.10) we get that

$$\frac{\mathrm{d}f_0}{\mathrm{d}z} + \frac{\mathrm{d}f_1}{\mathrm{d}z} + \frac{\mathrm{d}f_2}{\mathrm{d}z} = \alpha_0 + \alpha_1 + \alpha_2 = k$$

where k is a constant. Hence,

$$f_0 + f_1 + f_2 = kz + c$$

where c is the integration constant. Assuming that $k \neq 0$, we normalize the variables so that $k = -2$ and $c = 0$. This gives the constraints

$$f_0 + f_1 + f_2 = -2z, \quad \alpha_0 + \alpha_1 + \alpha_2 = -2. \qquad (1.11)$$

Under the normalisation constraint $f_0 + f_1 + f_2 = -2z$, the system of equations (1.8)-(1.10) is equivalent to $\mathrm{P_{IV}}$.

Proof. If we multiply the equation $f_0 + f_1 + f_2 = -2z$ by f_0 and then subtract equation (1.8) we find that

$$f_0^2 - \frac{\mathrm{d}f_0}{\mathrm{d}z} + 2f_0f_2 + 2zf_0 + \alpha_0 = 0.$$

Therefore,

$$f_2 = \frac{1}{2f_0}\left(\frac{\mathrm{d}f_0}{\mathrm{d}z} - f_0^2 - 2zf_0 - \alpha_0\right). \tag{1.12}$$

Similarly, if we multiply the equation $f_0 + f_1 + f_2 = -2z$ by f_0 and then add equation (1.8) we find that

$$f_0^2 + \frac{\mathrm{d}f_0}{\mathrm{d}z} + 2f_0f_1 + 2zf_0 + \alpha_0 = 0.$$

This tells us that

$$f_1 = -\frac{1}{2f_0}\left(\frac{\mathrm{d}f_0}{\mathrm{d}z} + f_0^2 + 2zf_0 + \alpha_0\right). \tag{1.13}$$

Substituting (1.12) and (1.13) into equation (1.9) gives the result

$$\frac{1}{4f_0^2}\left(-2f_0\frac{\mathrm{d}^2f_0}{\mathrm{d}z^2} + \left(\frac{\mathrm{d}f_0}{\mathrm{d}z}\right)^2 + 3f_0^4 + 8f_0^3z + f_0^2(4z^2 - 2\alpha_0 - 4\alpha_1 - 4) - \alpha_0^2\right) = 0.$$

Therefore,

$$\frac{\mathrm{d}^2f_0}{\mathrm{d}z^2} = \frac{1}{2f_0}\left(\left(\frac{\mathrm{d}f_0}{\mathrm{d}z}\right)^2 + 3f_0^4 + 8f_0^3z + f_0^2(4z^2 - 2\alpha_0 - 4\alpha_1 - 4) - \alpha_0^2\right).$$

Setting $w = f_0$ gives the result

$$\frac{\mathrm{d}^2w}{\mathrm{d}z^2} = \frac{1}{2w}\left(\frac{\mathrm{d}w}{\mathrm{d}z}\right)^2 + \frac{3}{2}w^3 + 4w^2z + w(2z^2 - \alpha_0 - 2\alpha_1 - 2) - \frac{\alpha_0^2}{2w}.$$

This is P_{IV} with $\alpha = \frac{\alpha_0}{2} + \alpha_1 + 1$ and $\beta = -\frac{\alpha_0^2}{2}$. □

Noumi and Yamada [67] showed that the system of equations (1.8)-(1.10) possesses a symmetry group of Bäcklund transformations acting on the tuple of solutions and parameters $(f_0, f_1, f_2 \mid \alpha_0, \alpha_1, \alpha_2)$ (see [67] for details). This symmetry group is the affine Weyl group $A_2^{(1)}$ (see [65, 67] for details). It follows from Noumi and Yamada [67] that the system (1.8)-(1.10) with the constraints (1.11) has the simple rational solutions

$$
\begin{array}{lll}
\text{(i)} & (f_0, f_1, f_2) = (-2z, 0, 0), & (\alpha_0, \alpha_1, \alpha_2) = (-2, 0, 0), \\
\text{(ii)} & (f_0, f_1, f_2) = \left(-\frac{2}{3}z, -\frac{2}{3}z, -\frac{2}{3}z\right), & (\alpha_0, \alpha_1, \alpha_2) = \left(-\frac{2}{3}, -\frac{2}{3}, -\frac{2}{3}\right).
\end{array}
$$

The rational solutions (i) and (ii) can be used as "seed solutions" to generate the hierarchy of rational solutions of $\mathrm{P_{IV}}$. Noumi and Yamada [67] showed that rational solutions arising from (i) can be expressed in terms of the generalised Hermite polynomials $H_{m,n}(z)$ and rational solutions arising from (ii) can be expressed in terms of the generalised Okamoto polynomials $Q_{m,n}(z)$, which will be discussed in the next chapter.

Noumi and Yamada [66] soon realised that the structure of the system of equations (1.8)-(1.10) can be generalised to any number of equations. This resulted in the introduction of A_N-Painlevé system, also known as the Noumi and Yamada system. The system of equations (1.8)-(1.19) is known as the A_2-Painlevé system. The A_{2n}-Painlevé system is a set of $2n+1$ non-linear differential equations defined as

$$
\frac{\mathrm{d}f_i}{\mathrm{d}z} + f_i \sum_{j=1}^{n} (f_{i+2j-1} - f_{i+2j}) = \alpha_i, \quad i = 0, 1, \ldots, 2n \mod (2n+1)
$$

with the (normalisation) constraints

$$
\sum_{j=0}^{2n} f_j = -2z, \qquad \sum_{j=0}^{2n} \alpha_j = -2.
$$

For example, the A_4-Painlevé system is the following

$$
\begin{aligned}
\frac{\mathrm{d}f_0}{\mathrm{d}z} + f_0(f_1 - f_2 + f_3 - f_4) &= \alpha_0, && (1.14)\\
\frac{\mathrm{d}f_1}{\mathrm{d}z} + f_1(f_2 - f_3 + f_4 - f_0) &= \alpha_1, && (1.15)\\
\frac{\mathrm{d}f_2}{\mathrm{d}z} + f_2(f_3 - f_4 + f_0 - f_1) &= \alpha_2, && (1.16)
\end{aligned}
$$

$$\begin{aligned}
\frac{\mathrm{d}f_3}{\mathrm{d}z} + f_3(f_4 - f_0 + f_1 - f_2) &= \alpha_3, && (1.17)\\
\frac{\mathrm{d}f_4}{\mathrm{d}z} + f_4(f_0 - f_1 + f_2 - f_3) &= \alpha_4, && (1.18)
\end{aligned}$$

where $\alpha_0, \alpha_1, \alpha_2, \alpha_3$ and α_4 are constants, with the constraints

$$f_0 + f_1 + f_2 + f_3 + f_4 = -2z, \quad \alpha_0 + \alpha_1 + \alpha_2 + \alpha_3 + \alpha_4 = -2. \tag{1.19}$$

It has been conjectured by Veselov [79] that all Wronskians of Hermite polynomials arise in connection to rational solutions of one of the A_N-Painlevé system. It follows from results found by Matsuda [60] (also see [58]) that the A_4-Painlevé system (1.14)-(1.18) with the constraints (1.19) has the simple rational solutions

$$\begin{array}{lll}
\text{(i)} & \boldsymbol{f} = (-2z, 0, 0, 0, 0), & \boldsymbol{\alpha} = (-2, 0, 0, 0, 0),\\
\text{(ii)} & \boldsymbol{f} = \left(-\frac{2}{3}z, -\frac{2}{3}z, -\frac{2}{3}z, 0, 0\right), & \boldsymbol{\alpha} = \left(-\frac{2}{3}, -\frac{2}{3}, -\frac{2}{3}, 0, 0\right),\\
\text{(iii)} & \boldsymbol{f} = \left(-\frac{2}{5}z, -\frac{2}{5}z, -\frac{2}{5}z, -\frac{2}{5}z, -\frac{2}{5}z\right), & \boldsymbol{\alpha} = \left(-\frac{2}{5}, -\frac{2}{5}, -\frac{2}{5}, -\frac{2}{5}, -\frac{2}{5}\right),
\end{array}$$

where $\boldsymbol{f} = (f_0, f_1, f_2, f_3, f_4)$ and $\boldsymbol{\alpha} = (\alpha_0, \alpha_1, \alpha_2, \alpha_3, \alpha_4)$. Filipuk and Clarkson [33] investigated the rational solutions that arise from the simple solutions found by Matsuda [60]. Filipuk and Clarkson [33] expressed rational solutions arising from (i) in terms of new polynomials that they introduced, called the *symmetric Hermite polynomials*. They also expressed rational solutions arising from (iii) in terms of new polynomials called the *symmetric Okamoto polynomials*.

Definition 5. The *symmetric Hermite polynomials* have the Wronskian representation

$$H_{m,n,r,s}(z) = \mathcal{W}\Big(\{H_j(z)\}_{j=m}^{m+n-1}; \{H_{m+n+j}(z)\}_{j=r}^{r+s-1}\Big),$$

where $H_n(z)$ is the n th Hermite polynomial.

Definition 6. The *symmetric Okamoto polynomials* have the Wronskian representation

$$Q_{m,n,r,s}(z) \quad = \quad \mathcal{W}\Big(\{H_{1+5j}(z)\}_{j=0}^{m-1}; \{H_{2+5j}(z)\}_{j=0}^{n-1}; \{H_{3+5j}(z)\}_{j=0}^{r-1}; \{H_{4+5j}(z)\}_{j=0}^{s-1}\Big)$$

where $H_n(z)$ is the n th Hermite polynomial.

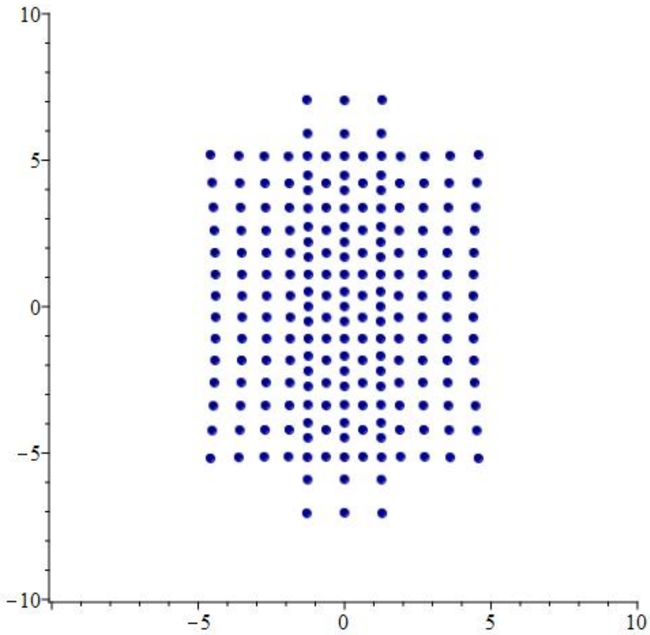

FIGURE 1.3: Plot of the roots of $H_{3,9,10,14}(z)$.

Filipuk and Clarkson [33] observed that the roots of the symmetric Hermite polynomials and symmetric Okamoto polynomials surprisingly form interesting structures and patterns in the complex plane. The plots in Figure 1.3 and Figure 1.4 are of the roots of the symmetric polynomial $H_{3,9,10,14}(z)$ and $Q_{3,9,10,14}(z)$, respectively. Further plots can be found in [33]. As the plots show, the structures formed by the roots of the symmetric Hermite and symmetric Okamoto polynomials are more complicated than the structures we have discussed so far in this chapter. The structures formed by the roots of the symmetric Hermite and symmetric Okamoto polynomials are yet to be described, except the case where the symmetric Okamoto polynomials are equal to the generalised Okamoto polynomials. The generalised

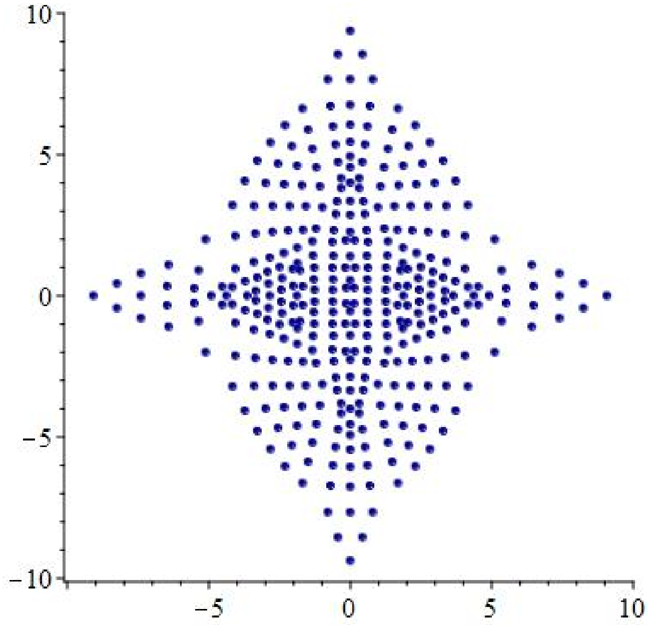

FIGURE 1.4: Plot of the roots of $Q_{3,9,10,14}(z)$.

Okamoto polynomials

$$Q_{m,n}(z) = \mathcal{W}\Big(\{H_{1+3j}(z)\}_{j=0}^{m-1}; \{H_{2+3j}(z)\}_{j=0}^{n-1}\Big),$$

which arise in connection to the A_2-Painlevé system, are also known as the 3-Okamoto polynomials because of the sequence of Hermite polynomials in the Wronskian. Similarly, the symmetric Okamoto polynomials, defined in Definition 6, which arise in connection to the A_4-Painlevé system can be called the 5-Okamoto polynomials.

It has been conjectured that the roots of the Wronskian of Hermite polynomials are simple, except possibly at the origin [32]. It follows from Theorem 3.1 and Remark 3.2 in [11] that the roots of the Wronskian of Hermite polynomials at the origin are of multiplicity

$$\frac{(p-q)(p-q+1)}{2}, \tag{1.20}$$

where p is the number of Hermite polynomials in the Wronskian that are of odd degree and q is number of Hermite polynomials in the Wronskian of even degree.

It has also been proven that if $P(z)$ is the Wronskian of Hermite polynomials then

$$P(z) = z^k \widetilde{P}(z^2), \tag{1.21}$$

where k is equal to (1.20) and $\widetilde{P}(z^2)$ is some polynomial [11]. This tells us that the roots of the Wronskian of Hermite polynomials are symmetric about the real and imaginary axis, e.g. see Figure 1.3 and Figure 1.4.

In Chapter 2, we explore how the structures formed by the roots of the 3-Okamoto polynomials $Q_{m,n}(z)$ in the complex plane depend on the parameters m and n. The structures and patterns formed by the roots of the 5-Okamoto polynomials (for example in Figure 1.4) are very surprising and intriguing, and unlike the structures we have discussed in this chapter. The beautiful structures and patterns formed by the roots of the 5-Okamoto polynomials $Q_{m,n,r,s}(z)$ motivate us to first investigate the roots of polynomials that we call 4-Okamoto polynomials $Q_{m,n,r}(z)$. We define the 4-Okamoto polynomials to be

$$Q_{m,n,r}(z) = \mathcal{W}\Big(\{H_{1+4j}(z)\}_{j=0}^{m-1}; \{H_{2+4j}(z)\}_{j=0}^{n-1}; \{H_{3+4j}(z)\}_{j=0}^{r-1}\Big).$$

In Chapter 3, we explore the structures formed by the roots of 4-Okamoto polynomials in the complex plane and the relationship between the structures and the parameters m, n and r.

We now continue our discussion of the A_4-Painlevé system. Earlier we discussed the simple solution

$$\text{(ii)} \quad \boldsymbol{f} = \left(-\frac{2}{3}z, -\frac{2}{3}z, -\frac{2}{3}z, 0, 0\right), \quad \boldsymbol{\alpha} = \left(-\frac{2}{3}, -\frac{2}{3}, -\frac{2}{3}, 0, 0\right),$$

due to Matsuda [60]. Recent work by Clarkson, Gómez-Ullate, Grandati and Milson [29] expressed rational solutions arising from (ii) in terms of a new polynomial $P_{m,n,r,s}(z)$ that they introduced.

Definition 7. The polynomial $P_{m,n,r,z}(z)$ has the Wronskian representation

$$P_{m,n,r,s}(z) = \mathcal{W}\Big(\{H_{1+3j}(z)\}_{j=0}^{m-1}; \{H_{2+3j}(z)\}_{j=0}^{n-1}; \{H_{r+3j}(z)\}_{j=0}^{s-1}\Big),$$

provided that

$$r \notin \{1, 4, \ldots, 3m-2, 2, 5, \ldots, 3n-1\}.$$

Similar, to the polynomials $H_{m,n,r,s}(z)$ and $Q_{m,n,r,s}(z)$ the roots of $P_{m,n,r,z}(z)$ also form surprising structures. Figure 1.5 shows the roots of $P_{8,16,18,5}(z)$ in the complex plane. Further plots can be found in [29].

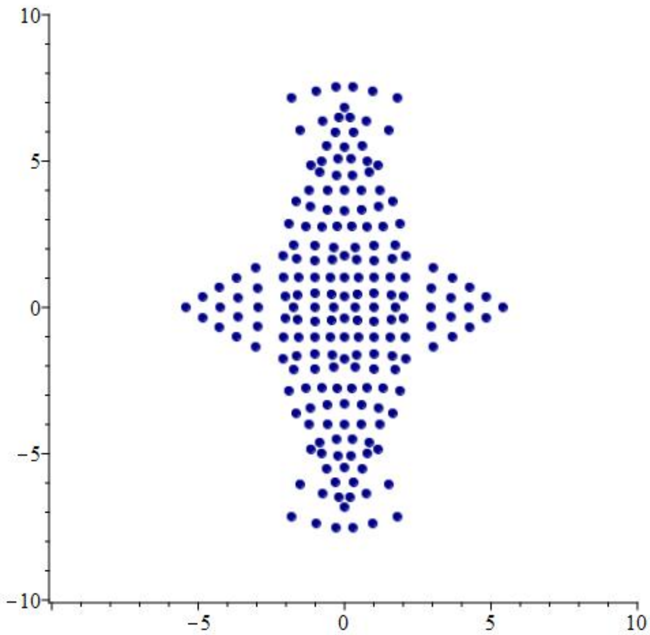

FIGURE 1.5: Plot of the roots of $P_{8,16,18,5}(z)$.

The Wronskian of polynomials are naturally associated with partitions since Wronskians are labelled by partitions (see [32]). In the next section of this chapter, we define partitions and explain how to visually represent partitions using Young diagrams and Maya diagrams. We also discuss cores and quotients of partitions. The cores and quotients of partitions have many applications and are of great interest in representation theory and number theory. Partitions are often used to study the structure of the Wronskian of polynomials. Recent work on the Wronskian of Hermite polynomials and their coefficients was studied by Bonneux, Dunning and Stevens [11] using the combinatorial concepts of cores and quotients. In 2021 Gómez-Ullate, Grandati and Milson [41] provided a complete classification of rational solutions of the A_{2n}-Painlevé system using Maya diagrams and partitions associated with some rational solution of the A_{2n}-Painlevé system.

1.3 Partitions and diagrams

In this section, we discuss partitions, Young diagrams, Maya diagrams and cores and quotient of partitions. The following definitions and theorems, as well as further examples can be found in [43, 50, 53, 82].

Definition 8. A *partition* λ of a positive integer Λ is a sequence $(\lambda_1, \lambda_2, \ldots, \lambda_m)$ of weakly decreasing positive integers such that $\lambda_1 + \lambda_2 + \cdots + \lambda_m = \Lambda$.

Example 1. For example, a partition of the integer 14 is

$$\begin{aligned} \lambda &= (5, 3, 2, 2, 1, 1) \\ &\equiv (5, 3, 2^2, 1^2). \end{aligned}$$

Definition 9. Given a partition $\lambda = (\lambda_1, \lambda_2, \ldots, \lambda_m)$, the *associated polynomial* $\mathcal{P}_\lambda(z)$ is given by

$$\mathcal{P}_\lambda(z) = \mathcal{W}\big(f_{n_1}, f_{n_2}, \ldots, f_{n_m}\big),$$

where f_{n_j} is a polynomial of degree n_j and

$$n_j = \lambda_j + m - j. \tag{1.22}$$

Definition 10. The *degree vector* associated with λ is the sequence

$$n_\lambda = (n_1, n_2, \ldots, n_m).$$

Example 2. For example, the polynomial associated with the partition $\lambda = (5, 3, 2^2, 1^2)$ is

$$\mathcal{P}_\lambda(z) = \mathcal{W}\big(f_{10}, f_7, f_5, f_4, f_2, f_1\big)$$

and the associated degree vector of λ is $n_\lambda = (10, 7, 5, 4, 2, 1)$.

Definition 11. The *size* of a partition $\lambda = (\lambda_1, \lambda_2, \ldots, \lambda_m)$ is denoted by

$$|\lambda| = \lambda_1 + \lambda_2 + \cdots + \lambda_m.$$

A partition can be visually represented by a Young diagram.

Definition 12. The *Young diagram* of $\lambda = (\lambda_1, \lambda_2, \ldots, \lambda_m)$ is a left-justified shape of m rows of boxes of length $\lambda_1, \lambda_2, \ldots, \lambda_m$.

Example 3. Figure 1.6 shows the Young diagram of $\lambda = (5, 3, 2^2, 1^2)$.

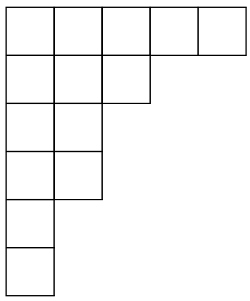

FIGURE 1.6: The Young diagram of $\lambda = (5, 3, 2^2, 1^2)$.

Definition 13. The *conjugate* λ^* of a partition λ is the partition found by reflecting the Young diagram of λ about the diagonal, so that rows become columns and columns become rows.

Example 4. Figure 1.7 shows that the conjugate of $\lambda = (5, 3, 2^2, 1^2)$ is $\lambda^* = (6, 4, 2, 1, 1)$.

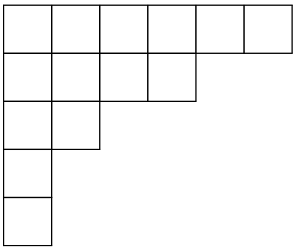

FIGURE 1.7: The Young diagram of the conjugate of $\lambda = (5, 3, 2^2, 1^2)$.

Definition 14. A partition λ is called *self-conjugate* if $\lambda = \lambda^*$.

Definition 15. Given a Young diagram the *hook* of a box in position (i, j), i.e. in the i th row and j th column, consists of all boxes to its right, the box itself and all the boxes below.

Example 5. Figure 1.8 shows the hook at position (2,2) of the Young diagram of $\lambda = (5, 3, 2^2, 1^2)$. The boxes that form the hook at position (2,2) have been coloured red.

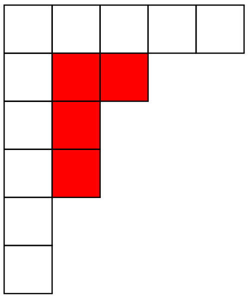

FIGURE 1.8: The Young diagram of $\lambda = (5, 3, 2^2, 1^2)$. The red boxes form the hook in position (2,2) of the Young diagram.

Definition 16. A hook has a corner, an arm ending in a hand, and a leg ending in a foot.

Example 6. Consider the hook in position (2,2) of the Young diagram in Figure 1.8. The corner of this hook is the box in position (2,2), the hand is the box in position (2,3), and the foot is the box in position (4,2).

Definition 17. The *hook length* of a box in position (i, j) is the number of boxes in the hook at position (i, j).

Example 7. Figure 1.8 shows that the hook length of the box in position (2,2) is 4. Therefore, we say that the hook in position (2,2) of the partition $\lambda = (5, 3, 2^2, 1^2)$ is of hook length 4. Figure 1.9 shows the Young diagram of $\lambda = (5, 3, 2^2, 1^2)$ and its hook lengths.

10	7	4	2	1
7	4	1		
5	2			
4	1			
2				
1				

FIGURE 1.9: The Young diagram of $\lambda = (5, 3, 2^2, 1^2)$ with the hook length of hooks in position (i, j).

Definition 18. A hook of length p is called a *p-hook*.

Example 8. Figure 1.9 shows that the Young diagram of $\lambda = (5, 3, 2^2, 1^2)$ has a 7-hook in position $(1, 2)$ and another in position $(2, 1)$.

Remark 1. The first column hook lengths of the Young diagram of λ are precisely the elements of the degree vector n_λ of λ.

Definition 19. The *rim* of the Young diagram refers to the set of boxes in position (i, j) of the Young diagram such that the boxes $(i + 1, j + 1)$ do not exist.

Example 9. Figure 1.10 shows the rim of the Young diagram of $\lambda = (5, 3, 2^2, 1^2)$.

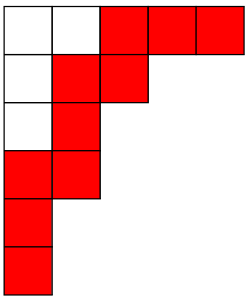

FIGURE 1.10: The Young diagram of $\lambda = (5, 3, 2^2, 1^2)$. The boxes coloured red form the rim of the Young diagram.

Definition 20. A *rim p-hook* consists of boxes from the hand to the foot of a p-hook along the rim of the Young diagram.

Remark 2. A rim p-hook is of length p i.e. it consists of p boxes.

Example 10. The 7-hooks of $\lambda = (5, 3, 2^2, 1^2)$ are in position $(1, 2)$ and $(2, 1)$. Figures 1.11 and 1.12 show the rim 7-hook corresponding with each of the 7-hooks of $\lambda = (5, 3, 2^2, 1^2)$.

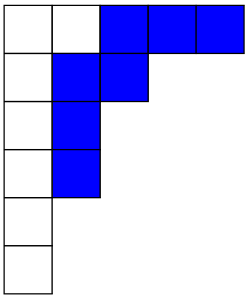

FIGURE 1.11: The Young diagram of $\lambda = (5, 3, 2^2, 1^2)$ has a 7-hook in position (1,2). The blue boxes form a rim 7-hook.

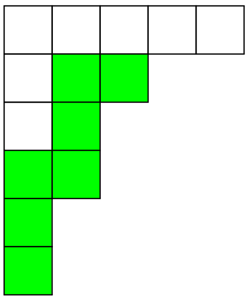

FIGURE 1.12: The Young diagram of $\lambda = (5, 3, 2^2, 1^2)$ has a 7-hook in position (2,1). The green boxes form a rim 7-hook.

Definition 21. The *p-core* of a partition is the partition corresponding to the Young diagram after all rim p-hooks have been removed.

Example 11. The 4-core of $\lambda = (5, 3, 2^2, 1^2)$ can be found by first removing the rim 4-hook in Figure 1.13 coloured by blue boxes and then the ones coloured red. Removing the coloured boxes in Figure 1.13 results in the Young diagram of (1^2). Since the partition (1^2) has no rim 4-hooks, i.e. there are no rim 4-hooks to remove, it means the 4-core of $\lambda = (5, 3, 2^2, 1^2)$ is (1^2).

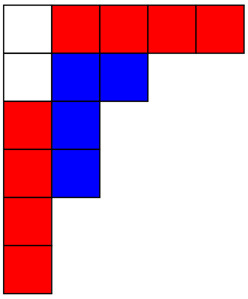

FIGURE 1.13: The Young diagram of $\lambda = (5, 3, 2^2, 1^2)$. The 4-core of λ can be found first removing the rim 4-hooks coloured by blue boxes and then the ones coloured by red boxes.

Alternatively, the 4-core of $\lambda = (5, 3, 2^2, 1^2)$ can be found in the following way.

Example 12. If we first remove the rim 4-hooks in Figure 1.14 that are coloured by red boxes and then the ones coloured blue, we are left with the partition (1^2).

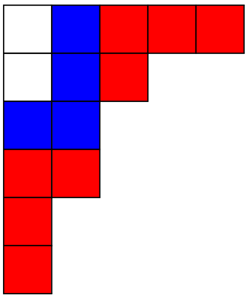

FIGURE 1.14: The Young diagram of $\lambda = (5, 3, 2^2, 1^2)$. The 4-core of λ can be found by first removing the rim 4-hooks coloured by red boxes and then the boxes coloured blue.

Figures 1.13 and 1.14 show that the 4-core of $\lambda = (5, 3, 2^2, 1^2)$ is (1^2).

Theorem 9. *Removing all rim p-hooks leads to a unique p-core irrespective of the order in which the hooks are removed.*

A partition is called a p-core if it does not contain any p-hooks. For example, Figure 1.9 shows that $\lambda = (5, 3, 2^2, 1^2)$ is a 3-core partition, since λ does not contain any 3-hooks. Similarly, $\lambda = (5, 3, 2^2, 1^2)$ is also a 6-core partition. Figure 1.9 shows that $\lambda = (5, 3, 2^2, 1^2)$ is not a 2-core partition, since it contains 2-hooks. In the following example we find the 2-core of $\lambda = (5, 3, 2^2, 1^2)$.

Example 13. Figure 1.15 shows that if we first remove the rim 2-hooks coloured by blue boxes, and then the ones coloured by red boxes, followed by the rim 2-hook coloured by green boxes, we are left with the Young diagram of (1^2). Since the partition (1^2) contains a 2-hook in position $(1,1)$ this means it contains a rim 2-hook. Therefore, the 2-core of $\lambda = (5,3,2^2,1^2)$ is the empty set.

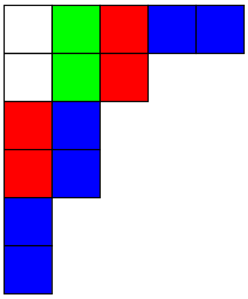

FIGURE 1.15: The Young diagram $\lambda = (5,3,2^2,1^2)$. The 2-core of λ can be found by first removing the rim 2-hooks coloured by blue boxes, then the ones coloured by red boxes and lastly the rim 2-hooks coloured by green boxes.

We later discuss how abacus displays of a partition can be used to find the p-core of the partition. We now discuss Maya diagrams which are often used to represent partitions visually. The Maya diagram of a partition is found using the border of the partition's Young diagram.

Definition 22. The *border* of a Young diagram refers to the boundary of the diagram that connects the northeast corner of the diagram to the southwest corner, along the southeast boundary of the Young diagram.

Example 14. Figure 1.16 shows the border of the Young diagram of $\lambda = (5,3,2^2,1^2)$.

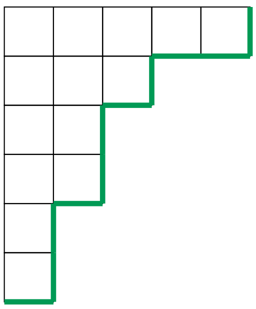

FIGURE 1.16: The Young diagram of $\lambda = (5,3,2^2,1^2)$ with green lines to highlight the border of the Young diagram.

Definition 23. The *Maya diagram* of a partition λ is a sequence of beads and empty beads that can be found using the Young diagram of λ. To find the Maya diagram of λ, start at the southwest corner of the Young diagram of λ and walk along the border of the diagram, placing a bead for each step up and an empty bead for each step to the right. Straightening out the diagram of beads and empty beads gives the Maya diagram of λ.

The partition λ of an integer $\Lambda = \lambda_1 + \lambda_2 + \cdots + \lambda_m$ is

$$\begin{aligned} \lambda &= (\lambda_1, \lambda_2, \ldots, \lambda_m) \\ &\equiv (\lambda_1, \lambda_2, \ldots, \lambda_m, 0, 0, 0, \ldots, 0). \end{aligned}$$

As a consequence, the Maya diagram of partitions contains of an infinite number of beads at the start of the diagram, and an infinite number of empty beads at the end of the diagram. For convenience, we will not include such beads in our examples.

Example 15. Figure 1.17 shows the Young diagram of $\lambda = (5, 3, 2^2, 1^2)$ with beads and empty beads placed along the border of the diagram. Figure 1.18 shows the Maya diagram of $\lambda = (5, 3, 2^2, 1^2)$.

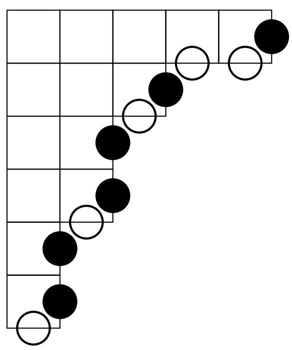

FIGURE 1.17: The Young diagrams of $\lambda = (5, 3, 2^2, 1^2)$ with beads and empty beads along the border of the diagram.

FIGURE 1.18: The Maya diagram of $\lambda = (5, 3, 2^2, 1^2)$.

Given the Maya diagram of a partition $\lambda = (\lambda_1, \lambda_2, \ldots, \lambda_m)$, the terms $\lambda_1, \lambda_2, \ldots, \lambda_m$ can be determined by counting the number of empty beads to the left of each bead starting from the right hand side of the Maya diagram.

The sequence of beads and empty beads in the Maya diagram of λ can be arranged into columns. If we read the Maya diagram from left to right starting with the first empty bead of the diagram and then arrange the beads and empty beads onto p columns it produces a display known as a *p-runner abacus display*. Since, the partition $\lambda = (\lambda_1, \lambda_2, \ldots, \lambda_m)$ of an integer is equivalent to $\lambda = (\lambda_1, \lambda_2, \ldots, \lambda_m, 0, 0, \ldots, 0)$, the abacus display of partitions include an infinite number of beads at the start of each runner and an infinite number of empty beads at the end of each runner of the abacus display. For convenience we will not be including these beads in our examples. Figure 1.19 shows the 4-runner abacus display of $\lambda = (5, 3, 2^2, 1^2)$. The 2-runner abacus display is shown in Figure 1.23.

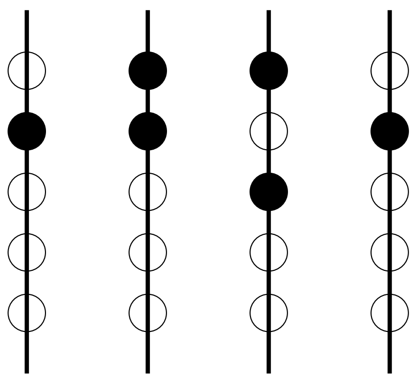

FIGURE 1.19: The 4-runner abacus display of $\lambda = (5, 3, 2^2, 1^2)$.

A partition λ is a p-core if and only if every bead in the p-runner abacus display of λ has a bead directly above it. Earlier, we discussed that $\lambda = (5, 3, 2^2, 1^2)$ is a 3-core since its does not contain any 3-hook. It is clear to see that λ is a 3-core from Figure 1.20.

If the p-runner abacus of λ contains empty beads directly above beads it shows that λ contains rim p-hooks. As discussed earlier, the p-core of λ is obtained by removing all rim p-hooks of λ. The rim p-hooks can be removed by pushing up all

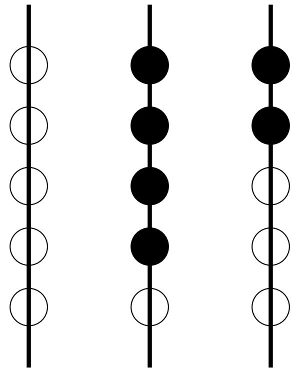

FIGURE 1.20: The 3-runner abacus display of $\lambda = (5, 3, 2^2, 1^2)$.

the beads in the p-runner abacus of λ up as far as they can go. Pushing up a bead by one place in the p-runner abacus display of λ is equivalent to removing a rim p-hook. Once the abacus display of the p-core is obtained, the p-core can be found by looking at the position of beads and empty beads to determine the corresponding Young diagram, i.e. the Young digram of the p-core. In the following example, we explain how to determine the 4-core of λ.

Example 16. Figure 1.21 is the result of pushing all the beads in Figure 1.19 up as far as they can go. Figure 1.21 shows that every bead in the display has a bead directly above it. This shows that the partition corresponding to Figure 1.21 is a 4-core partition. The position of the beads and empty beads in Figure 1.21 tells us that the Young diagram of the 4-core is of the form shown in Figure 1.22. Figure 1.22 shows that the 4-core of $\lambda = (5, 3, 2^2, 1^2)$ is the partition (1^2), which we found earlier.

Example 17. If we push all the beads in Figure 1.23 up as far as they can go we get Figure 1.24. Since all beads in Figure 1.24 contain a bead directly above it, we know that the corresponding partition is a 2-core. Figure 1.24 shows that the 2-core of $\lambda = (5, 3, 2^2, 1^2)$ is the empty set, since no beads appear after the first empty bead of each each runner.

Remark 3. A 2-core is always of the form

$$(m, m-1, m-2, \ldots, 1),$$

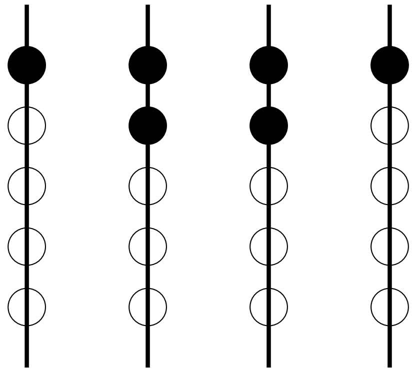

FIGURE 1.21: The 4-runner abacus display of the 4-core $\lambda = (5, 3, 2^2, 1^2)$.

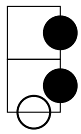

FIGURE 1.22: The Young diagram of the 4-core of $\lambda = (5, 3, 2^2, 1^2)$.

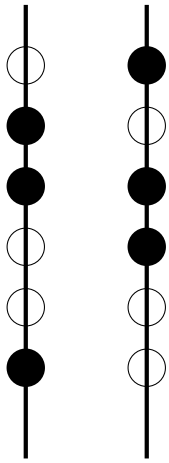

FIGURE 1.23: The 2-runner abacus display of $\lambda = (5, 3, 2^2, 1^2)$.

where $m \in \mathbb{Z}^+$. Partitions of this form are known as *staircase partition.*

Definition 24. The *p-quotient* of λ is an ordered set of p partitions where each partition describes how many places beads in each runner of the p-runner abacus display of λ have been pushed up by to form the the p-runner abacus display of the p-core of λ.

The following example explains how to find the 2-quotient (μ, ν) of $\lambda = (5, 3, 2^2, 1^2)$.

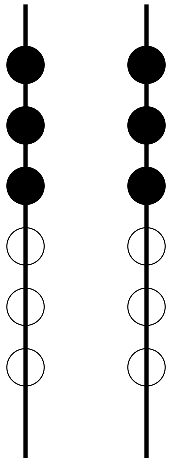

FIGURE 1.24: The 2-runner abacus display of the 2-core of $\lambda = (5, 3, 2^2, 1^2)$.

Example 18. Figure 1.23 shows the 2-runner abacus display of λ and Figure 1.24 shows the 2-runner abacus display of the 2-core of λ. To obtain Figure 1.24 from 1.23, all three beads in the first runner of Figure 1.23 need to be pushed up. The first and second bead in the first runner need to be pushed up by one place, and the third bead needs to be pushed up by three places. This tells us that the partition $\mu = (3, 1^2)$. The second runner of Figure 1.23 shows that two beads need to pushed up, each by one place in order to obtain Figure 1.24. This shows that the partition $\nu = (1^2)$. Therefore, the 2-quotient of $\lambda = (5, 3, 2^2, 1^2)$ is

$$\big((3, 1^2), (1^2)\big).$$

Remark 4. To ensure that the 2-quotient (μ, ν) obtained from the 2-runner abacus display of λ is ordered, i.e. that the first runner gives μ and the second runner gives ν, it is required that the second runner of the 2-runner abacus display contains at least as many beads as the first runner (see [82]). According to Wildon [82], including an additional bead to the start of the first runner and rearranging beads and empty beads to include the additional beads, allows the second runner to contain at least as many beads as the first.

Remark 5. With this convention to fix the order of the partitions μ and ν in the 2-quotient of λ, the correspondence between λ and pairs of 2-cores δ and

2-quotients (μ, ν) is bijective $(\delta, (\mu, \nu))$.

Remark 6. Recent findings on the ordering of p-quotients for $p > 2$ can be found in [10]. It is known that there is a bijective correspondence between λ and the pairs of p-cores and ordered p-quotients of λ (see [10]).

1.4 Thesis outline

Chapter 2 focuses on properties of the generalised Okamoto polynomials $Q_{m,n}(z)$. We first consider properties of the Okamoto polynomials $R_n(z)$ and $S_n(z)$ which are special cases of $Q_{m,n}(z)$. We then discuss structures formed by the roots of generalised Okamoto polynomials in the complex plane. In this chapter, we determine the explicit form of the family of partitions λ associated with $Q_{m,n}(z)$ and show that these partitions are 3-core partitions. We find that the relative size of m and n affects the structures formed by the roots of $Q_{m,n}(z)$ and the set of partitions λ associated with $Q_{m,n}(z)$. We determine the explicit form of the conjugate of partitions λ associated with $Q_{m,n}(z)$ by considering the general form of the Young diagram λ associated with $Q_{m,n}(z)$. The conjugate partitions of λ are used when we discuss the polynomials

$$R_{m,n}(z) = \mathrm{i}^d Q_{m,n}(-\mathrm{i}z),$$

where d is the degree of $Q_{m,n}(z)$. The motivation for investigating the polynomials $R_{m,n}(z)$ is to confirm our findings on the structures formed by the roots of $Q_{m,n}(z)$ in the complex plane. We determine the 2-cores and 2-quotients of λ associated with $Q_{m,n}(z)$ by considering the 2-runner abacus display of λ.

Chapter 3 is on properties of the 4-Okamoto polynomials $Q_{m,n,r}(z)$. We start by investigating the relationship between m, n and r and the structures formed by the roots of $Q_{m,n,r}(z)$ in the complex plane. In this chapter, we determine the explicit form of the family of partitions λ associated with $Q_{m,n,r}(z)$ and the conjugate of these partitions. We explain why the family of partitions λ associated with $Q_{m,n,r}(z)$ are 4-core partitions. We use the 2-runner abacus display of λ associated with $Q_{m,n,r}(z)$ to determine the 2-cores and 2-quotients of λ. The polynomials

$$R_{m,n,r}(z) = \mathrm{i}^d Q_{m,n,r}(-\mathrm{i}z),$$

where d is the degree of $Q_{m,n,r}(z)$ are discussed towards the end of this chapter. Chapter 3 ends with an investigation on the discriminant of a subset of the 4-Okamoto polynomials.

Chapter 2

The generalised Okamoto polynomials

In this chapter, we investigate properties of the generalised Okamoto polynomials $Q_{m,n}(z)$. The generalised Okamoto polynomials are naturally associated with a specific family of partitions. In this chapter, we explore how aspects of these partitions play a role in properties of $Q_{m,n}(z)$. We first discuss the structures formed by the roots of $Q_{m,n}(z)$ in the complex plane. We investigate the explicit form of the partitions λ associated with $Q_{m,n}(z)$ and the conjugate of λ. In this chapter, we also determine the 2-cores and 2-quotients of λ associated with $Q_{m,n}(z)$. The polynomials

$$R_{m,n}(z) = \mathrm{i}^d Q_{m,n}(-\mathrm{i}z),$$

where d is the degree of $Q_{m,n}(z)$ given in (2.1) are also discussed in this chapter. The motivation for studying the polynomials $R_{m,n}(z)$ is to check the structures formed by the roots of $Q_{m,n}(z)$ in the complex plane. We start this chapter by first considering the Okamoto polynomials $R_n(z)$ and $S_n(z)$, which are special cases of $Q_{m,n}(z)$.

The Okamoto polynomials are special polynomials associated with some rational solutions of $\mathrm{P_{IV}}$. The following definition is of the monic integer coefficient form of the Okamoto polynomials, defined by Okamoto [71].

Definition 25. The Okamoto polynomials $R_n(z)$ where n is an integer satisfy the differential-difference equation

$$R_{n+1}R_{n-1} = R_n\frac{\mathrm{d}^2R_n}{\mathrm{d}z^2} - \left(\frac{\mathrm{d}R_n}{\mathrm{d}z}\right)^2 + (z^2 - 2n - 1)R_n^2,$$

with $R_{-1}(z) = R_0(z) = 1$. The Okamoto polynomials $S_n(z)$ where n is an integer satisfy

$$S_{n+1}S_{n-1} = S_n\frac{\mathrm{d}^2S_n}{\mathrm{d}z^2} - \left(\frac{\mathrm{d}S_n}{\mathrm{d}z}\right)^2 + (z^2 - 2n)S_n^2,$$

with $S_0(z) = 1$ and $S_1(z) = z$.

The Okamoto polynomials are of degree $n(n+1)$ and n^2, respectively. The first few Okamoto polynomials can be found in Tables 2.1 and 2.2.

$$\begin{aligned}
R_1(z) &= z^2 - 1\\
R_2(z) &= z^6 - 5z^4 + 5z^2 - 5\\
R_3(z) &= z^{12} - 14z^{10} + 65z^8 - 140z^6 + 175z^4 - 350z^2 + 175\\
R_4(z) &= z^{20} + 10z^{18} - 5z^{16} - 240z^{14} - 630z^{12} - 364z^{10} - 2170z^8 - 3040z^6\\
&\quad -4396z^4 - 1390z^2 - 801
\end{aligned}$$

TABLE 2.1: Okamoto polynomials $R_n(z)$.

$$\begin{aligned}
S_1(z) &= z\\
S_2(z) &= z^4 - 2z^2 - 1\\
S_3(z) &= z^9 - 8z^7 + 14z^5 - 35z\\
S_4(z) &= z^{16} - 20z^{14} + 140z^{12} - 420z^{10} + 350z^8 + 980z^6 - 4900z^4 + 4900z^2\\
&\quad +1225
\end{aligned}$$

TABLE 2.2: Okamoto polynomials $S_n(z)$.

The Okamoto polynomials have the symmetric property (see [71])

$$R_{-n}(z) = \mathrm{i}^{-n(n-1)} R_{n-1}(\mathrm{i}z),$$

and

$$S_{-n}(z) = \mathrm{i}^{-n^2} S_n(\mathrm{i}z).$$

As a result, Okamoto polynomials with n positive are often studied. The Okamoto polynomials defined in Definition 25, for $n \geq 1$ can be written as the Wronskian of Hermite polynomials defined in Theorem 10 (see [67]). For convenience, the monic Hermite polynomials, also known as the probabilists' Hermite polynomials, can be used.

Definition 26. The probabilist's Hermite polynomial $\mathrm{He}_n(z)$ are defined as

$$\mathrm{He}_n(z) = (-1)^n \, \mathrm{e}^{\frac{z^2}{2}} \frac{\mathrm{d}^n}{\mathrm{d}z^n} \mathrm{e}^{-\frac{z^2}{2}}.$$

The n th probabilist's Hermite polynomial is of degree n. The first few probabilist's Hermite polynomials can be found in Table 2.3.

$$\begin{aligned}
\mathrm{He}_0(z) &= 1 \\
\mathrm{He}_1(z) &= z \\
\mathrm{He}_2(z) &= z^2 - 1 \\
\mathrm{He}_3(z) &= z^3 - 3z, \\
\mathrm{He}_4(z) &= z^4 - 6z^2 + 3 \\
\mathrm{He}_5(z) &= z^5 - 10z^3 + 15z
\end{aligned}$$

Table 2.3: The first few probabilist's Hermite polynomials.

Theorem 10. *The Okamoto polynomials for $n \geq 1$ have the Wronskian representation*

$$R_n(z) = c_n \mathcal{W}\Big(\big\{\mathrm{He}_{2+3j}(z)\big\}_{j=0}^{n-1}\Big),$$

$$S_n(z) = c_n \mathcal{W}\Big(\big\{\mathrm{He}_{1+3j}(z)\big\}_{j=0}^{n-1}\Big),$$

where

$$c_n = \prod_{i<j} \frac{1}{n_j - n_i},$$

ensures that polynomials are monic. The terms $n_1, n_2, \ldots, n_\ell$ are the degrees of the Hermite polynomials in the Wronskian.

Figure 2.1 shows the roots of $R_n(z)$ and $S_n(z)$ in the complex plane. Clarkson [22] observed that the roots of Okamoto polynomials form highly regular structures in the complex plane. Clarkson [22] found that the roots of $R_n(z)$ form two approximate equilateral triangles of size n, and the roots of $S_n(z)$ form two approximate equilateral triangles of size $n-1$, with an additional row of roots on a straight line between the two equilateral triangles. It is clear to see from the plots in Figure 2.1 that the equilateral triangle structures formed by the roots of Okamoto polynomials are bounded by curves.

Over a decade after the Okamoto polynomials were introduced, Noumi and Yamada [67] generalised the Okamoto polynomials so that all rational solutions of $\mathrm{P_{IV}}$ can be expressed in terms the generalised Hermite polynomials $H_{m,n}(z)$ and the generalised Okamoto polynomials $Q_{m,n}(z)$. We discussed the generalised Hermite polynomials in Chapter 1. Examples of generalised Hermite polynomials can be found in Table 1.5 and examples of structures formed by the roots of $H_{m,n}(z)$ can be found in Figure 1.2. To recap, Clarkson [22] found that the roots of $H_{m,n}(z)$ form an approximate rectangle structure of size $m \times n$.

The following definition is the monic integer coefficient form of the generalised Okamoto polynomials defined by Noumi and Yamada [67].

Definition 27. The generalised Okamoto polynomials $Q_{m,n}(z)$, where m and n are integers, satisfy the differential-difference equations

$$\begin{aligned}
Q_{m+1,n}Q_{m-1,n} &= Q_{m,n}\frac{\mathrm{d}^2 Q_{m,n}}{\mathrm{d}z^2} - \left(\frac{\mathrm{d}Q_{m,n}}{\mathrm{d}z}\right)^2 + (z^2 - 2m + n)Q_{m,n}^2, \\
Q_{m,n+1}Q_{m,n-1} &= Q_{m,n}\frac{\mathrm{d}^2 Q_{m,n}}{\mathrm{d}z^2} - \left(\frac{\mathrm{d}Q_{m,n}}{\mathrm{d}z}\right)^2 + (z^2 + m - 2n - 1)Q_{m,n}^2,
\end{aligned}$$

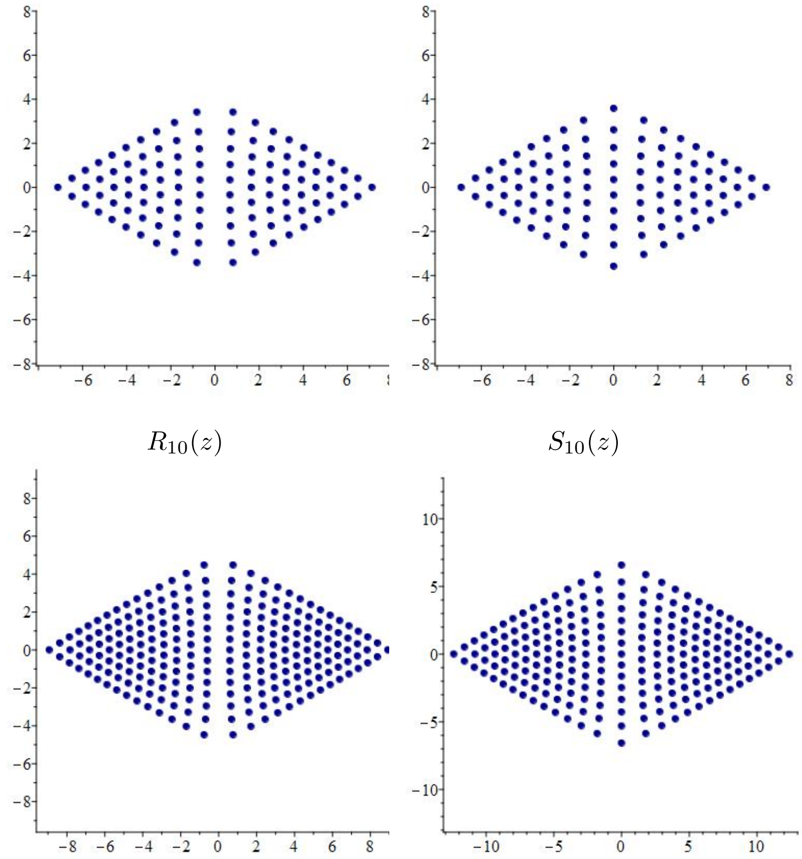

$R_{10}(z)$ $S_{10}(z)$

$R_{15}(z)$ $S_{15}(z)$

FIGURE 2.1: Plot of roots of $R_n(z)$ and $S_n(z)$ for $n = 10$ and $n = 15$.

with $Q_{0,-1}(z) = Q_{0,0}(z) = Q_{1,-1}(z) = 1$ and $Q_{1,0}(z) = z$.

The generalised Okamoto polynomials $Q_{m,n}(z)$ are of degree

$$d = m^2 + n^2 - mn + n. \tag{2.1}$$

Examples of $Q_{m,n}(z)$ are given in Table 2.4.

Noumi and Yamada showed that $Q_{m,n}(z)$ can be written as the Wronskian of Hermite polynomials. The Wronskian representation of $Q_{m,n}(z)$, defined in Definition 27, in terms of the probabilist's Hermite polynomials is given in Theorem 11 (see [67]).

$$
\begin{aligned}
Q_{1,1}(z) &= z^2+1\\
Q_{1,2}(z) &= z^5-5z\\
Q_{2,1}(z) &= z^4+2z^2-1\\
Q_{2,2}(z) &= z^6+5z^4+5z^2+5\\
Q_{2,3}(z) &= z^{10}+5z^8-10z^6-50z^4-75z^2+25\\
Q_{3,3}(z) &= z^{12}+14z^{10}+65z^8+140z^6+175z^4+350z^2+175\\
Q_{3,4}(z) &= z^{17}+16z^{15}+60z^{13}-160z^{11}-1650z^9-4400z^7-7700z^5+9625z\\
Q_{5,3}(z) &= z^{22}+21z^{20}+105z^{18}-455z^{16}-5950z^{14}-19110z^{12}-19110z^{10}\\
&\quad +31850z^8-111475z^6-557375z^4-111475z^2-111475
\end{aligned}
$$

TABLE 2.4: Generalised Okamoto polynomials $Q_{m,n}(z)$.

Theorem 11. *The generalised Okamoto polynomials $Q_{m,n}(z)$ where m and n are positive integers have the Wronskian representation*

$$Q_{m,n}(z) = c_{m,n}\mathcal{W}\Big(\big\{\mathrm{He}_{1+3j}(z)\big\}_{j=0}^{m-1}\,;\,\big\{\mathrm{He}_{2+3j}(z)\big\}_{j=0}^{n-1}\Big), \tag{2.2}$$

where

$$c_{m,n} = \prod_{i<j}\frac{1}{n_j-n_i}, \tag{2.3}$$

ensures that $Q_{m,n}(z)$ is monic. The terms $n_1, n_2, \ldots, n_\ell$ are the degrees of the Hermite polynomials in the Wronskian.

It is clear from Theorems 10 and 11 that the polynomials $Q_{n,0}(z)$ and $S_n(z)$ are equal, and the polynomials $Q_{0,n}(z)$ and $R_n(z)$ are equal.

Alternatively, the generalised Okamoto polynomials can be defined by the polynomials $\Omega_{m,n}(z)$ and $\Sigma_{m,n}(z)$ introduced by Clarkson (see [22] and [26], respectively). Note that in [22] and [26] the polynomials $\Omega_{m,n}(z)$ that I defined in Theorem 12, are called $Q_{m,n}(z)$, and the polynomials $\Sigma_{m,n}(z)$ that I defined in Theorem 13, are called $Q_{-m,-n}(z)$ in [26].

Theorem 12. *The generalised Okamoto polynomials $\Omega_{m,n}(z)$ where m and n are non-negative integers have the Wronskian representation*

$$\Omega_{m,n}(z) = c_{m,n}\mathcal{W}\Big(\big\{\mathrm{He}_{1+3j}(z)\big\}_{j=0}^{m+n-2}\,;\,\big\{\mathrm{He}_{2+3j}(z)\big\}_{j=0}^{n-2}\Big),$$

where $c_{m,n}$ is defined in (2.3).

Theorem 13. *The generalised Okamoto polynomials $\Sigma_{m,n}(z)$ where m and n are non-negative integers have the Wronskian representation*

$$\Sigma_{m,n}(z) = c_{m,n}\mathcal{W}\Big(\big\{\mathrm{He}_{1+3j}(z)\big\}_{j=0}^{m-1}\,;\,\big\{\mathrm{He}_{2+3j}(z)\big\}_{j=0}^{m+n-1}\Big),$$

where $c_{m,n}$ is defined in (2.3).

Figures 2.3 and 2.5 respectively show the roots of $\Omega_{m,n}(z)$ and $\Sigma_{m,n}(z)$ in the complex plane. All of the plots in this chapter from Figure 2.3 onwards, exclude any roots at the origin. Clarkson observed that the roots of both polynomials form approximate equilateral triangle and rectangle structures in the complex plane. Figure 2.2 illustrates the structures observed by Clarkson. In this thesis, we use the term "blocks" to refer to structures formed by the roots of polynomials. The notation $A - C$, shown in Figure 2.2, refer to the different types of blocks formed by the roots of generalised Okamoto polynomials.

The blocks A–C illustrated in Figure 2.2 are as follows:

- Block A are equilateral triangles on the imaginary axis.
- Block B are equilateral triangles on the real axis.
- Block C is a rectangle that lies around the origin, and is of width c_1, height c_2, and size $c_1 \times c_2$.

Clarskon [22] investigated the roots of $\Omega_{m,n}(z)$ in the complex plane, and found that the roots form A blocks of size $n-1$, B blocks of size $m-1$, and C blocks

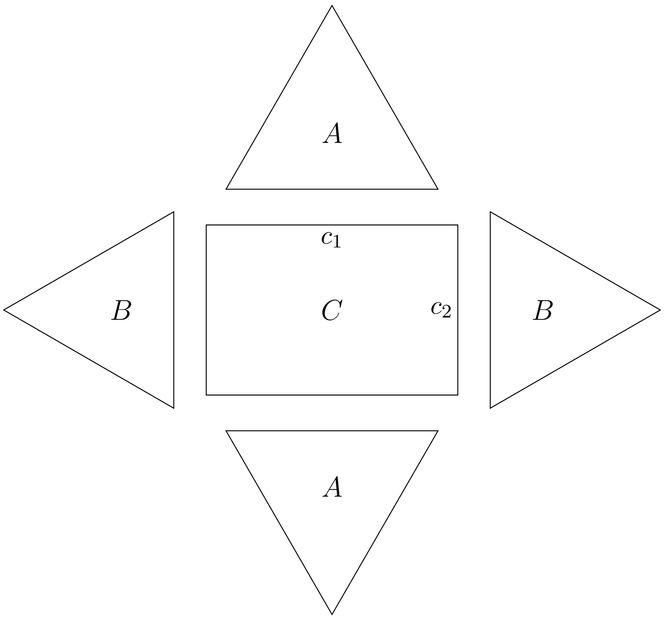

Figure 2.2: Blocks formed by roots of generalised Okamoto polynomials.

of size $n \times m$. A summary of the size of blocks formed by $\Omega_{m,n}(z)$ can be found in Table 2.5.

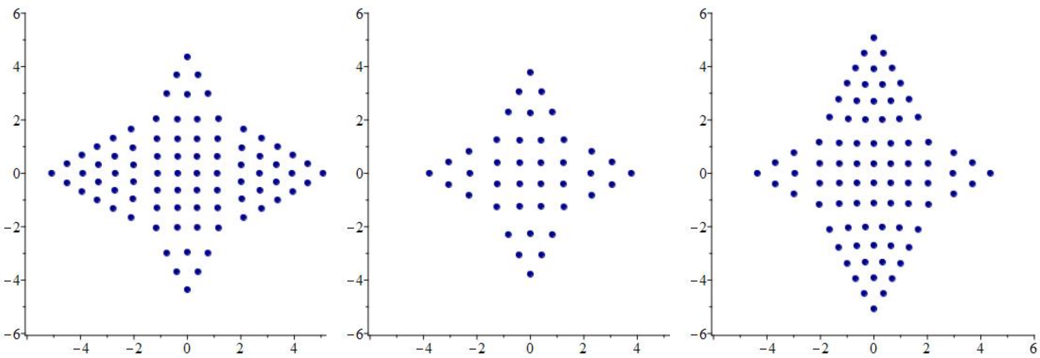

$\Omega_{7,4}(z)$ $\Omega_{4,4}(z)$ $\Omega_{4,7}(z)$

Figure 2.3: Plot of roots of $\Omega_{7,4}(z)$, $\Omega_{4,4}(z)$ and $\Omega_{4,7}(z)$.

Block	$\Omega_{m,n}(z)$
A	$(n-1)$-triangle
B	$(m-1)$-triangle
C	$n \times m$ rectangle

Table 2.5: Blocks formed by roots of $\Omega_{m,n}(z)$.

A comparison of Theorems 10 and 12 shows that

$$\Omega_{m,n}(z) = c_{m+n-1,n-1}\, Q_{m+n-1,n-1}(z). \tag{2.4}$$

To recap, the parameters m and n of $\Omega_{m,n}(z)$ are non-negative integers. It follows from (2.4) and Table 2.5, that the roots of $Q_{m,n}(z)$ when $m > n$, form the blocks found in Table 2.6. The plots in Figure 2.4 show examples of blocks formed by the roots of $Q_{m,n}(z)$ when $m > n$.

Block	$Q_{m,n}(z)$ with $m > n$
A	n-triangle
B	$(m-n-1)$-triangle
C	$(n+1) \times (m-n)$ rectangle

TABLE 2.6: Blocks formed by the roots of $Q_{m,n}(z)$ when $m > n$.

Figure 2.5 show the blocks formed by the roots of $\Sigma_{m,n}(z)$. Clarkson [26] found that the roots of $\Sigma_{m,n}(z)$ form the blocks found in Table 2.7.

Block	$\Sigma_{m,n}(z)$
A	m-triangle
B	n-triangle
C	$m \times n$ rectangle

TABLE 2.7: Blocks formed by roots of $\Sigma_{m,n}(z)$.

A comparison of Theorems 10 and 13 shows that

$$\Sigma_{m,n}(z) = c_{m,m+n} Q_{m,m+n}(z). \tag{2.5}$$

To recap, the parameters m and n of $\Sigma_{m,n}(z)$ are non-negative integers. It follows from (2.5) and Table 2.7, that the roots of $Q_{m,n}(z)$ when $n > m$, form the blocks found in Table 2.8. The plots in Figure 2.6 show examples of blocks formed by the roots of $Q_{m,n}(z)$ when $n > m$.

The plots in Figure 2.7 show the roots of generalised Okamoto polynomials $Q_{n,n}(z)$. Figure 2.7 shows that the roots of $Q_{n,n}(z)$ form A blocks of size n, and B and C

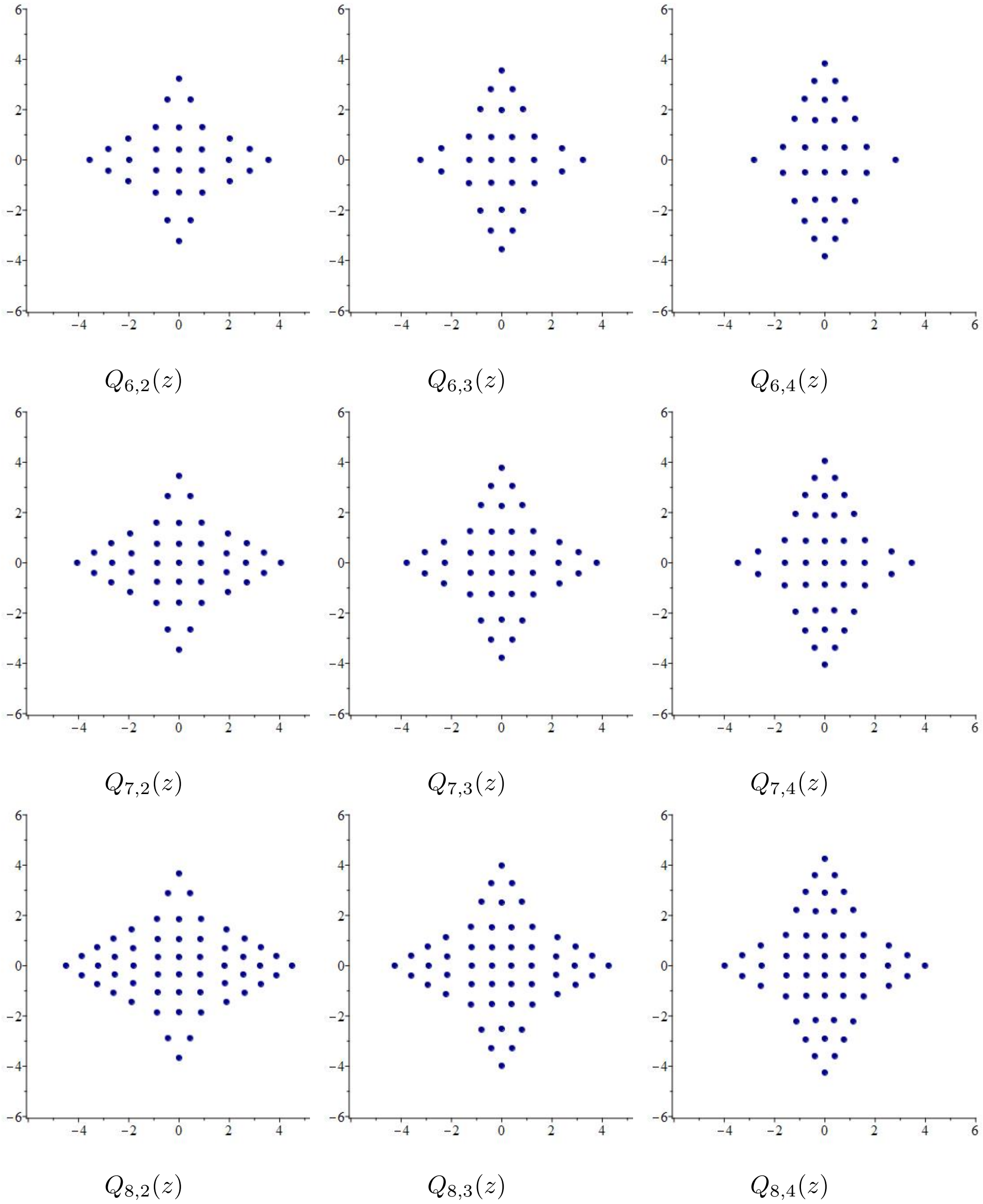

FIGURE 2.4: Plot of roots of $Q_{m,n}(z)$ with $m > n$.

Block	$Q_{m,n}(z)$ with $n > m$
A	m-triangle
B	$(n-m)$-triangle
C	$m \times (n-m)$ rectangle

TABLE 2.8: Blocks formed by the roots of $Q_{m,n}(z)$ when $n > m$.

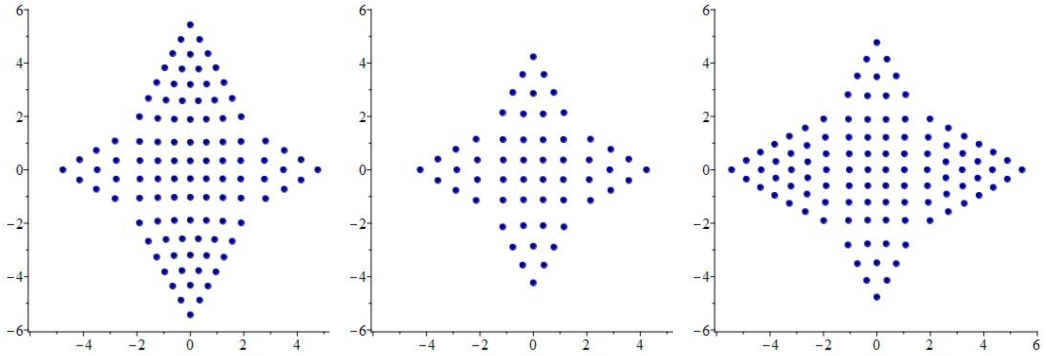

$\Sigma_{7,4}(z)$ $\Sigma_{4,4}(z)$ $\Sigma_{4,7}(z)$

FIGURE 2.5: Plot of roots of $\Sigma_{7,4}(z)$, $\Sigma_{4,4}(z)$ and $\Sigma_{4,7}(z)$.

blocks that are "empty", i.e. of size zero. A summary of the blocks formed by $Q_{n,n}(z)$ can be found in Table 2.9.

Block	$Q_{n,n}(z)$
A	n-triangle

TABLE 2.9: Blocks formed by the roots of $Q_{n,n}(z)$.

Table 2.10 gives a summary of the size of blocks $A-C$ formed by roots of $Q_{m,n}(z)$ for each parameter condition of m and n. A comparison of the results in Table

Block	when $m > n$	when $m = n$	when $m < n$
A	n	n	m
B	$m-n-1$		$n-m$
C	$(n+1)\times(m-n)$		$m\times(n-m)$

TABLE 2.10: Size of blocks formed by roots of $Q_{m,n}(z)$ when $m > n$, $m = n$ or $m < n$.

2.10 show that the size of block A is the smaller parameter out of m and n. By introducing the terms a and b, the results in Table 2.10 can be simplified. Let a denote the smaller parameter out of m and n, and let b denote the difference between the larger and smaller parameter out of m and n. By also introducing

$$\gamma = \begin{cases} 0 & \text{when } m < n \\ 1 & \text{when } m > n. \end{cases}$$

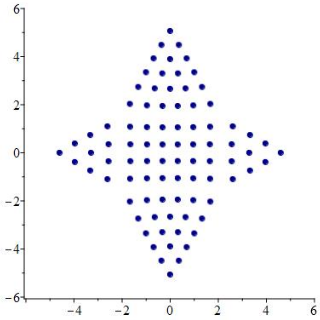

$Q_{6,10}(z)$ $Q_{6,11}(z)$ $Q_{6,12}(z)$

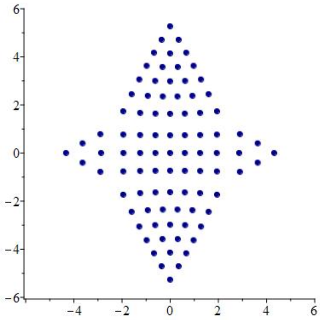

$Q_{7,10}(z)$ $Q_{7,11}(z)$ $Q_{7,12}(z)$

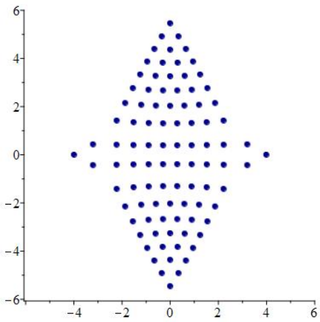

$Q_{8,10}(z)$ $Q_{8,11}(z)$ $Q_{8,12}(z)$

FIGURE 2.6: Plot of roots of $Q_{m,n}(z)$ with $n > m$.

we can simplify the results in Table 2.10 to Table 2.11. Note that when $a = 0$ block A is empty, and when $b = 0$, blocks B and C are empty.

Block	size of blocks formed by $Q_{m,n}(z)$
A	a
B	$b - \gamma$
C	$(a + \gamma) \times b$

TABLE 2.11: Size of blocks formed by roots of $Q_{m,n}(z)$.

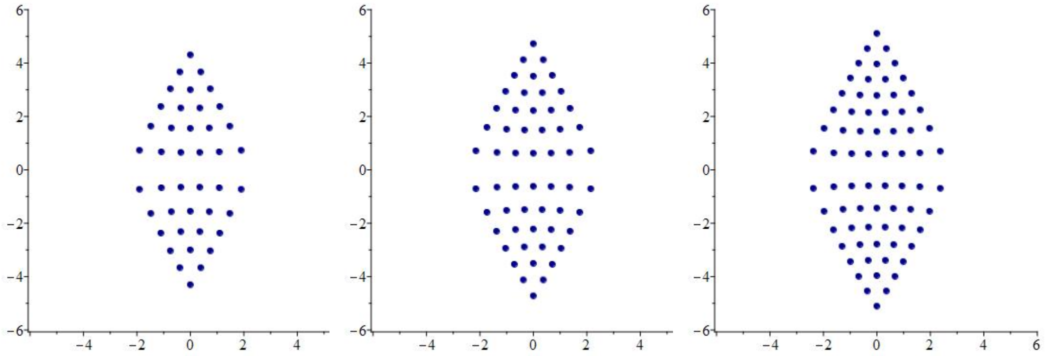

$Q_{6,6}(z)$ $Q_{7,7}(z)$ $Q_{8,8}(z)$

FIGURE 2.7: Plot of roots of $Q_{n,n}(z)$ for $n = 6, \ldots, 8$.

2.1 The partition λ associated with $Q_{m,n}(z)$

The generalised Okamoto polynomials are naturally associated with a family of partitions. The partitions associated with the generalised Okamoto polynomials $\Omega_{m,n}(z)$ and $\Sigma_{m,n}(z)$ can be found in [26]. The partitions associated with $Q_{m,n}$ can be derived from the partitions associated with $\Omega_{m,n}(z)$ and $\Sigma_{m,n}(z)$. The motivation for studying the partitions λ associated with $Q_{m,n}(z)$ is to explore how aspects of these partitions play a role in properties of $Q_{m,n}(z)$. In this section, we determine the explicit form of the partitions λ associated with $Q_{m,n}(z)$. We then use the explicit form of λ to find its conjugate partition λ^*. For convenience, we introduce the notation $\lambda_{m,n}$ to denote the partition λ associated with $Q_{m,n}(z)$, and the notation $\lambda^*_{m,n}$ to denote the conjugate of $\lambda_{m,n}$. Towards the end of this chapter, we determine the 2-cores and 2-quotients of $\lambda_{m,n}$.

2.1.1 The partition λ

As discussed in Chapter 1, the parts λ_j in the partition λ associated with the Wronskian $\mathcal{W}(f_{n_1}, f_{n_2}, \ldots, f_{n_\ell})$ are defined as

$$\lambda_j = n_j + j - \ell. \tag{2.6}$$

We are interested in the partition λ associated with

$$Q_{m,n}(z) = c_{m,n}\mathcal{W}\Big(\left\{\mathrm{He}_{1+3j}(z)\right\}_{j=0}^{m-1};\ \left\{\mathrm{He}_{2+3j}(z)\right\}_{j=0}^{n-1}\Big). \tag{2.7}$$

By the definition of λ, the associated degree vector of $\lambda_{m,n}$ is $n_\lambda = (n_1, n_2, \ldots, n_\ell)$, where $n_1, n_2, \ldots, n_\ell$ are the degrees of the Hermite polynomials in (2.7), ordered from large to small.

Theorem 14. *When parameters are equal*

$$\lambda_{n,n} = \left(\left\{(j)^2\right\}_{j=1}^{n}\right).$$

Proof. The generalised Okamoto polynomial

$$Q_{n,n}(z) = c_{n,n}\mathcal{W}\Big(\left\{\mathrm{He}_{1+3j}(z)\right\}_{j=0}^{n-1};\ \left\{\mathrm{He}_{2+3j}(z)\right\}_{j=0}^{n-1}\Big),$$

therefore, the degree vector associated with $\lambda_{n,n}$ is

$$n_\lambda = (3n-1, 3n-2, 3n-4, 3n-5, \ldots, 1).$$

It follows from (2.6) that

$$\lambda_{n,n} = \big(n, n, n-1, n-1, \ldots, 1, 1\big).$$

□

Theorem 15. *When $m > n$ the partition*

$$\lambda_{m,n} = \left(\left\{n-1+2j\right\}_{j=1}^{m-n};\ \left\{(j)^2\right\}_{j=1}^{n}\right).$$

Proof. When $m > n$ the degree vector associated with $\lambda_{m,n}$ is

$$n_\lambda = (3m-2, 3m-5, \ldots, 3n+1, 3n-1, 3n-2, 3n-4, \ldots, 1).$$

It follows from (2.6) that when $m > n$

$$\lambda_{m,n} = \big(2m-n-1, 2m-n-3, \dots, n+1, n, n, n-1, \dots, 1\big).$$

$\square$

Theorem 16. *When $n > m$ the partition*

$$\lambda_{m,n} = \left(\left\{m+2j\right\}_{j=1}^{n-m}; \left\{(j)^2\right\}_{j=1}^{m}\right).$$

Proof. When $n > m$ the degree vector associated with $\lambda_{m,n}$ is

$$n_\lambda = (3n-1, 3n-4, 3n-7, \dots, 3m+2, 3m-1, 3m-2, \dots, 1).$$

It follows from (2.6) that when $n > m$

$$\lambda_{m,n} = \big(2n-m, 2n-m-2, \dots, m+2, m, m, m-1, \dots, 1\big).$$

$\square$

A summary of the partitions $\lambda_{m,n}$ for all three parameter conditions of m and n can be found in Table 2.12.

case no.	condition	partition $\lambda_{m,n}$
1	$m > n$	$\left(\left\{n-1+2j\right\}_{j=1}^{m-n}; \left\{(j)^2\right\}_{j=1}^{n}\right)$
2	$m = n$	$\left(\left\{(j)^2\right\}_{j=1}^{n}\right)$
3	$m < n$	$\left(\left\{m+2j\right\}_{j=1}^{n-m}; \left\{(j)^2\right\}_{j=1}^{m}\right)$

TABLE 2.12: The partitions $\lambda_{m,n}$ for all three parameter conditions of m and n.

The partitions in Table 2.12 are unordered, since the upper limit of each sequence in Table 2.12 gives the largest term of the sequence, and the lower limit, i.e. $j = 1$ gives the smallest term of each sequence. A comparison of the results in Table

2.12 shows that all partitions contain "double" terms, i.e. terms of the form $(z)^2$, where z is a positive integer. When m and n are not equal, the partitions $\lambda_{m,n}$ also contain "single" terms, i.e. terms of the form z. A comparison of the sequences in Table 2.12 shows that the upper limit of the sequence of single terms can be described by the relative size of m and n. Similarly, each sequence in Table 2.12 can be expressed in terms of the relative size of m and n. By introducing the terms a, b and γ the partitions in Table 2.12 can be simplified to the following theorem.

Theorem 17. *The partition $\lambda_{m,n}$ for all parameter conditions of m and n is*

$$\lambda_{m,n} = \left(\left\{a - \gamma + 2j\right\}_{j=1}^{b}; \left\{(j)^2\right\}_{j=1}^{a}\right), \tag{2.8}$$

where a denotes the smaller parameter, b denotes the difference between the larger and smaller parameter out of m and n, and

$$\gamma = \begin{cases} 0 & \text{when } m < n \\ 1 & \text{when } m > n. \end{cases}$$

Our aim is to now determine the explicit form the conjugate partition $\lambda^*_{m,n}$ using the Young diagram of $\lambda_{m,n}$. Earlier we discussed that $\lambda_{m,n}$ consists of single and double terms when m and n are not equal (see Table 2.12). This tells us that the Young diagrams of $\lambda_{m,n}$, when m and n are not equal, will consist of single rows, i.e. consecutive rows that are of different length, and double rows, i.e. two consecutive rows of the same length.

Remark 7. It follows from (2.8) that when m and n are not equal, the Young diagram of $\lambda_{m,n}$ consists of b single rows and a sets of double rows. When m and n are not equal, row b of the Young diagram of $\lambda_{m,n}$ is simply the shortest single row of the diagram. It follows from (2.8) that the difference in length between row b and row $b+1$, is one when $m > n$, and two when $n > m$. When $m > n$, we call $Q_{m,n}(z)$ a case 1 polynomial, and when $n > m$ we call $Q_{m,n}(z)$ a case 2 polynomial.

Figure 2.8 shows examples of $\lambda_{m,n}$ and the Young diagram of $\lambda_{m,n}$ when m and n are not equal. Figures 2.9 and 2.10 show the general form of the Young diagram of $\lambda_{m,n}$ when $m > n$ and $n > m$, respectively. The coloured boxes in row b of the diagrams highlight the difference in length between row b and row $b+1$.

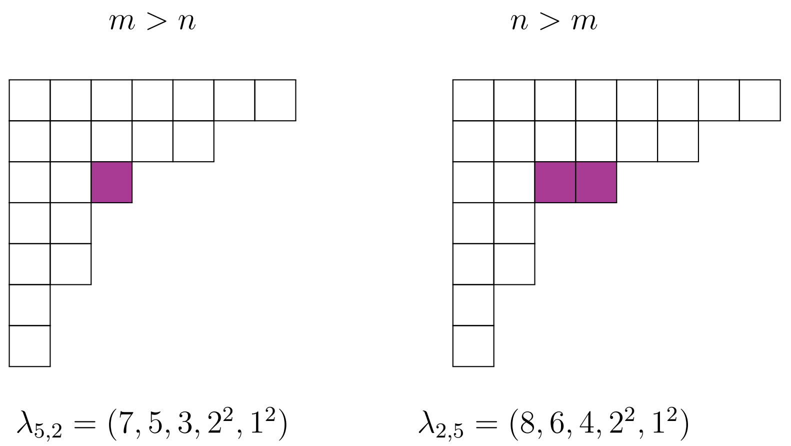

FIGURE 2.8: Examples of $\lambda_{m,n}$ and the Young diagram of $\lambda_{m,n}$ when m and n are not equal. Row b of the Young digram of $\lambda_{m,n}$, when $m > n$ or $n > m$ is the shortest single row of the diagram. Row b of each diagram in this figure contain purple coloured boxes to highlight the difference in length between row b and row $b+1$.

If the Young diagram of $\lambda_{m,n}(z)$ consists of single and double rows it follows from Remark 7, that the parameters m and n are not equal. The parameters m and n can be found by first determining the terms a and b. The term b is the number of single rows in the Young diagram, and the term $2a$ is the number of rows that form double rows in the Young diagram. To recap, a denotes the smaller parameter our of m and n, and b denotes the difference between the larger and smaller parameter out of m and n. Table 2.13 can be used as a criteria to determine the parameter condition of m and n.

Remark 8. It follows from (2.8) that the Young diagram of $\lambda_{n,n}$ consists of n "sets" of double rows, i.e. $2n$ rows that form double rows, and no single rows. Therefore, the total number of rows in the Young diagram of $\lambda_{n,n}$ is $2n$.

Figure 2.11 shows the general form of the Young diagram of $\lambda_{n,n}$.

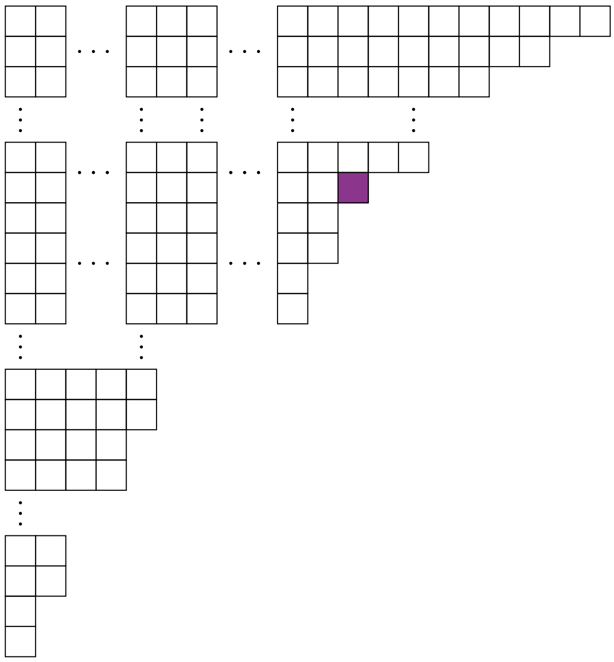

FIGURE 2.9: The Young diagram of $\lambda_{m,n}$ when $m > n$. Row b of this Young diagram is the shortest single row of the diagram. Row b contains a purple coloured box to highlight the difference in length between row b and row $b + 1$.

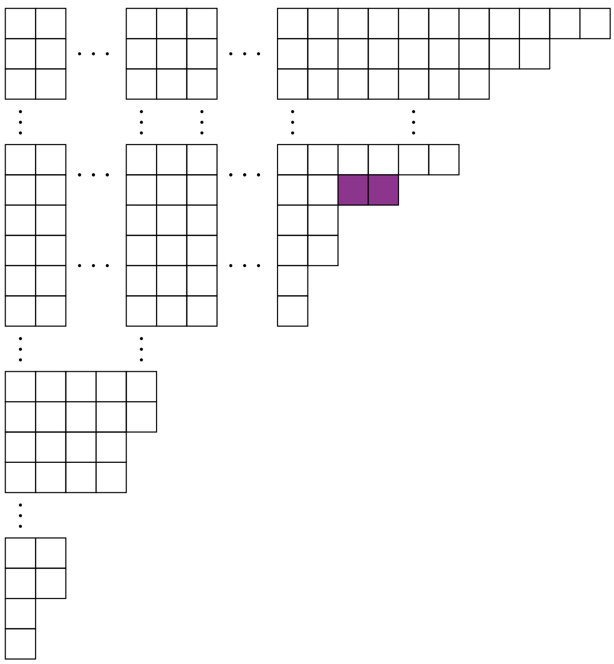

FIGURE 2.10: The Young diagram of $\lambda_{m,n}$ when $n > m$. Row b of this Young diagram is the shortest single row of the diagram. Row b contains purple coloured boxes to highlight the difference in length between row b and row $b + 1$.

case no	condition	row b and $b+1$
1	$m > n$	1
3	$n > m$	2

TABLE 2.13: Difference in length between row b and $b+1$ of the Young diagram of $\lambda_{m,n}$. When m and n are not equal, row b of the Young diagram of $\lambda_{m,n}$ is the shortest single row of the Young diagram.

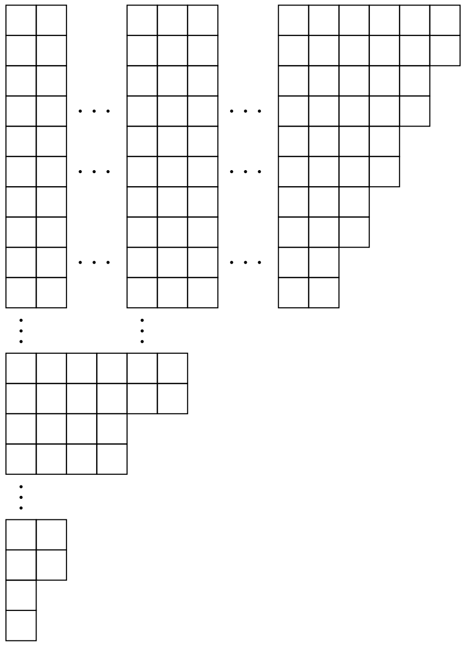

FIGURE 2.11: The Young diagram of $\lambda_{n,n}$. This Young diagram consists of $2n$ rows.

2.1.2 The conjugate of λ

We have determined the explicit form of the partitions $\lambda_{m,n}$ and the general form of the Young diagram of $\lambda_{m,n}$. Our aim is to now determine the explicit form of the conjugate partition of $\lambda_{m,n}$.

Theorem 18. *The conjugate partition of $\lambda_{n,n}$ is*

$$\lambda^*_{n,n} = \left(\left\{2n - 2j + 2\right\}_{j=1}^{n}\right).$$

Proof. Figure 2.11 shows the general form of the Young diagram of $\lambda_{n,n}$. The first column of this Young diagram is of length $2n$. The second column is of length $2n-2$, the third column is of length $2n-4$ and so on. Therefore, the conjugate partition of $\lambda_{n,n}$ is

$$\lambda^*_{n,n} = (2n, 2n-2, 2n-4, \ldots, 2).$$

□

Theorem 19. *The conjugate partition of $\lambda_{m,n}$ when $m > n$ is*

$$\lambda^*_{m,n} = \left(\left\{m+n-2j+2\right\}_{j=1}^{n+1}; \left\{(j)^2\right\}_{j=1}^{m-n-1}\right).$$

Proof. When $m > n$ the partition

$$\lambda_{m,n} = \left(\left\{n-1+2j\right\}_{j=1}^{m-n}; \left\{(j)^2\right\}_{j=1}^{n}\right). \tag{2.9}$$

The general form of the Young diagram of $\lambda_{m,n}$ when $m > n$, can be found in Figure 2.9. The row containing the purple coloured box in Figure 2.9 is row b of the Young diagram. This row is of length $n+1$. As a result, the Young diagram of $\lambda^*_{m,n}$ when $m > n$, contains a column of length $n+1$. Figure 2.12 shows the Young diagram of $\lambda^*_{m,n}$ when $m > n$. The box outlined in purple indicates the position of the purple coloured box in Figure 2.9.

Figure 2.12 shows that the Young diagram of $\lambda^*_{m,n}$ when $m > n$, consists of $n+1$ single rows. It follows from (2.9) that the first column of the Young diagram of $\lambda_{m,n}$ is of length $m+n$. Therefore, the first row in Figure 2.12 is of length $m+n$. Figure 2.12 shows that consecutive single rows decrease in length by two. This mean the single rows in the Young diagram of $\lambda^*_{m,n}$ when $m > n$, are of length

$$m+n-2j+2, \quad j = 1, 2, \ldots, n+1.$$

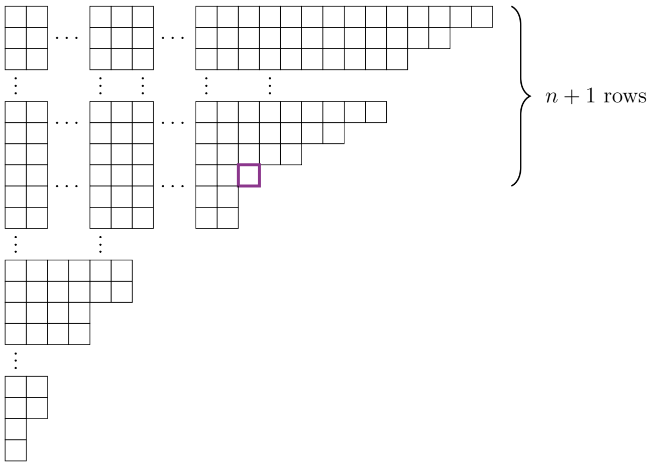

Figure 2.12: The Young diagram of $\lambda^*_{m,n}$ when $m > n$.

It follows from (2.9) that the first row of the Young diagram of $\lambda_{m,n}$ when $m > n$ is of length $2m - n + 1$. Hence, the first column of the Young diagram $\lambda^*_{m,n}$ in Figure 2.12 is of length $2m - n + 1$. Figure 2.12 shows that the Young diagram of $\lambda^*_{m,n}$ consists of single and double rows. We can see that there are $n + 1$ single rows in the diagram, therefore, the remaining $2(m - n - 1)$ rows of the diagram form double rows.

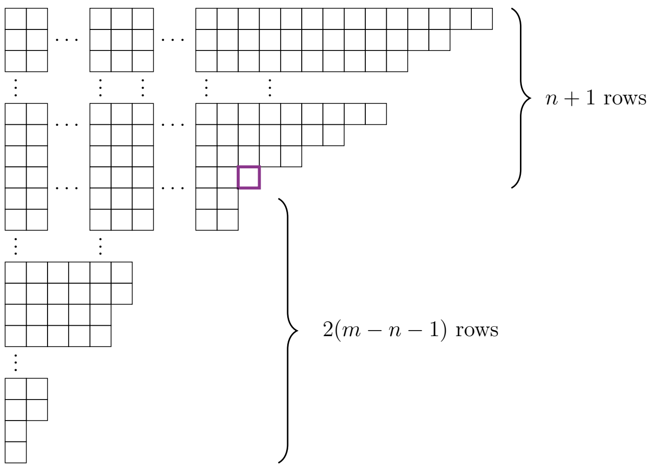

Figure 2.13: The Young diagram of $\lambda^*_{m,n}$ when $m > n$ with brackets indicating the number of rows in the diagram.

Figure 2.13 also shows that consecutive double rows decrease in length by one, and that the shortest double row of the diagram is of length one. Therefore, the rows that form double rows in the Young diagram of $\lambda_{m,n}$ when $m > n$, are of length

$$(j)^2, \quad j = 1, \ldots, m - n - 1.$$

□

Theorem 20. *The conjugate partition of $\lambda_{m,n}$ when $n > m$ is*

$$\lambda^*_{m,n} = \left(\left\{m + n - 2j + 2\right\}_{j=1}^{m} ; \left\{(j)^2\right\}_{j=1}^{n-m}\right).$$

Proof. When $n > m$ the partition

$$\lambda_{m,n} = \left(\left\{m + 2j\right\}_{j=1}^{n-m} ; \left\{(j)^2\right\}_{j=1}^{m}\right). \tag{2.10}$$

Figure 2.10 shows the general form of the Young diagram of $\lambda_{m,n}$ when $n > m$. It follows from (2.10) that the first row of the Young diagram in Figure 2.10 is of length $2n - m$, and the length of row b of the diagram is $m + 2$. The row containing the purple coloured boxes in Figure 2.10 is row b of the Young diagram. Figure 2.14 shows the Young diagram of $\lambda^*_{m,n}$ when $n > m$. The boxes outlined in purple indicates the position of the purple coloured boxes in Figure 2.10.

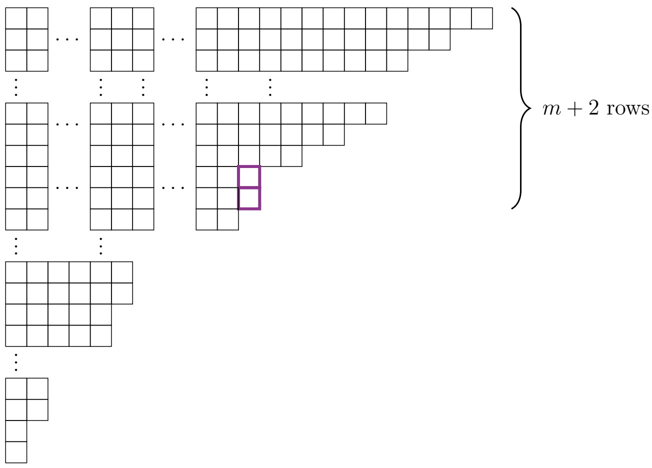

FIGURE 2.14: The Young diagram of $\lambda^*_{m,n}$ when $n > m$.

Figure 2.14 shows that the rows that contain a box outlined in purple, form double rows i.e two consecutive rows of the same length. Therefore, the Young diagram in Figure 2.14 consists of m single rows. The longest single row in Figure 2.14 is of length $m+n$ and consecutive single rows decrease in length by two. Hence, Figure 2.14 shows that the Young diagram of $\lambda^*_{m,n}$ when $n > m$, consists of single rows of length

$$m+n-2j+2, \quad j = 1, 2, \ldots, m.$$

It follows from (2.14) that the first column of the Young diagram of λ^* in Figure 2.14 is of length $2n-m$. Figure 2.14 shows that the Young diagram consists of m single rows. This means the remaining $2(n-m)$ rows form double rows.

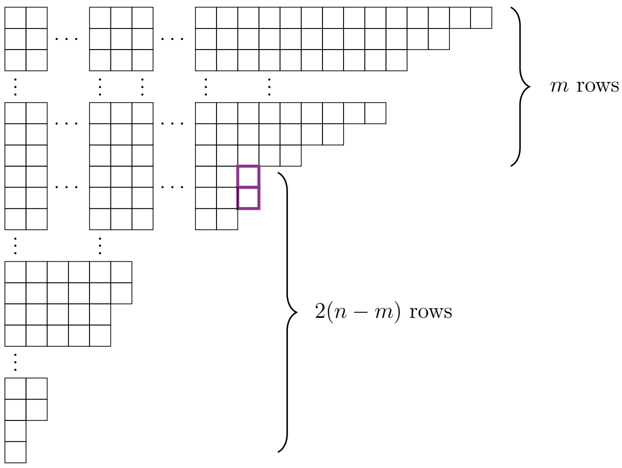

FIGURE 2.15: The Young diagram of $\lambda^*_{m,n}$ when $n > m$ with brackets indicating the number of rows in the diagram.

Figure 2.15 shows that consecutive double rows decrease in length by one. Therefore, the Young diagram of $\lambda^*_{m,n}$ when $n > m$ consists of double rows of length

$$(j)^2, \quad j = 1, 2, \ldots, n-m.$$

$\square$

A summary of the conjugate partitions $\lambda^*_{m,n}(z)$ can be found in Table 2.14.

case no.	condition	partition $\lambda^*_{m,n}$
1	$m > n$	$\left(\left\{m+n-2j+2\right\}_{j=1}^{n+1};\left\{(j)^2\right\}_{j=1}^{m-n-1}\right)$
2	$m = n$	$\left(\left\{2n-2j+2\right\}_{j=1}^{n}\right)$
3	$m < n$	$\left(\left\{m+n-2j+2\right\}_{j=1}^{m};\left\{(j)^2\right\}_{j=1}^{n-m}\right)$

TABLE 2.14: The partitions $\lambda^*_{m,n}$ for all three parameter conditions of m and n.

2.1.3 The 2-core of λ

The explicit form of the partition $\lambda^*_{m,n}$ for all parameter conditions of m and n are given in Table 2.14. In Chapter 1, we discussed how to determine the 2-core of λ using the 2-runner abacus display of λ. In order to find the 2-runner abacus display of λ we require the Maya diagram of λ.

The Maya diagram diagram of $\lambda_{m,n}$ can be found by placing beads and empty beads along the border of the Young diagram of $\lambda_{m,n}$. The Maya diagram of $\lambda_{m,n}$ will consist of empty beads in position $0+3j$, and beads in position $1+3j$ and $2+3j$. If we arrange the Maya digram of $\lambda_{m,n}$, from left to right, onto three runners, we get the abacus display shown in Figure 2.16. The first runner in Figure 2.16 contains no beads, the second runner contains m beads, and the third runner contains n beads. Figure 2.16 shows that every bead in the 3-runner abacus display $\lambda_{m,n}$ has a bead directly above it. Therefore, $\lambda_{m,n}$ is a 3-core partition for all parameters of m and n.

Theorem 21. *When m is odd the 2-core of $\lambda_{m,n}$ is*

$$\delta = \begin{cases} \emptyset & \text{when } n \text{ is odd} \\ (1) & \text{when } n \text{ is even.} \end{cases}$$

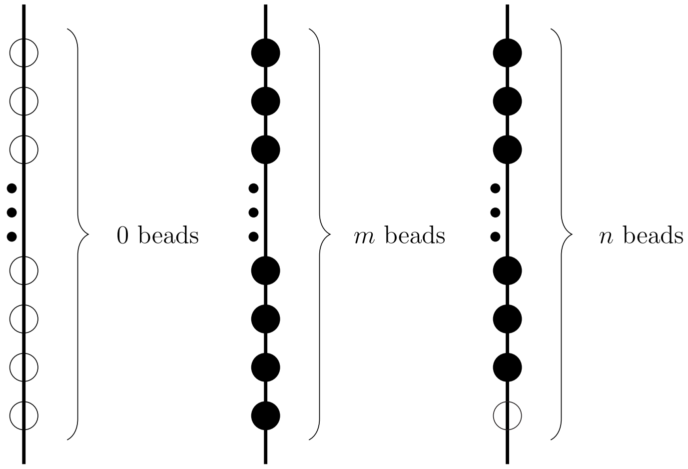

FIGURE 2.16: The 3-runner abacus display of $\lambda_{m,n}$.

Proof. Figure 2.17 shows the 2-runner abacus display of $\lambda_{m,n}$, when m and n are odd, and $m > n$. Both runners in Figure 2.17 contain the same number of beads. Therefore, if we push all the beads up as far as they can go, we find that no beads appear after the first empty bead of the abacus display. Hence, when m and n are odd and $m > n$, the 2-core of $\lambda_{m,n}$ is the empty set.

Figure 2.18 shows the 2-runner abacus display of $\lambda_{m,n}$ when m and n are odd and $n > m$. Since the number of beads in each runner is the same, the 2-core is the empty set.

Figure 2.19 shows the 2-runner abacus display of $\lambda_{n,n}$. As the number of beads in both runners is the same it means the 2-core of $\lambda_{n,n}$ is the empty set. Therefore, when m and n are odd and $m = n$, the 2-core is the empty set.

Figures 2.20 and 2.21 show the 2-runner abacus display of $\lambda_{m,n}$, when m is odd and n is even. The second runner in both figures contain one more bead than the first runner of the figure. Therefore, it follows from Figures 2.20 and 2.21 that a bead appears after the first empty bead of the abacus display. Hence, the 2-core of $\lambda_{m,n}$, when m is odd and n is even, is (1).

□

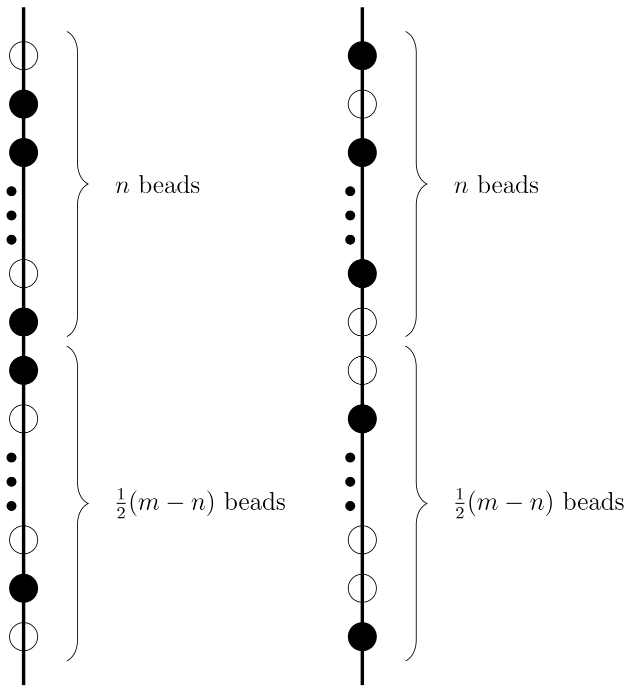

FIGURE 2.17: The 2-runner abacus display of $\lambda_{m,n}$ when m and n are odd with $m > n$.

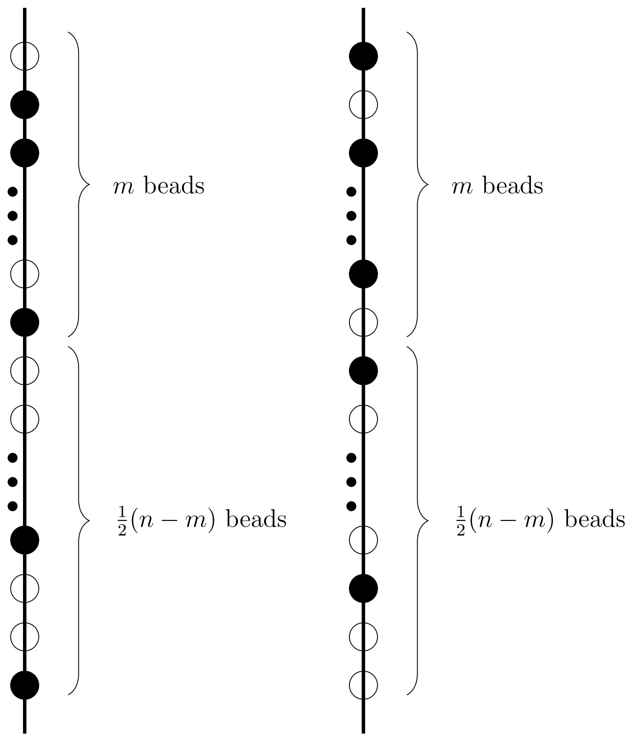

FIGURE 2.18: The 2-runner abacus display of $\lambda_{m,n}$ when m and n are odd and $n > m$.

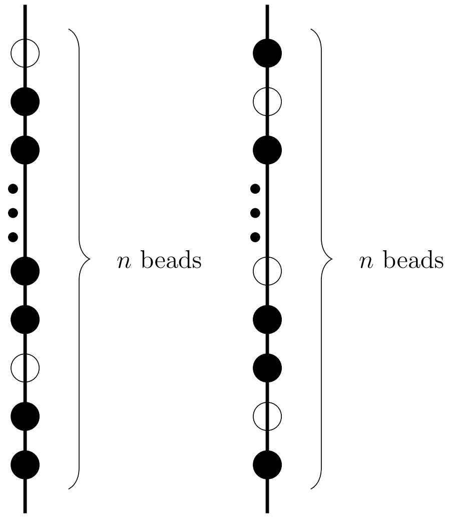

FIGURE 2.19: The 2-runner abacus display of $\lambda_{n,n}$.

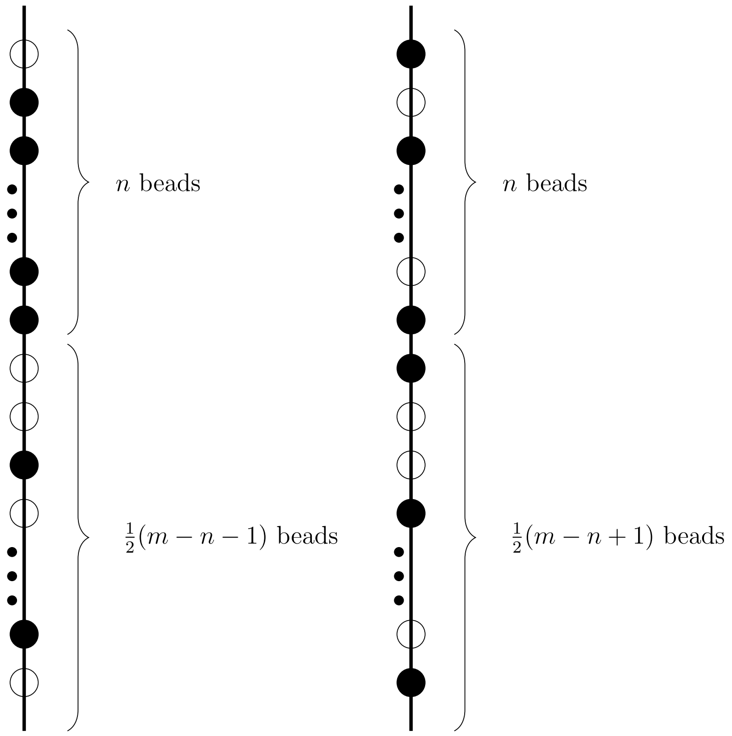

FIGURE 2.20: The 2-runner abacus display of $\lambda_{m,n}$ when m is odd, n is even and $m > n$.

Theorem 22. *When m is even the 2-core of $\lambda_{m,n}$ is the empty set.*

Proof. Similar to the proof of Theorem 21. $\square$

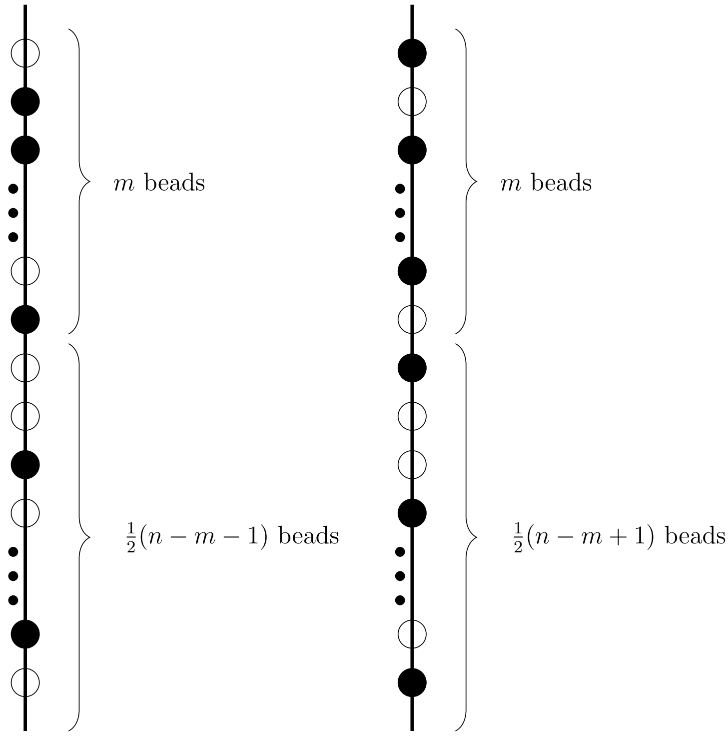

FIGURE 2.21: The 2-runner abacus display of $\lambda_{m,n}$ when m is odd, n is even and $n > m$.

2.1.4 The 2-quotient of λ

The 2-quotient (μ, ν) of a partition λ can found by making a note of how many places beads in the first and second runner of the 2-runner abacus display of λ are pushed up by, to form the 2-runner abacus display of the 2-core of λ. Interestingly, we found that whether parameters are odd or even effects the 2-cores of $\lambda_{m,n}$.

Theorem 23. *The 2-quotient (μ, ν) of $\lambda_{2n,2n}$ is*

$$\mu = \big(n^2,\, (n-1)^2,\, (n-2)^2, \ldots, (1)^2\big),$$

$$\nu = \big(n,\, (n-1)^2,\, (n-2)^2, \ldots, (1)^2\big).$$

Proof. Figure 2.22 shows the 2-runner abacus display of $\lambda_{2n,2n}$. All $2n$ beads in the first runner shown in Figure 2.22, need to be pushed up to form the abacus display of the 2-core. Figure 2.22 shows that $2j$ th and the $2j-1$ th beads need to be pushed up by j places. Therefore, the partition μ in the 2-quotient of $\lambda_{2n,2n}$ is

$$\mu = \big(n^2, (n-1)^2, (n-2)^2, \dots, 1^2\big).$$

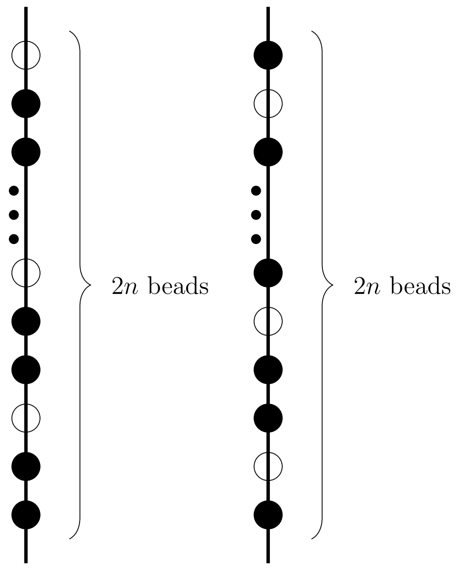

FIGURE 2.22: The 2-runner abacus display of $\lambda_{2n,2n}$.

The second runner in Figure 2.22 contains $2n-1$ beads that need to be pushed up. The $2j$ th and $2j+1$ th beads in this runner need to be pushed up by j places to produce the abacus display of the 2-core. This means the last bead i.e. the $2n$ th bead of the display needs to be pushed up by n places. The $2n-2$ th and $2n-1$ th bead need to be pushed up by $n-1$ places, and so on. Hence, the partition ν in the 2-quotient of $\lambda_{2n,2n}$ is

$$\nu = \big(n, (n-1)^2, (n-2)^2, \dots, 1^2\big).$$

□

Theorem 24. *The 2-quotient* (μ,ν) *of* $\lambda_{2n+1,2n+1}(z)$ *is*

$$\mu = \big(n+1,\, n^2,\, (n-1)^2,\, \ldots, (1)^2\,\big),$$

$$\nu = \big(\,n^2, (n-1)^2, (n-2)^2, \ldots, (1)^2\,\big).$$

Proof. The first runner in Figure 2.23 shows that the $2j-1$ th and $2j$ th beads need to be pushed up by j places to form the abacus display of the 2-core. This means the last bead i.e. the $2n+1$ th bead needs to be pushed by $n+1$ places. The $2n$ th and $2n-1$ th bead need to pushed up by n places, and so on. Therefore, the partition μ in the 2-quotient of $\lambda_{2n+1,2n+1}$ is

$$\mu = \big(n+1, n^2, (n-1)^2, \ldots, 1^2\big).$$

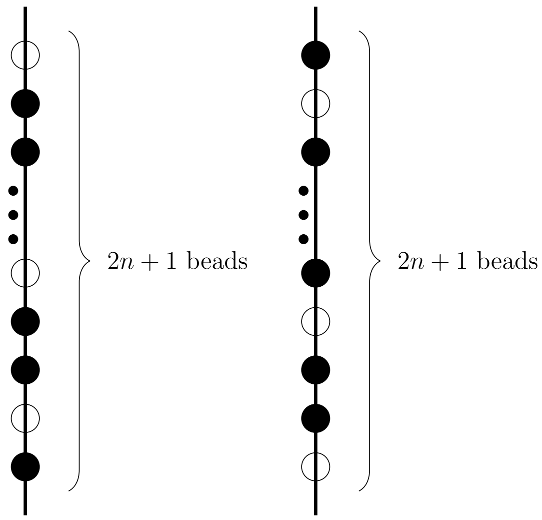

FIGURE 2.23: The 2-runner abacus display of $\lambda_{2n+1,2n+1}$.

The second runner in Figure 2.23 shows that the $2j$ th and $2j+1$ th beads need to be pushed up by j places. Therefore, the partition ν in the 2-quotient of $\lambda_{2n+1,2n+1}$ is

$$\nu = \big(n^2, (n-1)^2, (n-2)^2, \ldots, 1^2\big).$$

□

Theorem 25. *The 2-quotients of $\lambda_{m,n}$ can be found in Tables 2.15 and 2.16. The 2-quotients in both tables are ordered.*

polynomial	partition μ	partition ν
$Q_{2m,2n}(z)$	$\left(\{m+2j-1\}_{j=1}^{n-m};\{(j)^2\}_{j=1}^{m}\right)$	$\left(\{m+2j-2\}_{j=1}^{n-m+1};\{(j)^2\}_{j=1}^{m-1}\right)$
$Q_{2m,2n+1}(z)$	$\left(\{m+2j-2\}_{j=1}^{n-m+1};\{(j)^2\}_{j=1}^{m-1}\right)$	$\left(\{m+2j-1\}_{j=1}^{n-m+1};\{(j)^2\}_{j=1}^{m}\right)$
$Q_{2m+1,2n+1}(z)$	$\left(\{m+2j-1\}_{j=1}^{n-m+1};\{(j)^2\}_{j=1}^{m}\right)$	$\left(\{m+2j-1\}_{j=1}^{n-m};\{(j)^2\}_{j=1}^{m}\right)$
$Q_{2m+1,2n}(z)$	$\left(\{m+2j-1\}_{j=1}^{n-m};\{(j)^2\}_{j=1}^{m}\right)$	$\left(\{m+2j-1\}_{j=1}^{n-m};\{(j)^2\}_{j=1}^{m}\right)$

TABLE 2.15: The 2-quotients of $\lambda_{m,n}$ when $n \geq m$.

polynomial	partition μ	partition ν
$Q_{2m,2n}(z)$	$\left(\{n+2j\}_{j=1}^{m-n};\{(j)^2\}_{j=1}^{n}\right)$	$\left(\{n+2j\}_{j=1}^{m-n-1};\{(j)^2\}_{j=1}^{n}\right)$
$Q_{2m,2n+1}(z)$	$\left(\{n+2j\}_{j=1}^{m-n-1};\{(j)^2\}_{j=1}^{n}\right)$	$\left(\{n+2j+1\}_{j=1}^{m-n-1};\{(j)^2\}_{j=1}^{n+1}\right)$
$Q_{2m+1,2n+1}(z)$	$\left(\{n+2j+1\}_{j=1}^{m-n-1};\{(j)^2\}_{j=1}^{n+1}\right)$	$\left(\{n+2j\}_{j=1}^{m-n};\{(j)^2\}_{j=1}^{n}\right)$
$Q_{2m+1,2n}(z)$	$\left(\{n+2j\}_{j=1}^{m-n};\{(j)^2\}_{j=1}^{n}\right)$	$\left(\{n+2j\}_{j=1}^{m-n};\{(j)^2\}_{j=1}^{n}\right)$

TABLE 2.16: The 2-quotients of $\lambda_{m,n}$ when $m > n$.

Proof. Similar to the proof of Theorems 23 and 24. □

2.2 The $R_{m,n}(z)$ polynomials

It is known that the Wronskian of Hermite polynomials $\mathcal{P}_\lambda(z)$ satisfies

$$\mathcal{P}_\lambda(z) = \mathrm{i}^d\, \mathcal{P}_{\lambda^*}(-\mathrm{i}z), \tag{2.11}$$

where d is the degree of $\mathcal{P}_\lambda(z)$. The polynomial $\mathcal{P}_\lambda(z)$ is associated with the partition λ, and the polynomial $\mathcal{P}_{\lambda^*}(z)$ is associated with the conjugate of λ. It follows from (2.11) that the generalised Okamoto polynomials

$$Q_{m,n}(z) = \mathrm{i}^d\, Q_{s,t}(-\mathrm{i}z), \tag{2.12}$$

where d is defined in (2.1), and s and t are positive integers, such that $\lambda^*_{m,n} = \lambda_{s,t}$. For convenience, we introduce the polynomials $R_{m,n}(z)$ defined in the following definition.

Definition 28. Define $R_{m,n}(z)$ as

$$R_{m,n}(z) = \mathrm{i}^d\, c_{m,n}\mathcal{W}\Big(\big\{\mathrm{He}_{1+3j}(-\mathrm{i}z)\big\}_{j=0}^{m-1}\,;\,\big\{\mathrm{He}_{2+3j}(-\mathrm{i}z)\big\}_{j=0}^{n-1}\Big),$$

where $c_{m,n}$ is defined in (2.3) and d is defined in (2.1) .

It follows form (2.12) that there exists positive s and t, such that

$$Q_{m,n}(z) = R_{s,t}(z).$$

Our aim is to find the polynomials $R_{s,t}(z)$ using the partitions $\lambda^*_{m,n}$. The motivation for studying the $R_{m,n}(z)$ polynomials, is to check the blocks formed by the roots of $Q_{m,n}(z)$. Since the roots of $R_{m,n}(z)$ are the negative conjugate of the roots of $Q_{m,n}(z)$, there is a 90 degree rotation between the blocks formed by the roots of both polynomials. Figure 2.2 shows an illustration of the blocks $A - C$ formed by the roots of generalised Okamoto polynomials. Figure 2.24 shows how the blocks in Figure 2.2 look after a 90 degree rotation.

We are interested in the polynomials $R_{s,u}(z)$ equal to $Q_{m,n}(z)$. By Definition 28, the polynomials

$$R_{s,u}(z) = \mathrm{i}^{\mathrm{d}}Q_{s,t}(-\mathrm{i}z).$$

Therefore, we can check the blocks formed by the roots of $Q_{m,n}(z)$, by checking if there is a 90 degree rotation between the blocks formed by the roots of $Q_{m,n}(z)$ and the blocks formed by the roots of $Q_{s,t}(z)$. We can find the blocks formed by the roots of $Q_{s,t}(z)$ by considering the parameter condition of s and t.

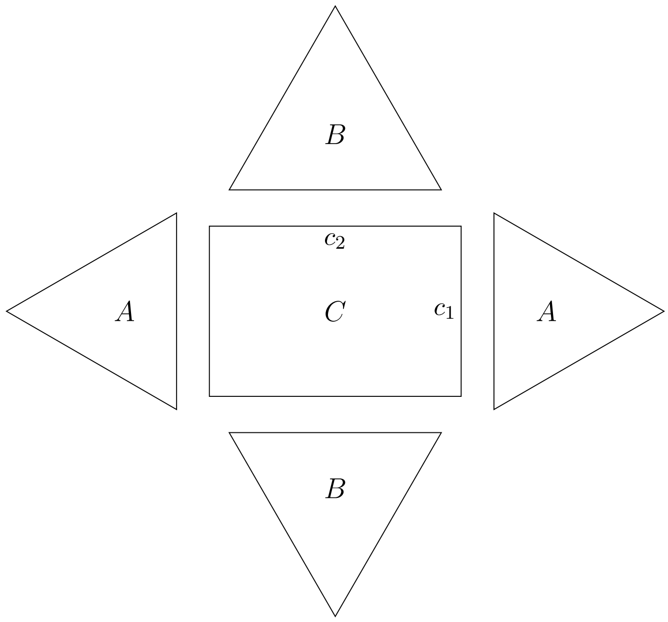

FIGURE 2.24: A 90 degree rotation of the blocks formed by roots of generalised Okamoto polynomials, shown in Figure 2.2.

Theorem 26. *When $m > n$ the polynomials $Q_{m,n}(z)$ and $R_{m,\,m-n-1}(z)$ are equal.*

Proof. When $m > n$ the partition

$$\lambda^*_{m,n} = \left(\left\{m + n - 2j + 2\right\}_{j=1}^{n+1}; \left\{(j)^2\right\}_{j=1}^{m-n-1}\right).$$

Figure 2.25 shows the general form of the Young diagram of $\lambda^*_{m,n}$ when $m > n$. Since the Young diagram in Figure 2.25 consists of single and double terms, it follows from Remark 7, that the parameters s and t are not equal. Figure 2.25 consists of $n + 1$ single rows and $m - n - 1$ sets of double rows. This means $b = n+1$ and $a = m-n-1$ of $R_{s,t}(z)$. This tells us that the parameters of $R_{s,t}(z)$ are m and $m - n - 1$. Row b of the Young diagram in Figure 2.25 is the $n + 1$ th row of the diagram. Figure 2.25 shows that the difference in length between row b and row $b + 1$ is one. This means $R_{s,t}(z)$ is a case 1 polynomial when $m > n$. Therefore, the polynomial associated with $\lambda^*_{m,n}$ when $m > n$, is $R_{m,\,m-n-1}(z)$.

□

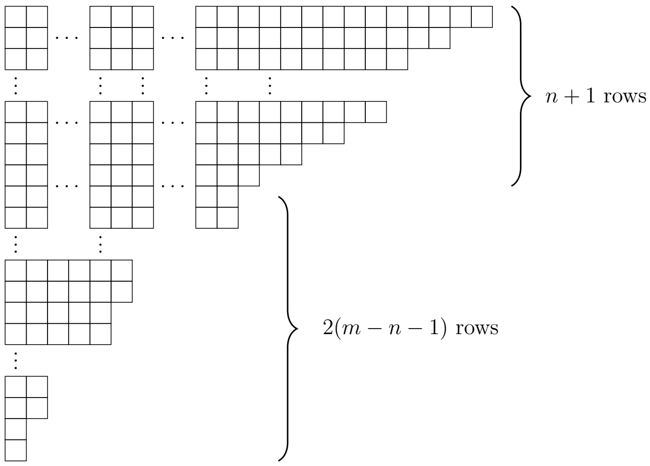

FIGURE 2.25: The Young diagram of $\lambda^*_{m,n}$ when $m > n$ with brackets indicating the number of rows in the diagram.

Suppose we want to check the results in Table 2.17. We have proven that when $Q_{m,n}(z)$ when $m > n$, i.e. when $Q_{m,n}(z)$ is a case 1 polynomial, it is equal to the case 1 polynomial, $R_{m,\,m-n-1}(z)$. It follows from the results in Table 2.17 that the roots of $Q_{m,\,m-n-1}(z)$ form the blocks found in Table 2.18. A comparison of the blocks in Tables 2.17 and 2.18 shows a 90 degree rotation between the blocks formed by the roots of $Q_{m,n}(z)$ and $Q_{m,\,m-n-1}(z)$, when $m > n$, as expected.

Block	$Q_{m,n}(z)$ with $m > n$
A	n-triangle
B	$(m-n-1)$-triangle
C	$(n+1)\times(m-n)$ rectangle

TABLE 2.17: Blocks formed by the roots of $Q_{m,n}(z)$ when $m > n$.

Block	$Q_{m,\,m-n-1}(z)$ with $m > n$
A	$(m-n-1)$-triangle
B	n-triangle
C	$(m-n)\times(n+1)$ rectangle

TABLE 2.18: Blocks formed by the roots of $Q_{m,\,m-n-1}(z)$ when $m > n$.

Theorem 27. *When $n > m$ the polynomials $Q_{m,n}(z)$ and $R_{n-m,\,n}(z)$ are equal.*

Proof. When $n > m$ the partition

$$\lambda^*_{m,n} = \left(\left\{ m + n - 2j + 2 \right\}_{j=1}^{m} ; \left\{ (j)^2 \right\}_{j=1}^{n-m} \right).$$

The general form of the Young diagram of $\lambda^*_{m,n}$ when $n > m$ can be found in Figure 2.15. The Young diagram of $\lambda^*_{m,n}$ when $n > m$, consists of m single rows and $n - m$ sets of double rows. Therefore, it follows from (2.9) that $b = m$ and $a = n - m$ of $R_{s,t}(z)$, when $n > m$. This tells us that the parameters of $R_{s,t}(z)$ are n and $n - m$. Row b of the Young diagram in Figure 2.15 is the m th row of the diagram. Figure 2.15 shows that the difference in length between row b and row $b + 1$ is two. Therefore, $R_{s,t}(z)$ is a case 3 polynomial, when $n > m$. Hence, the polynomial associated with $\lambda^*_{m,n}$ when $n > m$, is $R_{n-m,n}(z)$. □

Table 2.19 shows that there is a 90 degree rotation between the blocks formed by the roots of $Q_{m,n}(z)$ and $Q_{n-m,n}(z)$, when $n > m$.

Block	$Q_{m,n}(z)$ with $n > m$	$Q_{n-m,n}(z)$ with $n > m$
A	m-triangle	$(n - m)$-triangle
B	$(n - m)$-triangle	m-triangle
C	$m \times (n - m)$ rectangle	$(n - m) \times m$ rectangle

TABLE 2.19: Blocks formed by the roots of $Q_{m,n}(z)$ and $Q_{n-m,n}(z)$ when $n > m$.

Theorem 28. *The polynomials $Q_{n,n}(z)$ and $R_{0,n}(z)$ are equal.*

Proof. The partition

$$\lambda^*_{n,n} = \left(\left\{ 2n - 2j + 2 \right\}_{j=1}^{n} \right).$$

Figure 2.26 shows the Young diagram of $\lambda^*_{n,n}$. This Young diagram consists of n single rows and zero sets of double rows. This means $b = n$ and $a = 0$ of $R_{s,t}(z)$. Hence, the parameters of $R_{s,t}(z)$ are 0 and n. Row b of the Young diagram in Figure 2.26 is the n th row of the diagram. Figure 2.26 shows that the difference in length between row b and row $b+1$ is two. Hence, $R_{s,t}(z)$ is a case 3 polynomial when $m = n$. Therefore, the polynomial associated with $\lambda^*_{n,n}$ is $R_{0,n}(z)$.

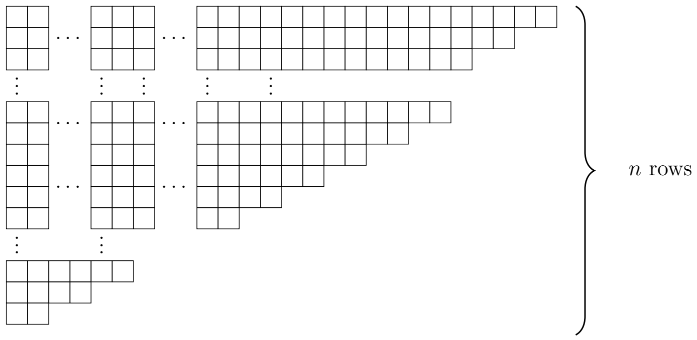

FIGURE 2.26: The Young diagram of $\lambda^*_{n,n}$.

$\square$

In the proof above, we saw that when $Q_{m,n}(z)$ is a case 2 polynomial i.e. when $m = n$, it is equal to the case 3 polynomial $R_{0,n}(z)$. Earlier in this chapter, we found that the roots of $Q_{n,n}(z)$ form A blocks of size n and B and C blocks that are empty i.e. of size zero. It follows from Table 2.8 that the roots of $Q_{0,n}(z)$ form empty A and C blocks, and B blocks of size n. This confirms that the roots of $Q_{n,n}(z)$ form A blocks of size n.

Chapter 3

The 4-Okamoto polynomials

We now discuss the 4-Okamoto polynomials $Q_{m,n,r}(z)$, defined in Definition 29. The 4-Okamoto polynomials are naturally associated with a specific family of partitions. In this chapter, we explore how aspects of these partitions play a role in properties of $Q_{m,n,r}(z)$. We first investigate the structures formed by the roots of $Q_{m,n,r}(z)$ in the complex plane. We then find the explicit form of the partition λ of $Q_{m,n,r}(z)$ and its conjugate partition λ^*, and later the 2-core and 2-quotient of λ. The polynomials

$$R_{m,n,r}(z) = \mathrm{i}^d Q_{m,n,r}(-\mathrm{i}z),$$

where d is the degree of $Q_{m,n,r}(z)$ given in (3.3), are also investigated in this chapter. The polynomials $R_{m,n,r}(z)$ will be used to confirm our observations on the structures formed by the roots of $Q_{m,n,r}(z)$. In the end of this chapter, we determine the discriminant of a subset of the 4-Okamoto polynomials.

Definition 29. The 4-Okamoto polynomials $Q_{m,n,r}(z)$, where m, n and r are positive integers are given by

$$Q_{m,n,r}(z) = c_{m,n,r}\mathcal{W}\Big(\big\{\mathrm{He}_{1+4j}(z)\big\}_{j=0}^{m-1}\,;\,\big\{\mathrm{He}_{2+4j}(z)\big\}_{j=0}^{n-1}\,;\,\big\{\mathrm{He}_{3+4j}(z)\big\}_{j=0}^{r-1}\Big), \quad (3.1)$$

where

$$c_{m,n,r} = \prod_{i<j} \frac{1}{n_j - n_i}, \tag{3.2}$$

ensures that $Q_{m,n,r}(z)$ is monic. The terms $n_1, n_2, \ldots, n_\ell$ are the degrees of the Hermite polynomials in the Wronskian.

It follows from results in [32] that the Wronskian of Hermite polynomials $\mathcal{W}(H_{n_1}, H_{n_2}, \ldots, H_{n_\ell})$ is of degree

$$\sum_{j=1}^{\ell} n_j - \frac{1}{2}\ell(\ell-1).$$

Therefore, the 4-Okamoto polynomials are of degree

$$d = \frac{3}{2}(m^2 + n^2 + r^2) - mn - mr - nr - \frac{1}{2}m + \frac{1}{2}n + \frac{3}{2}r. \tag{3.3}$$

In Chapter 2, we discussed the structure of blocks formed by the roots of $Q_{m,n}(z)$, and how the relative size of m and n affects block size. The results in that chapter motivate us to investigate the structure of blocks formed by the roots of 4-Okamoto polynomials. Since the 4-Okamoto polynomials depend on three parameters m, n and r it means there are thirteen possible parameter conditions to consider. The parameter conditions of $Q_{m,n,r}(z)$ include six cases where all parameters are not equal, one case where all are equal and six cases where two parameters are equal.

3.1 Roots of $Q_{m,n,r}(z)$ in the complex plane

We now discuss the blocks formed by the roots of $Q_{m,n,r}(z)$. It follows from (1.20), (1.21), and Definition 29, that the multiplicity of roots of $Q_{m,n,r}(z)$ at the origin is

$$k = \frac{(m + r - n)(m + r - n + 1)}{2}, \tag{3.4}$$

and

$$Q_{m,n,r}(z) = z^k \widetilde{P}(z^2). \tag{3.5}$$

Later in this chapter we determine the 2-core of λ associated with $Q_{m,n,r}(z)$. The size of these 2-core partitions confirm that the multiplicity of roots of $Q_{m,n,r}(z)$ at the origin is equal to (3.4). The relationship between the size of 2-cores and the multiplicity of roots of Wronskian of Hermite polynomials at the origin, is explained in Theorem 3.1 and Remark 3.2 of [11].

The factorised form of $Q_{m,n,r}(z)$ in (3.5) tells us that the roots of $Q_{m,n,r}(z)$ are symmetric about the real and imaginary axis. This symmetry can be seen in plots such as Figures 3.1 and 3.2. For convenience, the plots in this chapter exclude any roots at the origin.

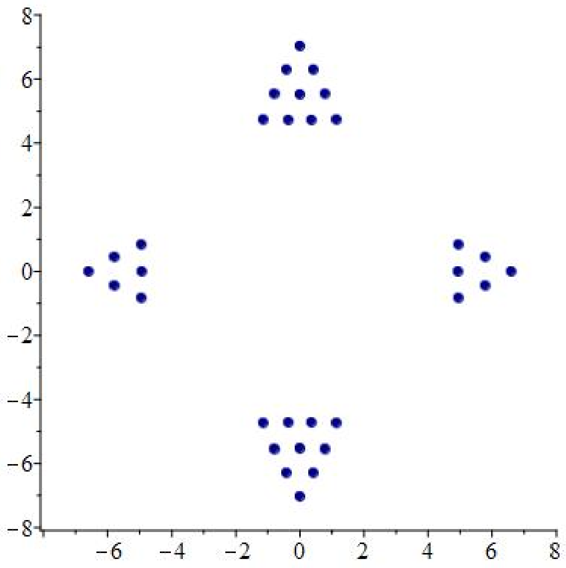

FIGURE 3.1: Plot of roots of $Q_{8,4,11}(z)$.

In the generalised Okamoto chapter, we discussed that the roots of $Q_{m,n}(z)$ form triangle blocks that lie on the real axis, triangle blocks that lie on the imaginary axis, and a rectangle block that lies around the origin. Figure 3.1 shows that the roots of $Q_{m,n,r}(z)$ also form triangle blocks that lie on the real axis and imaginary axis. Figure 3.2 shows that the roots of $Q_{m,n,r}(z)$ form rectangle blocks that lie

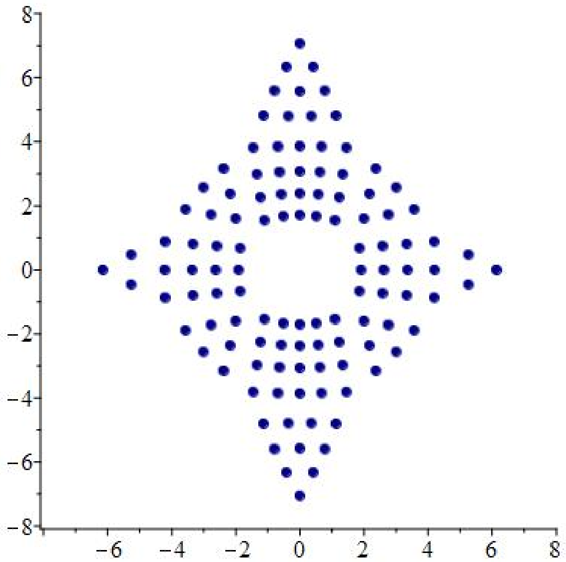

FIGURE 3.2: Plot of roots of $Q_{11,8,4}(z)$.

on the real and imaginary axis, unlike the roots of $Q_{m,n}(z)$, that form a single rectangle block centred at the origin. Figure 3.2 also shows that the roots of 4-Okamoto polynomials form triangle blocks that lie in each quadrant of the complex plane. A comparison between the triangle blocks that lie on the real axis in Figures 3.1 and 3.2 shows that the block size is different, i.e. in Figure 3.1 the block is of size three and in Figure 3.2 the block is of size two. This shows that the relative size of m, n and r affects the size of blocks formed by the roots of $Q_{m,n,r}(z)$. Our aim is to investigate the size and structure of blocks formed by the roots of 4-Okamoto polynomials.

Figures 3.3 and 3.4 show examples of blocks formed by roots of $Q_{m,n,r}(z)$. The plots show rectangle and triangle blocks that lie on the real and imaginary axis. Plots, such as of the roots of $Q_{2,16,11}(z)$ in Figure 3.3, and $Q_{3,7,13}(z)$ in Figure 3.4, show equilateral triangle blocks that appear in each quadrant of the complex plane. The blocks formed by the roots of $Q_{3,10,5}(z)$ and $Q_{4,11,8}(z)$ in Figure 3.4 show that triangle blocks appear around the origin. The shape of the blocks around the origin is unclear from Figures 3.3 and 3.4, however, enlarged images of the plots show that blocks around the origin change shape. Figures 3.3 and

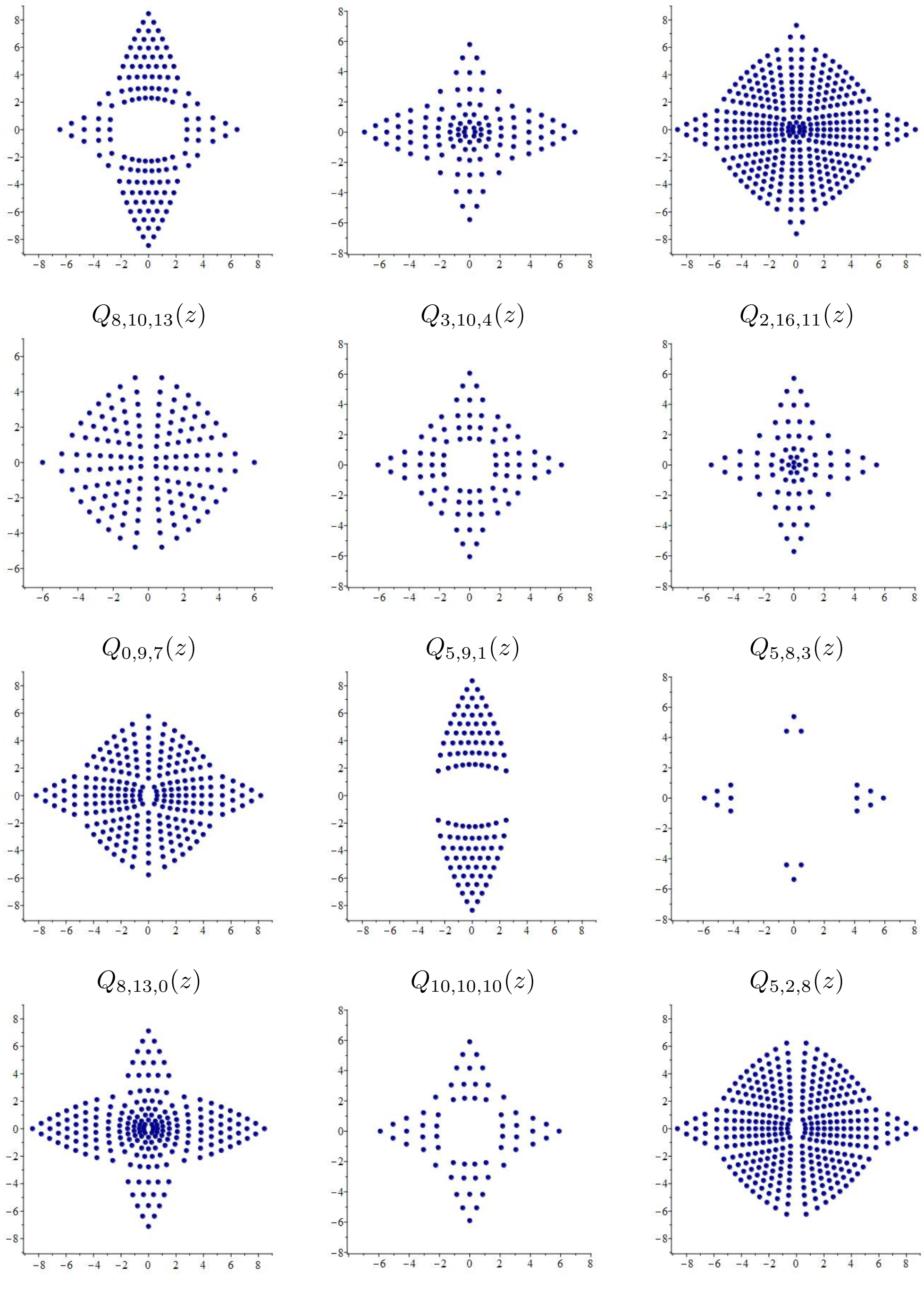

$Q_{8,10,13}(z)$ $Q_{3,10,4}(z)$ $Q_{2,16,11}(z)$

$Q_{0,9,7}(z)$ $Q_{5,9,1}(z)$ $Q_{5,8,3}(z)$

$Q_{8,13,0}(z)$ $Q_{10,10,10}(z)$ $Q_{5,2,8}(z)$

$Q_{5,14,5}(z)$ $Q_{9,5,3}(z)$ $Q_{0,15,10}(z)$

FIGURE 3.3: Plot of roots of $Q_{m,n,r}(z)$.

3.4 show that the roots of $Q_{m,n,r}(z)$ form a total of sixteen blocks (e.g. roots of $Q_{4,11,8}(z)$ in Figure 3.4) where some blocks can be empty, i.e. of size zero (e.g. roots of $Q_{10,3,6}(z)$ in Figure 3.4 show only four non-empty blocks). An illustration

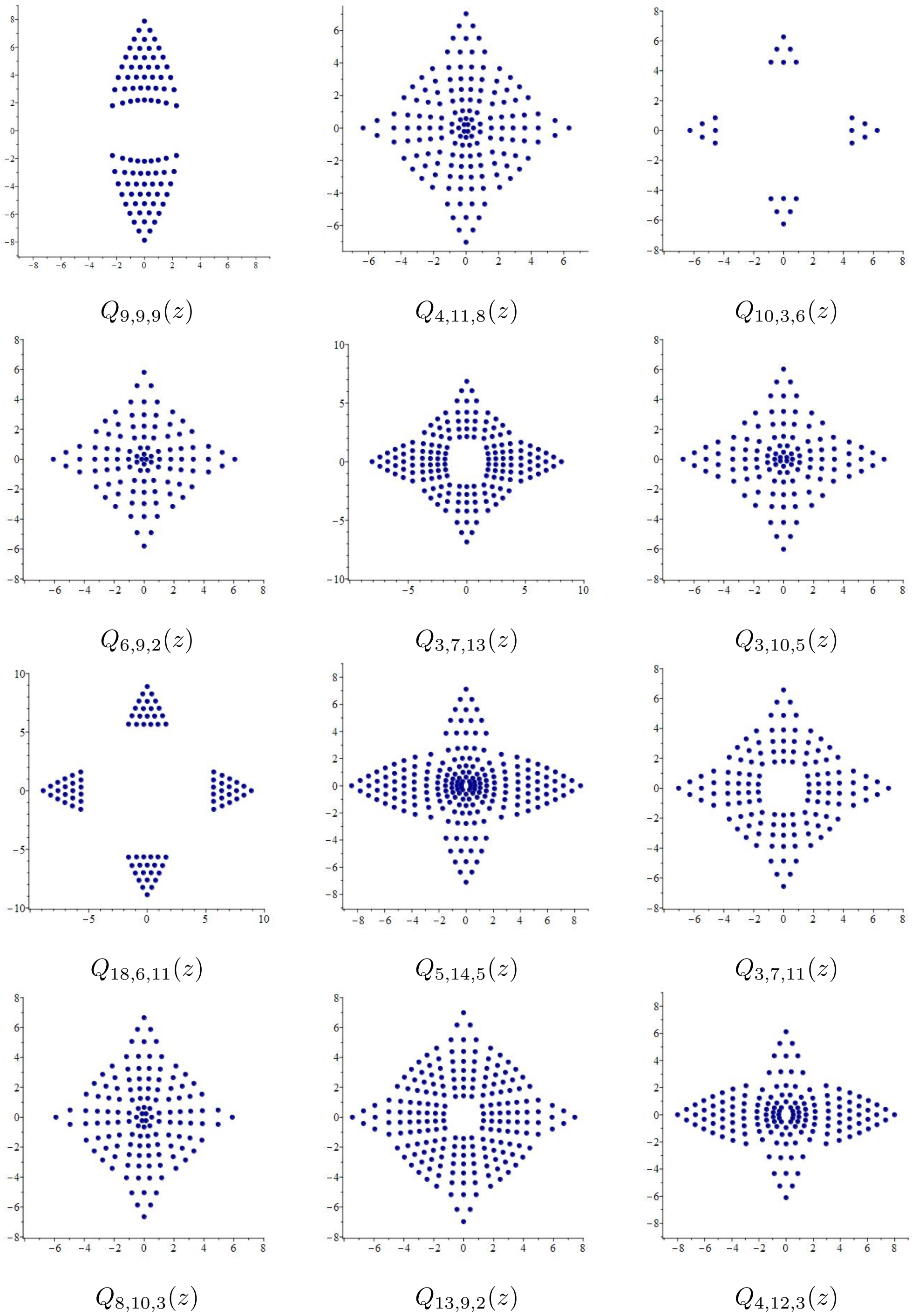

FIGURE 3.4: Further plots of roots of $Q_{m,n,r}(z)$.

of the sixteen blocks formed by the roots of $Q_{m,n,r}(z)$ can be found in Figure 3.5. The notation A–G (shown in Figure 3.5) refer to the different types of blocks formed by roots of $Q_{m,n,r}(z)$.

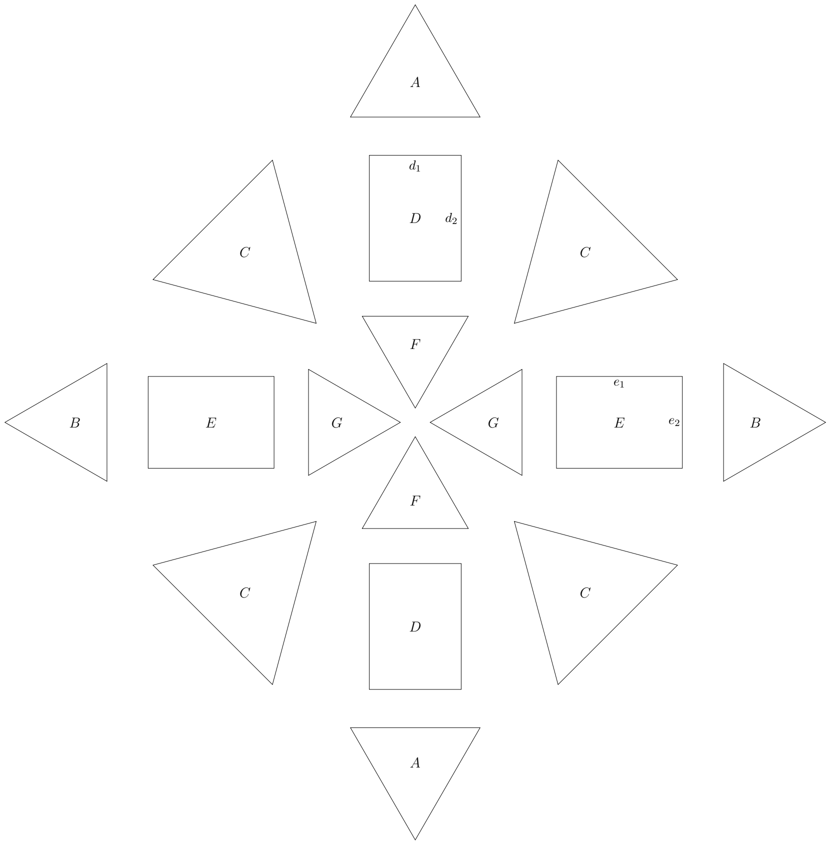

FIGURE 3.5: Blocks formed by roots of $Q_{m,n,r}(z)$.

To summarise, the blocks A–G illustrated in Figure 3.5 are as follows:

- Block A are equilateral triangles on the imaginary axis.
- Block B are equilateral triangles on the real axis.
- Block C are equilateral triangles that lies in each quadrant of the complex plane.
- Block D are rectangles that lies on the imaginary axis with width d_1, height d_2, and size $d_1 \times d_2$.
- Block E are rectangles that lies on the real axis with width e_1, height e_2, and size $e_1 \times e_2$.
- Block F lie on the imaginary axis and change shape. Further investigation is required.

- Block G lie on the real axis and change shape. Further investigation is required.

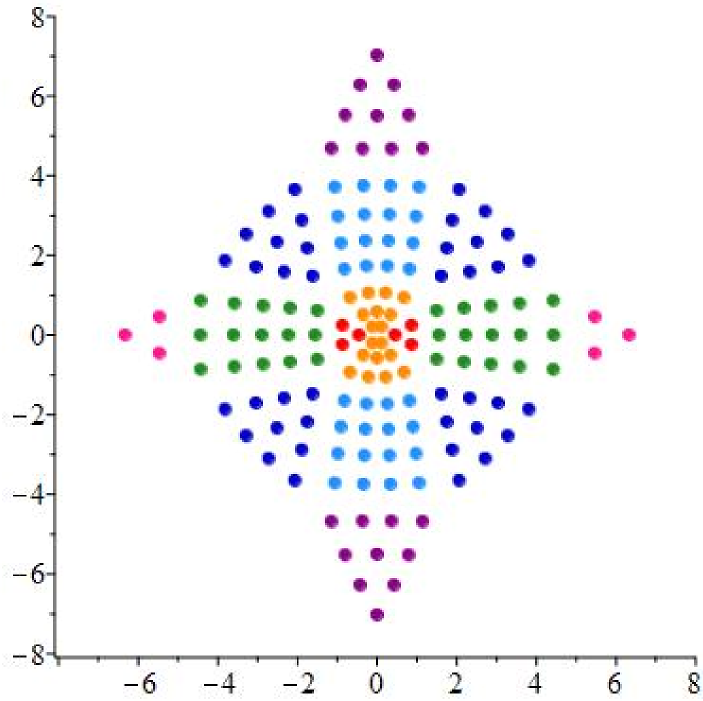

FIGURE 3.6: Plot of roots of $Q_{4,11,8}(z)$ with colour coded roots.

Figures 3.6 and 3.7 show colour coded roots of 4-Okamoto polynomials. Roots that form F blocks are coloured orange and roots that form G blocks are coloured red. A comparison between the plots in Figures 3.6 and 3.7 shows that block F can take the form of an isosceles triangle (e.g. $Q_{4,11,5}(z)$) or a trapezoid (e.g. $Q_{4,11,8}(z)$). Similarly, Figures 3.6 and 3.7 show that block G can also take the form of an isosceles triangle (e.g. $Q_{4,11,8}(z)$) or a trapezoid (e.g. $Q_{4,11,5}(z)$). The plots in Figures 3.6 and 3.7 show that the parameters of $Q_{m,n,r}(z)$ affect the shape of blocks F and G. A comparison between Figures 3.6 and 3.7 shows that blocks are of different size in each plot, for example, block C formed by roots of $Q_{4,11,8}(z)$ is of size 4 and block C formed by roots of $Q_{4,11,5}(z)$ is of size 1. This suggests that the parameters m, n and r affect the size of blocks. Our aim is to investigate the relationship between parameters m, n and r and the structure of blocks formed by the roots of $Q_{m,n,r}(z)$, for all thirteen parameter conditions. To investigate the

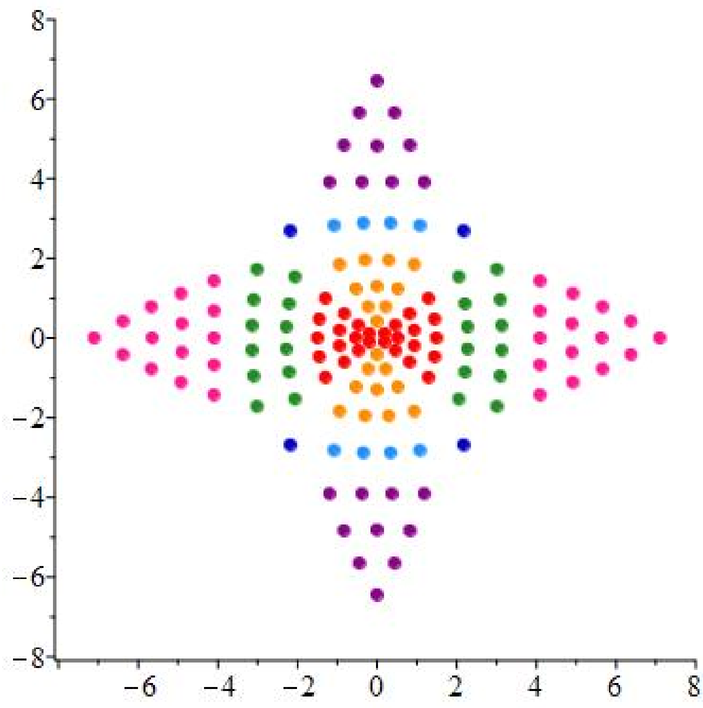

FIGURE 3.7: Plot of roots of $Q_{4,11,5}(z)$ with colour coded roots.

size and shape of blocks, we keep two parameters constant and increase the third parameter by increments of one.

The plots in Figure 3.8 are of the roots of 4-Okamoto polynomials with the parameter condition $m > n > r$. Figure 3.8 shows that blocks F and G are empty when $m > n > r$. The plots also show that when $m > n > r$ block A is of size r. The results in Table 3.1 state the size of blocks formed by the roots of $Q_{10,7,3}(z)$, $Q_{10,7,4}(z)$ and $Q_{10,7,5}(z)$, shown in Figure 3.8.

Block	$Q_{10,7,3}(z)$	$Q_{10,7,4}(z)$	$Q_{10,7,5}(z)$
A	3-triangle	4-triangle	5-triangle
B	2-triangle	2-triangle	2-triangle
C	3-triangle	2-triangle	1-triangle
D	4×4 rectangle	5×3 rectangle	6×2 rectangle
E	4×3 rectangle	3×3 rectangle	3×3 rectangle

TABLE 3.1: Blocks formed by the roots of $Q_{10,7,3}(z)$, $Q_{10,7,4}(z)$ and $Q_{10,7,5}(z)$ shown in Figure 3.8.

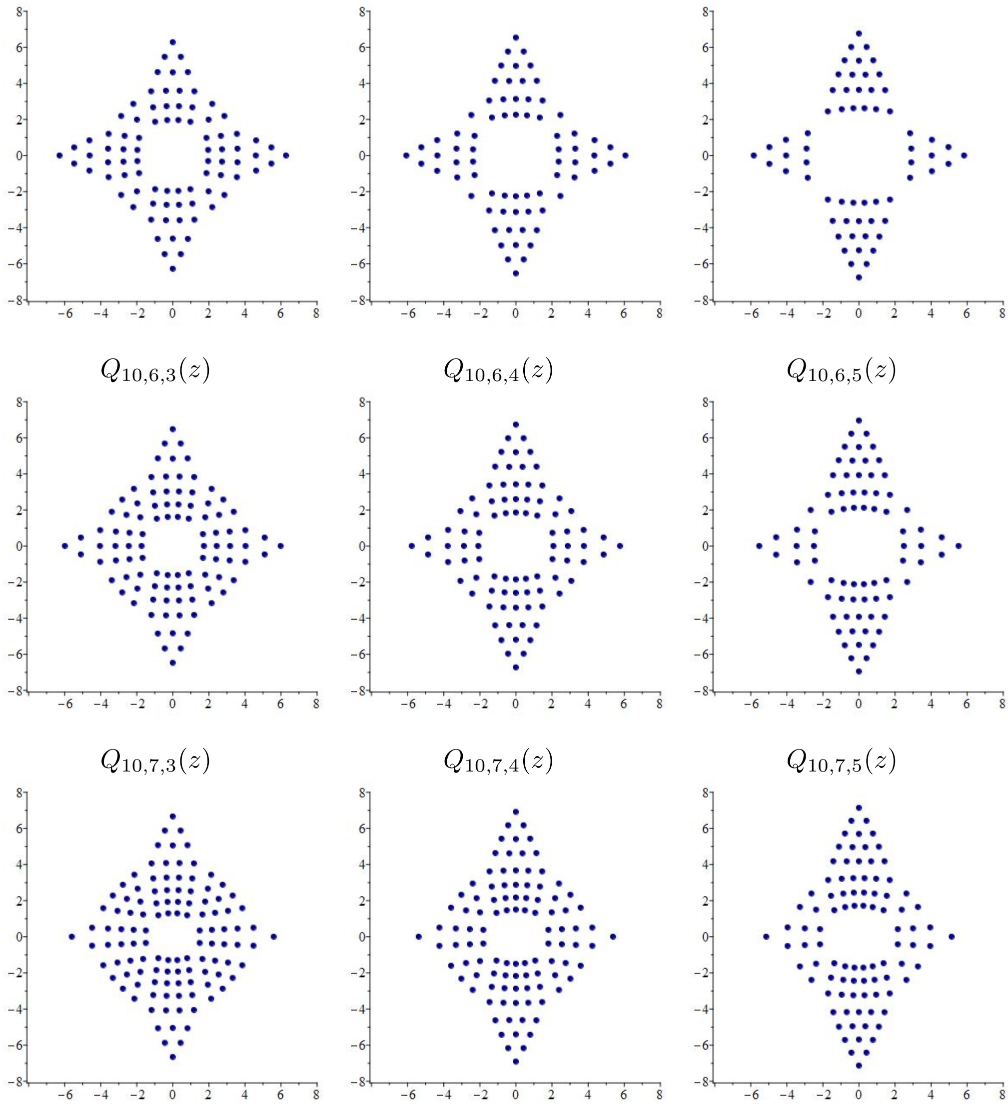

$Q_{10,6,3}(z)$ $Q_{10,6,4}(z)$ $Q_{10,6,5}(z)$

$Q_{10,7,3}(z)$ $Q_{10,7,4}(z)$ $Q_{10,7,5}(z)$

$Q_{10,8,3}(z)$ $Q_{10,8,4}(z)$ $Q_{10,8,5}(z)$

FIGURE 3.8: Plot of roots of $Q_{m,n,r}(z)$ with $m > n > r$.

The results in Table 3.1 and the plots in Figure 3.8 show that when m and n are fixed and r increases by one, the size of block B remains unchanged. A comparison of plots in Figure 3.8 and additional plots, show that when $m > n > r$, block B is of size $m - n - 1$. Figure 3.8 and Table 3.1 show that when m and n are fixed, and r increases by one, the size of block C decreases by one. The plots in Figure 3.8 shows that block C is of size $n - r - 1$ when $m > n > r$. The results in Table 3.1 show that when $m > n > r$, block D is of width $r + 1$ and length $n - r$. Similarly, block E is of width $(n-r)$ and length $(m-n)$. The general size of blocks when $m>n>r$ can be found in Table 3.2.

Block	$Q_{m,n,r}(z)$ with $m>n>r$
A	r-triangle
B	$(m-n-1)$-triangle
C	$(n-r-1)$-triangle
D	$(r+1)\times(n-r)$ rectangle
E	$(n-r)\times(m-n)$ rectangle

TABLE 3.2: Blocks formed by the roots of $Q_{m,n,r}(z)$ when $m>n>r$.

Examples of blocks formed by the roots of $Q_{m,n,r}(z)$ when $m>r>n$ can be found in Figure 3.9. Figure 3.9 shows that when m and r are fixed and n increases by one, the size of block A also increases by one. Figure 3.9 also shows that block B is unaffected by an increase in n, and blocks $C-G$ are empty. The general size of blocks when $m>r>n$ can be found in Table 3.3.

Block	$Q_{m,n,r}(z)$ with $m>r>n$
A	n-triangle
B	$(m-r-1)$-triangle

TABLE 3.3: Blocks formed by the roots of $Q_{m,n,r}(z)$ when $m>r>n$.

The plots in Figure 3.10 are of the roots of $Q_{m,n,r}(z)$ with $r>m>n$. Figure 3.10 shows that when m and r are fixed and n increases by one, block B remains unchanged and block A increase in size by one. The size of the blocks formed by roots of $Q_{m,n,r}(z)$ when $r>m>n$ can be found in Table 3.4.

Block	$Q_{m,n,r}(z)$ with $r>m>n$
A	n-triangle
B	$(r-m)$-triangle

TABLE 3.4: Blocks formed by the roots of $Q_{m,n,r}(z)$ when $r>m>n$.

Figure 3.11 shows examples of blocks formed by the roots of $Q_{m,n,r}(z)$ with $r>n>m$. Interestingly, the blocks F and G have been empty for all the parameter

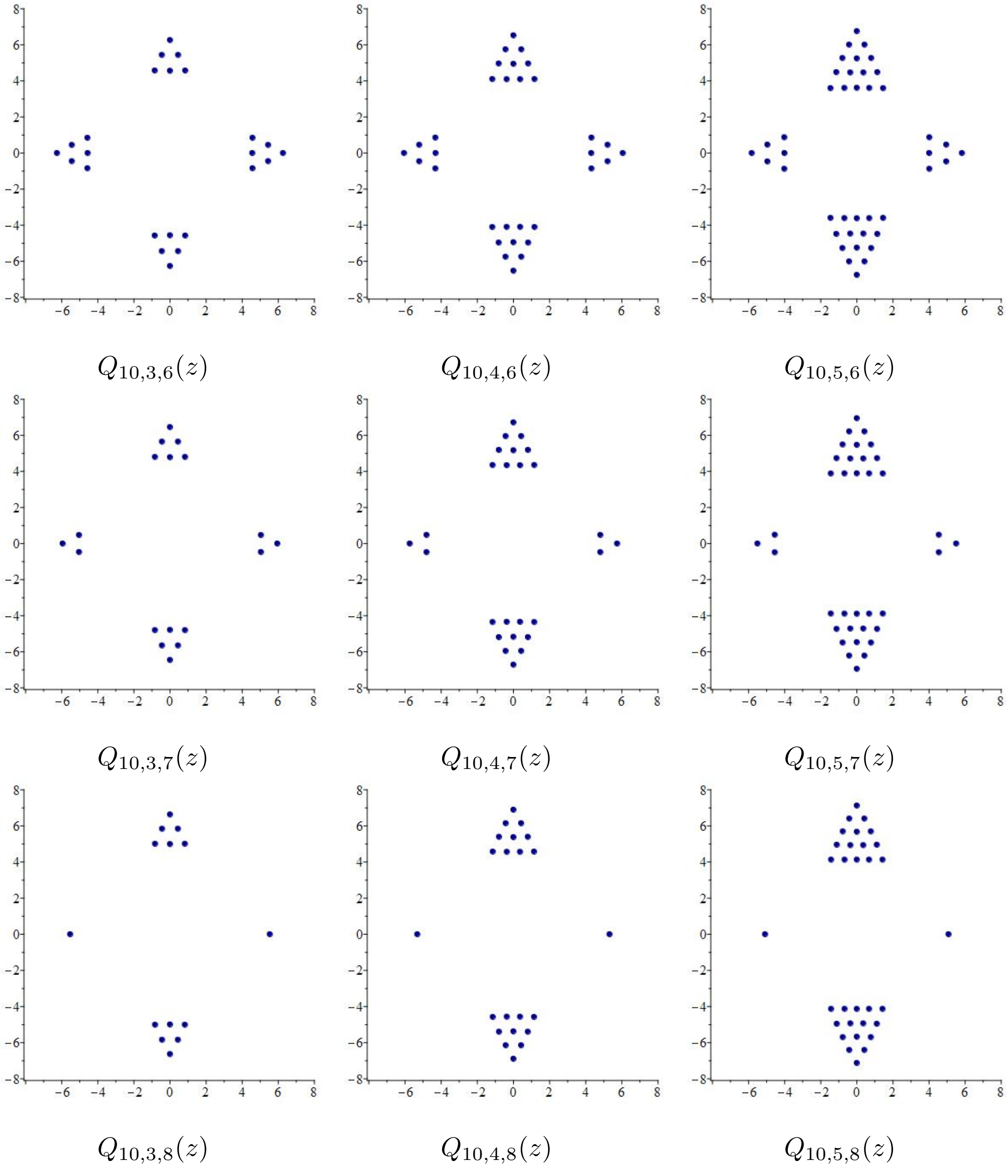

FIGURE 3.9: Plot of roots of $Q_{m,n,r}(z)$ with $m > r > n$.

conditions of $Q_{m,n,r}(z)$ discussed so far. Figure 3.11 shows that when n and r are fixed, and m increases by one; the size of block A increases by one, the size of block B remains unchanged, and, the size of block C decreases by one. The size of the blocks formed by roots of $Q_{m,n,r}(z)$ when $r > n > m$ can be found in Table 3.5.

So far, we have discussed the blocks formed by the roots of $Q_{m,n,r}(z)$ when the parameters m, n and r are not equal. We have seen that when the parameters are

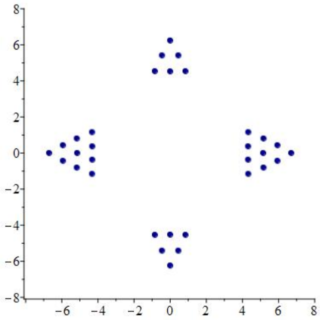

$Q_{6,3,10}(z)$

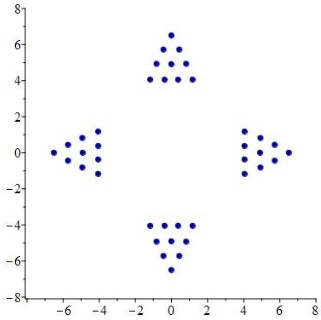

$Q_{6,4,10}(z)$

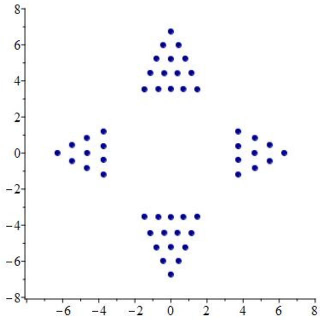

$Q_{6,5,10}(z)$

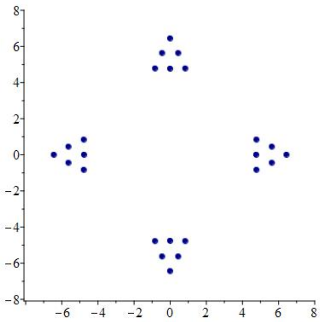

$Q_{7,3,10}(z)$

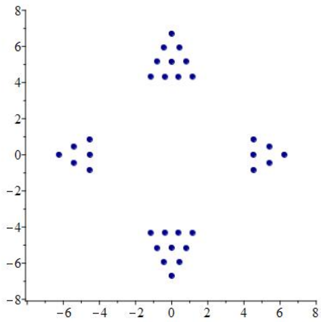

$Q_{7,4,10}(z)$

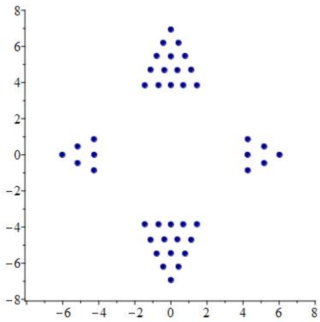

$Q_{7,5,10}(z)$

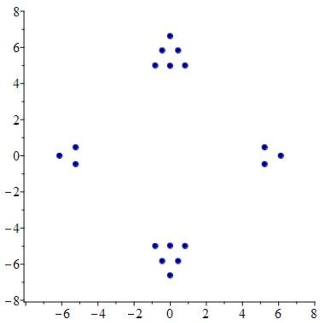

$Q_{8,3,10}(z)$

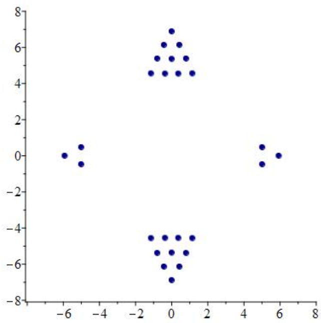

$Q_{8,4,10}(z)$

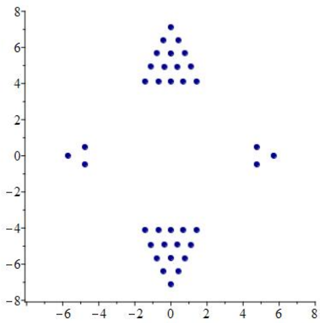

$Q_{8,5,10}(z)$

FIGURE 3.10: Plot of roots of $Q_{m,n,r}(z)$ with $r > m > n$.

Block	$Q_{m,n,r}(z)$ with $r > n > m$
A	m-triangle
B	$(r-n)$-triangle
C	$(n-m)$-triangle
D	$m \times (n-m)$ rectangle
E	$(n-m) \times (r-n)$ rectangle

TABLE 3.5: Blocks formed by the roots of $Q_{m,n,r}(z)$ when $r > n > m$.

not equal, and n is the smallest parameter blocks $C - G$ are empty, and when n is the second largest parameter blocks $F - G$ are empty. We now consider what happens when parameters are not equal and n is the largest parameter.

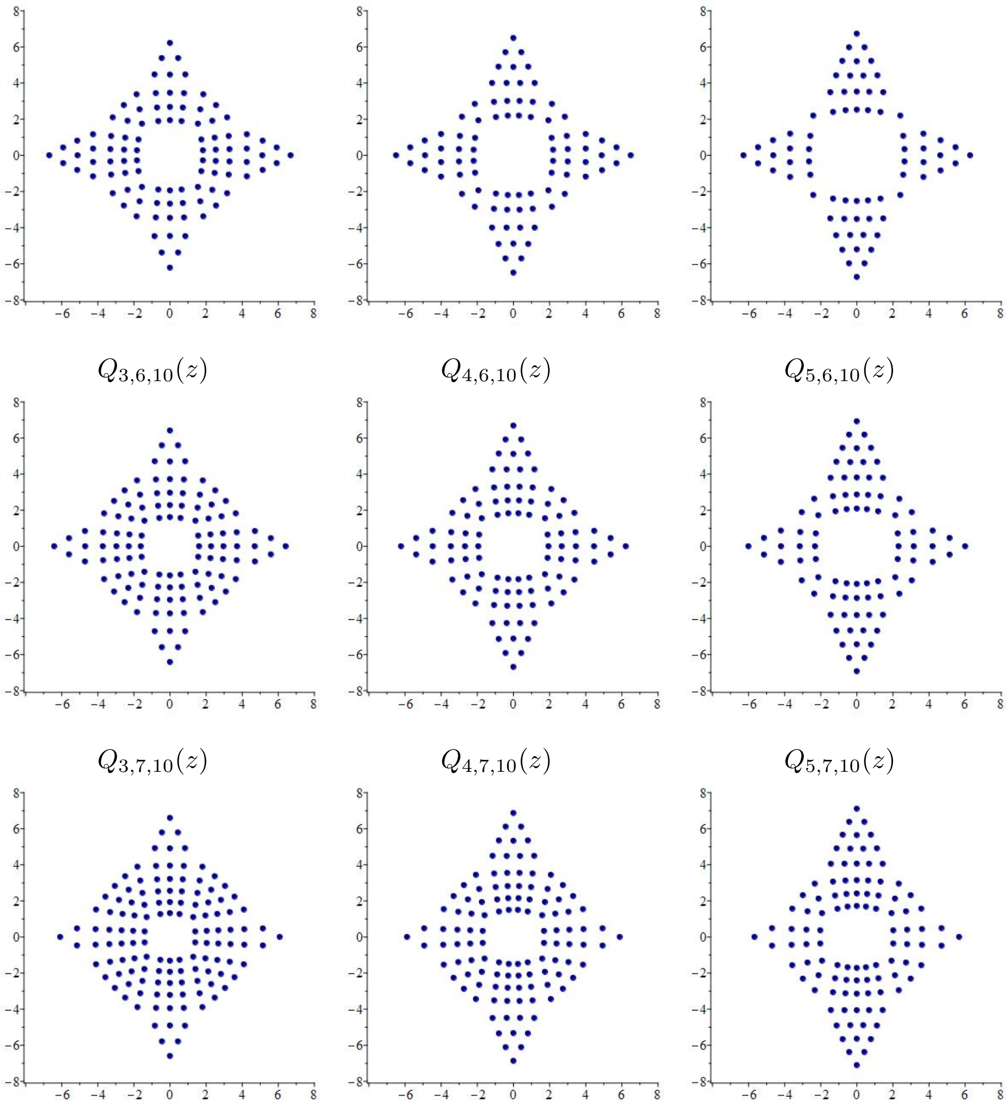

$Q_{3,6,10}(z)$ $Q_{4,6,10}(z)$ $Q_{5,6,10}(z)$

$Q_{3,7,10}(z)$ $Q_{4,7,10}(z)$ $Q_{5,7,10}(z)$

$Q_{3,8,10}(z)$ $Q_{4,8,10}(z)$ $Q_{5,8,10}(z)$

FIGURE 3.11: Plot of roots of $Q_{m,n,r}(z)$ with $r > n > m$.

The plots in Figure 3.12 are of the roots of $Q_{m,n,r}(z)$ with $n > m > r$. The plots show that when $n > m > r$ the blocks $A - G$ are non-empty. The size and shape of blocks $A - E$ can be clearly identified by looking at Figure 3.12. The size of blocks $A - E$ when $n > m > r$ can be found in Table 3.6.

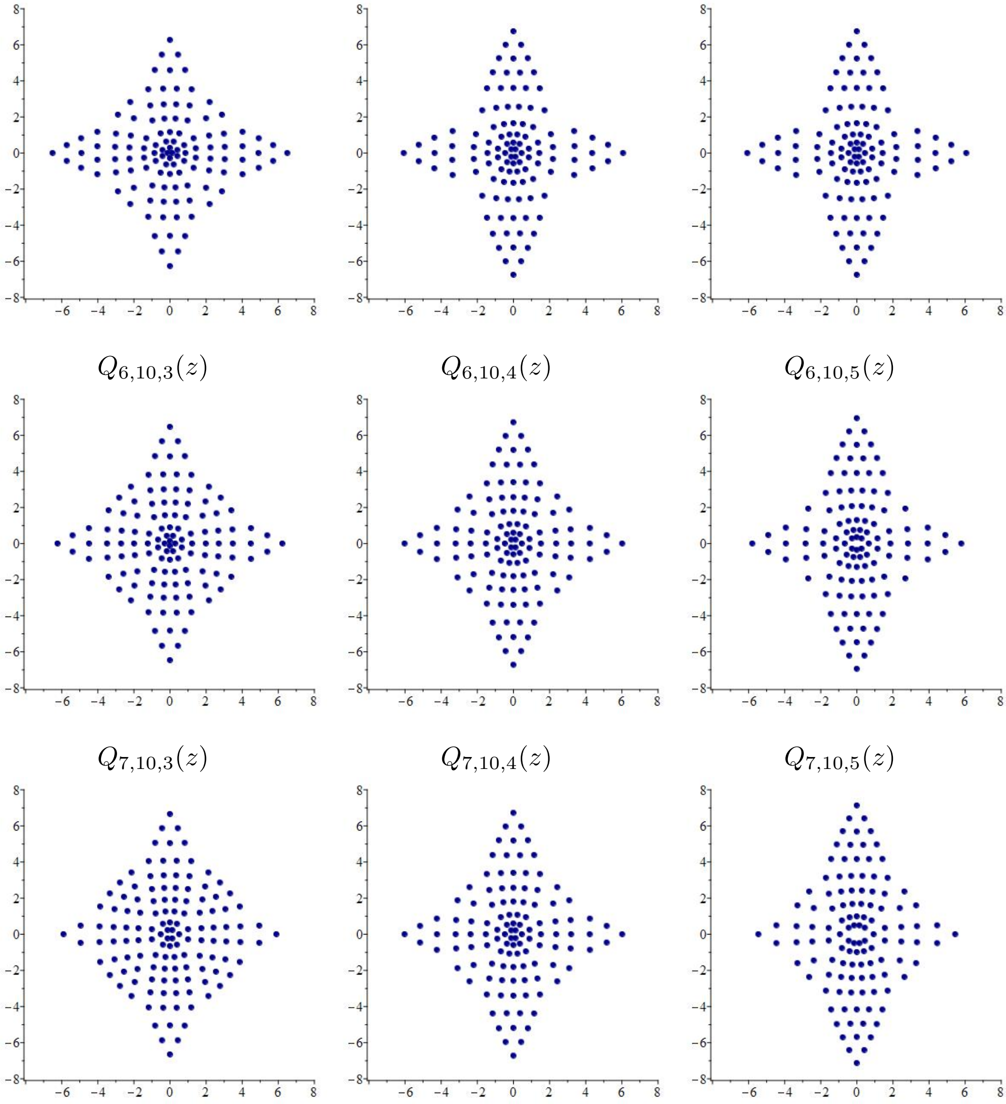

$Q_{6,10,3}(z)$ $Q_{6,10,4}(z)$ $Q_{6,10,5}(z)$

$Q_{7,10,3}(z)$ $Q_{7,10,4}(z)$ $Q_{7,10,5}(z)$

$Q_{8,10,3}(z)$ $Q_{8,10,4}(z)$ $Q_{8,10,5}(z)$

FIGURE 3.12: Plot of roots of $Q_{m,n,r}(z)$ with $n > m > r$.

Block	$Q_{m,n,r}(z)$ with $n > m > r$
A	r-triangle
B	$(n-m)$-triangle
C	$(m-r-1)$-triangle
D	$(r+1)\times(m-r)$ rectangle
E	$(m-r-1)\times(n-m)$ rectangle

TABLE 3.6: Blocks $A - E$ formed by the roots of $Q_{m,n,r}(z)$ when $n > m > r$.

Our aim is to now determine the size and shape of blocks F and G when $n > m > r$. The plots in Figure 3.13 show the blocks formed by the roots of $Q_{6,10,r}$ for $r = 2, \ldots, 5$. Roots that form F blocks in Figure 3.13 are coloured orange and roots that form G blocks are coloured red. Figure 3.14 shows the plots in Figure 3.13 zoomed in at the origin.

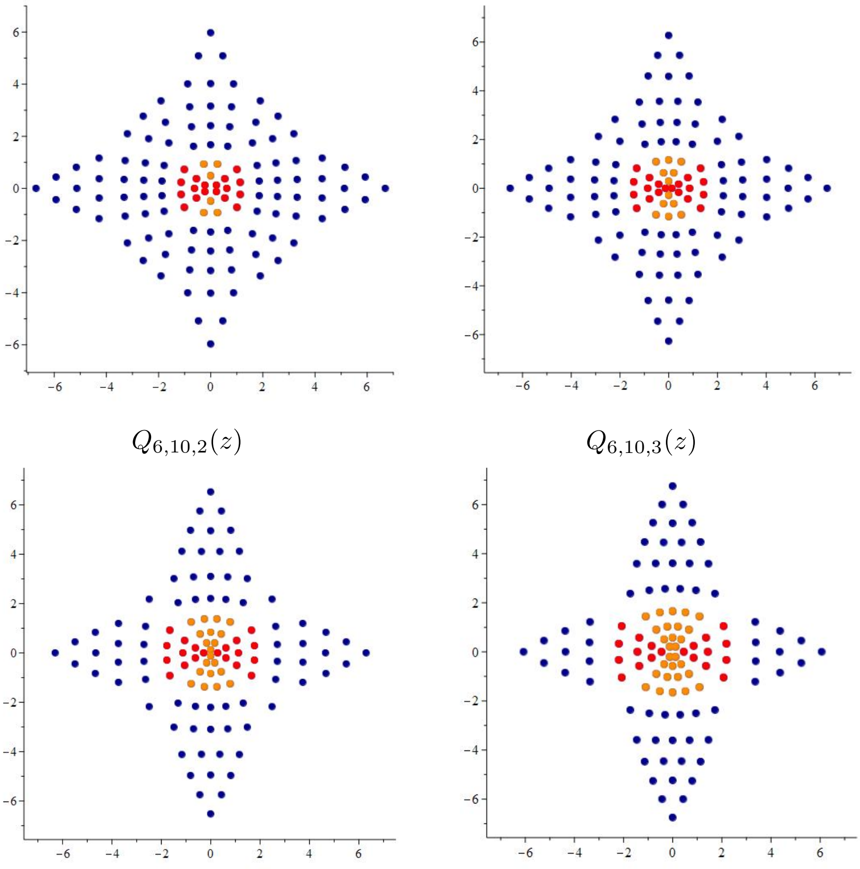

$Q_{6,10,2}(z)$ $Q_{6,10,3}(z)$

$Q_{6,10,4}(z)$ $Q_{6,10,5}(z)$

FIGURE 3.13: Plot of roots of $Q_{6,10,r}(z)$ for $r = 2, \ldots, 5$ with the condition $n > m > r$.

Similar to Figures 3.6 and 3.7, the blocks F and G in Figure 3.13 are either isosceles triangles or trapezoids. When a block is a trapezoid we will describe it as a trapezoid of size

$$h \times l,$$

where h is the height of the trapezoid and l is the length of the long base of the trapezoid. The size and shape of blocks F and G formed by the roots of $Q_{6,10,r}(z)$ for $r = 2, \ldots, 5$ (shown in Figures 3.13 and 3.14) can be found in Table 3.7.

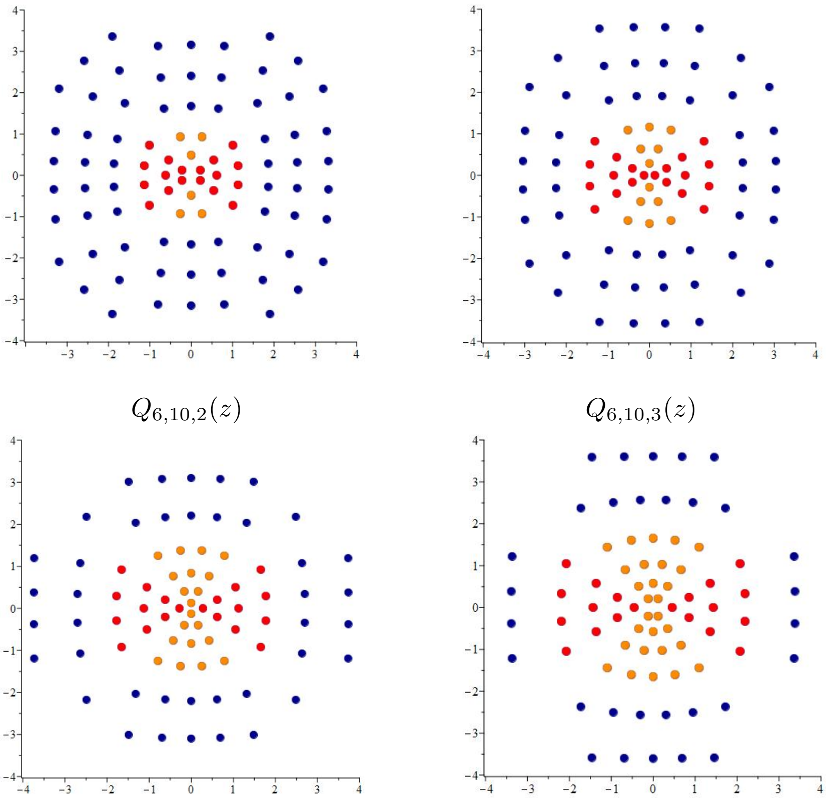

$Q_{6,10,2}(z)$ $Q_{6,10,3}(z)$

$Q_{6,10,4}(z)$ $Q_{6,10,5}(z)$

FIGURE 3.14: Plots in Figure 3.13 zoomed in at the origin.

Block	$Q_{6,10,2}(z)$	$Q_{6,10,3}(z)$	$Q_{6,10,4}(z)$	$Q_{6,10,5}(z)$
F	2-triangle	3-triangle	4-triangle	4×5 trapezoid
G	3×4 trapezoid	4-triangle	4-triangle	4-triangle

TABLE 3.7: Blocks F and G formed by the roots of $Q_{6,10,r}(z)$ for $r = 2, \ldots, 5$ as shown in Figures 3.13 and 3.14.

Further investigation shows that when $n > m > r$, block F is a triangle when $n \geq m + r$ and a trapezoid when $n < m + r$. Similarly, when $n > m > r$, block G is a triangle when $n \leq m + r + 1$ and a trapezoid when $n > m + r + 1$. The size and shape of blocks formed by the roots of $Q_{m,n,r}(z)$ when $n > m > r$ can be found in Table 3.8.

Block	$Q_{m,n,r}(z)$ when $n > m > r$
A	r-triangle
B	$(n-m)$-triangle
C	$(m-r-1)$-triangle
D	$(r+1)\times(m-r)$ rectangle
E	$(m-r-1)\times(n-m)$ rectangle
F	r-triangle when $n \geq m+r$
	$(n-m)\times r$ trapezoid when $n < m+r$
G	$(n-m)$-triangle when $n \leq m+r+1$
	$(r+1)\times(n-m)$ trapezoid when $n > m+r+1$

Table 3.8: Blocks formed by the roots of $Q_{m,n,r}(z)$ when $n > m > r$.

Figures 3.15 and 3.16 show examples of blocks formed by the roots of $Q_{m,n,r}(z)$ when $n > r > m$. The roots that form the F and G blocks are coloured in both figures. Examples of the size and shape of F and G blocks when $n > m > r$ can be found in Table 3.9. Interestingly, further investigation shows that when $n > r > m$ the shape of block F and G depends on the size of n, $m+r$ and $m+r+1$, similar to when $n > m > r$. The size and shape of blocks formed by the roots of $Q_{m,n,r}(z)$ when $n > r > m$ can be found in Table 3.10.

Block	$Q_{2,10,6}(z)$	$Q_{3,10,6}(z)$	$Q_{4,10,6}(z)$	$Q_{5,10,6}(z)$
F	2-triangle	3-triangle	4-triangle	4×5 trapezoid
G	2×3 trapezoid	3-triangle	3-triangle	3-triangle

Table 3.9: Blocks F and G formed by the roots of $Q_{m,10,6}(z)$ for $m = 2,\ldots,5$ as shown in Figures 3.15 and 3.16.

So far, we have considered the blocks formed by the roots of $Q_{m,n,r}(z)$ with parameters that are non-equal. We now consider what happens when parameters are equal. Figure 3.17 shows examples of blocks formed by the roots of $Q_{n,n,n}(z)$. Figure 3.17 suggests that the roots of $Q_{n,n,n}(z)$ form two triangle blocks of size $n-1$, and two rectangle blocks of size $1\times n$, i.e. A blocks of size $n-1$ and E blocks of size $1\times n$.

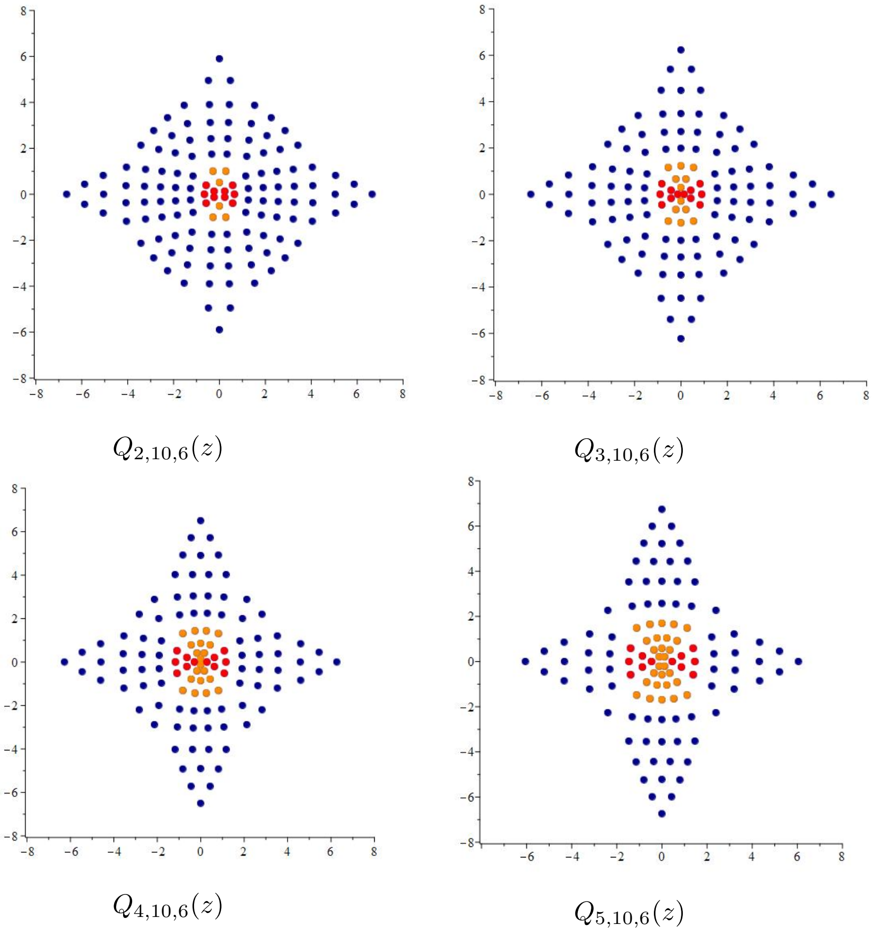

FIGURE 3.15: Plot of roots of $Q_{m,10,6}(z)$ for $m = 2, \ldots, 5$ with the condition $n > r > m$.

Block	$Q_{m,n,r}(z)$ when $n > r > m$
A	m-triangle
B	$(n-r-1)$-triangle
C	$(r-m)$-triangle
D	$m \times (r-m)$ rectangle
E	$(r-m+1) \times (n-r)$ rectangle
F	m-triangle when $n \geq m+r$
	$(n-r) \times m$ trapezoid when $n < m+r$
G	$(n-r-1)$-triangle when $n \leq m+r+1$
	$m \times (n-r-1)$ trapezoid when $n > m+r+1$

TABLE 3.10: Blocks formed by the roots of $Q_{m,n,r}(z)$ when $n > r > m$.

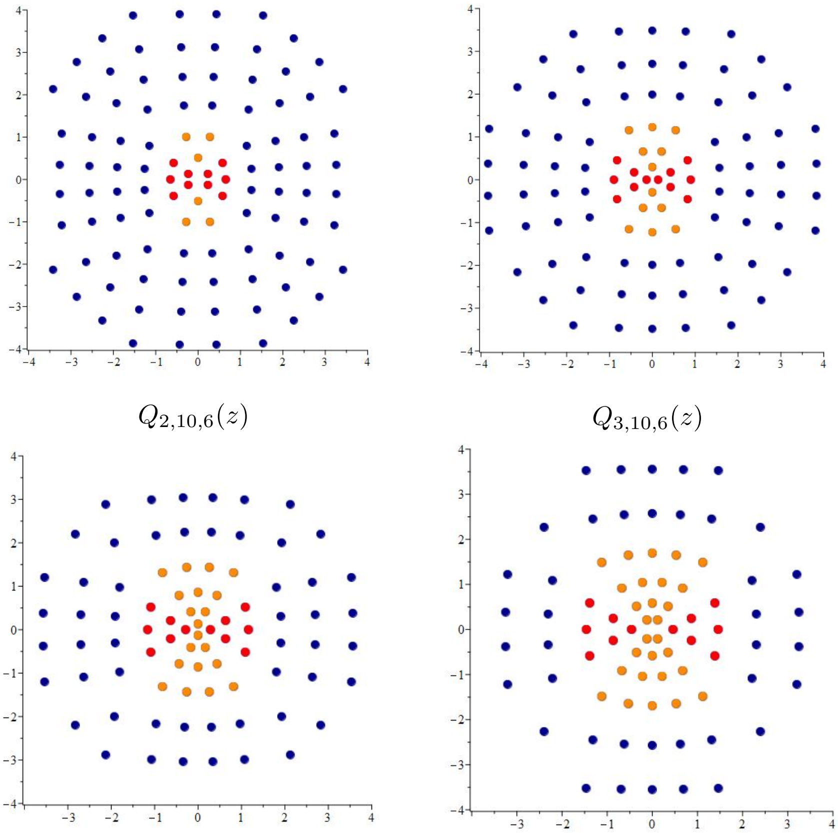

$Q_{2,10,6}(z)$ $Q_{3,10,6}(z)$

$Q_{4,10,6}(z)$ $Q_{5,10,6}(z)$

FIGURE 3.16: Plots in Figure 3.15 zoomed in at the origin.

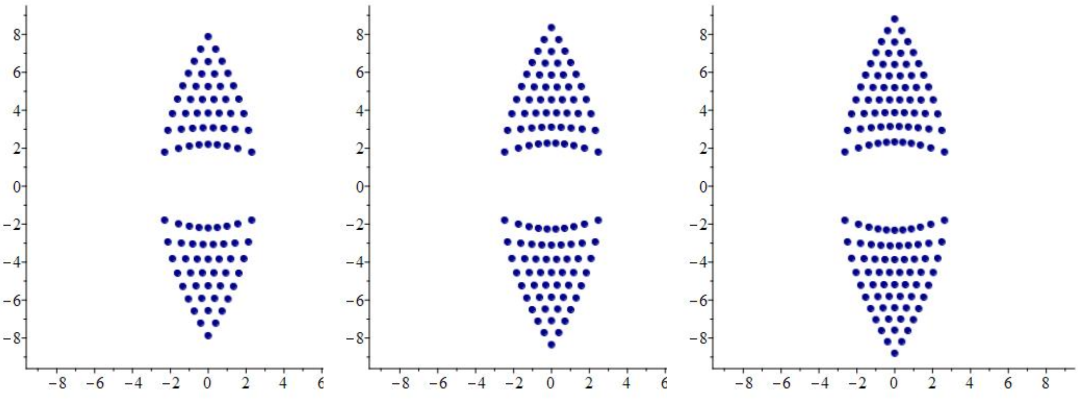

$Q_{9,9,9}(z)$ $Q_{10,10,10}(z)$ $Q_{11,11,11}(z)$

FIGURE 3.17: Plot of the roots of $Q_{n,n,n}(z)$ for $n = 9, \ldots, 11$.

A comparison of the blocks formed by the roots of $Q_{m,n,r}(z)$ when parameters are not equal, shows that the size of block A is the smallest parameters out of m, n

and r. Therefore, it follows that the roots of $Q_{n,n,n}(z)$ form A blocks of size n and $B-G$ blocks that are empty. Table 3.11 states the size of blocks when all parameters are equal. A summary of the size and shape of blocks when parameters are not equal can be found in Tables 3.12-3.15.

Block	$Q_{m,n,r}(z)$ with $m=n=r$
A	n-triangle

TABLE 3.11: Blocks formed by roots of $Q_{n,n,n}(z)$.

In Chapter 2, we discussed that the roots of $Q_{n,n}(z)$ also forms A blocks of size n. A comparison between plots show that the roots of 4-Okamoto polynomials $Q_{n,n,n}(z)$ form A blocks that are concave, and roots of generalised Okamoto polynomials $Q_{n,n}(z)$ form A blocks that are convex. The reason as to why this is the case is yet to be determined.

Block	$Q_{m,n,r}(z)$ when $m>r>n$	$Q_{m,n,r}(z)$ when $r>m>n$
A	n-triangle	n-triangle
B	$(m-r-1)$-triangle	$(r-m)$-triangle

TABLE 3.12: Blocks formed when $m>r>n$ or $r>m>n$.

Block	$Q_{m,n,r}(z)$ when $m>n>r$	$Q_{m,n,r}(z)$ when $r>n>m$
A	r-triangle	m-triangle
B	$(m-n-1)$-triangle	$(r-n)$-triangle
C	$(n-r-1)$-triangle	$(n-m)$-triangle
D	$(r+1)\times(n-r)$ rectangle	$m\times(n-m)$ rectangle
E	$(n-r)\times(m-n)$ rectangle	$(n-m)\times(r-n)$ rectangle

TABLE 3.13: Blocks formed when $m>n>r$ or $r>n>m$.

We now investigate the blocks formed by the roots of $Q_{m,n,r}(z)$ when two parameters are equal. Figure 3.18 shows examples of blocks formed by the roots of $Q_{m,n,r}(z)$ when $m<n=r$, $m>n=r$ and $m=n>r$. The results in Tables 3.16-3.18 state the size of blocks when $m<n=r$, $m>n=r$ and $m=n>r$.

The plots in Figure 3.19 show examples of blocks formed by the roots of $Q_{m,n,r}(z)$ when $m=n<r$, $m=r>n$ and $n>r=m$. The size and shape of blocks formed

Block	$Q_{m,n,r}(z)$ when $n > m > r$
A	r-triangle
B	$(n-m)$-triangle
C	$(m-r-1)$-triangle
D	$(r+1)\times(m-r)$ rectangle
E	$(m-r-1)\times(n-m)$ rectangle
F	r-triangle when $n \geq m+r$
	$(n-m)\times r$ trapezoid when $n < m+r$
G	$(n-m)$-triangle when $n \leq m+r+1$
	$(r+1)\times(n-m)$ trapezoid when $n > m+r+1$

TABLE 3.14: Blocks formed when $n > m > r$.

Block	$Q_{m,n,r}(z)$ when $n > r > m$
A	m-triangle
B	$(n-r-1)$-triangle
C	$(r-m)$-triangle
D	$m\times(r-m)$ rectangle
E	$(r-m+1)\times(n-r)$ rectangle
F	m-triangle when $n \geq m+r$
	$(n-r)\times m$ trapezoid when $n < m+r$
G	$(n-r-1)$-triangle when $n \leq m+r+1$
	$m\times(n-r-1)$ trapezoid when $n > m+r+1$

TABLE 3.15: Blocks formed when $n > r > m$.

Block	$Q_{m,n,r}(z)$ with $m < n = r$
A	m-triangle
B	
C	$(n-m)$-triangle
D	$m\times(n-m)$-rectangle

TABLE 3.16: Blocks formed by the roots of $Q_{m,n,r}(z)$ when $m < n = r$.

Block	$Q_{m,n,r}(z)$ with $m > n = r$
A	n-triangle
B	$(m-n-1)$-triangle

TABLE 3.17: Blocks formed by the roots of $Q_{m,n,r}(z)$ when $m > n = r$.

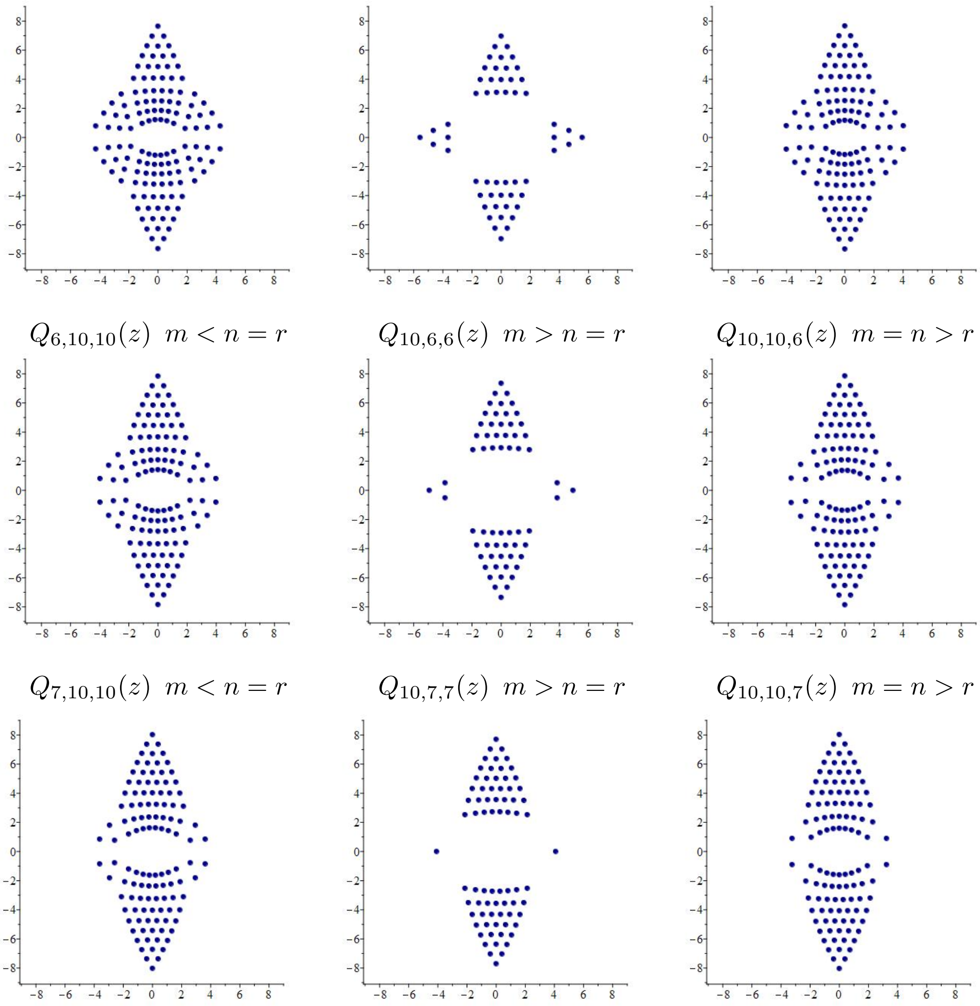

$Q_{6,10,10}(z)$ $m < n = r$ $Q_{10,6,6}(z)$ $m > n = r$ $Q_{10,10,6}(z)$ $m = n > r$

$Q_{7,10,10}(z)$ $m < n = r$ $Q_{10,7,7}(z)$ $m > n = r$ $Q_{10,10,7}(z)$ $m = n > r$

$Q_{8,10,10}(z)$ $m < n = r$ $Q_{10,8,8}(z)$ $m > n = r$ $Q_{10,10,8}(z)$ $m = n > r$

FIGURE 3.18: Plot of roots of $Q_{m,n,r}(z)$ with $m < n = r$, $m > n = r$ and $m = n > r$.

Block	$Q_{m,n,r}(z)$ with $m = n > r$
A	r-triangle
B	
C	$(n - r - 1)$-triangle
D	$(r + 1) \times (n - r)$-rectangle

TABLE 3.18: Blocks formed by the roots of $Q_{m,n,r}(z)$ when $m = n > r$.

when $m < n = r$ and when $m = r > n$ can clearly be seen in Figure 3.19. The size and shape of blocks when $m < n = r$ and $m = r > n$ can be found in Tables 3.19 and 3.20, respectively.

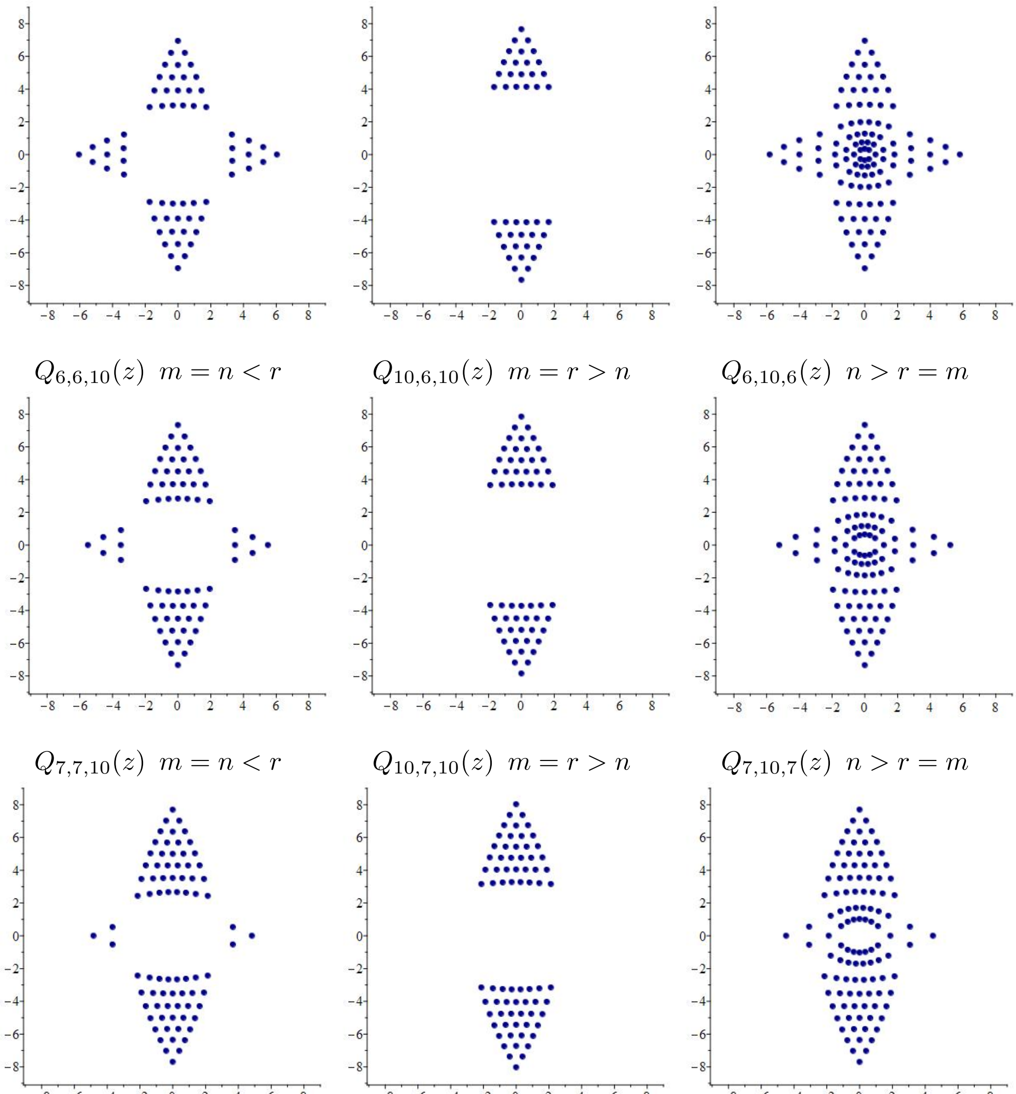

$Q_{6,6,10}(z)$ $m = n < r$ | $Q_{10,6,10}(z)$ $m = r > n$ | $Q_{6,10,6}(z)$ $n > r = m$

$Q_{7,7,10}(z)$ $m = n < r$ | $Q_{10,7,10}(z)$ $m = r > n$ | $Q_{7,10,7}(z)$ $n > r = m$

$Q_{8,8,10}(z)$ $m = n < r$ | $Q_{10,8,10}(z)$ $m = r > n$ | $Q_{8,10,8}(z)$ $n > r = m$

FIGURE 3.19: Plot of roots of $Q_{m,n,r}(z)$ with $m = n < r$, $m = r > n$ and $n > r = m$
.

Block	$Q_{m,n,r}(z)$ with $m = n < r$
A	m-triangle
B	$(r - m)$-triangle

TABLE 3.19: Blocks formed by the roots of $Q_{m,n,r}(z)$ when $m = n < r$.

Figure 3.19 shows that when $n > r = m$ blocks F and G are non-empty. Further investigation shows that when $n > r = m$, block F is triangle of size m when $n \geq 2m$ and a trapezoid of size $(n - m) \times m$ when $n > 2m$. Similarly, block G is

Block	$Q_{m,n,r}(z)$ with $m = r > n$
A	n-triangle

TABLE 3.20: Blocks formed by the roots of $Q_{m,n,r}(z)$ when $m = r > n$.

triangle of size $n-m-1$ when $n \leq 2m+1$, and a trapezoid of size $m \times (n-m-1)$ when $n > 2m+1$. Similar to when all parameters are non-equal and n is the largest parameter, when $n > r = m$, the shape of blocks F and G depend on the size of n, $m+r$ and $m+r+1$. The size and shape of blocks formed by the roots of $Q_{m,n,r}(z)$ when $n > r = m$ can be found in Table 3.21.

Block	$Q_{m,n,r}(z)$ with $n > r = m$
A	m-triangle
B	$(n-m-1)$-triangle
C	
D	
E	$1 \times (n-m)$ rectangle
F	m-triangle when $n \geq 2m$ $(n-m) \times m$ trapezoid when $n < 2m$
G	$(n-m-1)$-triangle when $n \leq 2m+1$ $m \times (n-m-1)$ trapezoid when $n > 2m+1$

TABLE 3.21: Blocks formed by the roots of $Q_{m,n,r}(z)$ when $n > r = m$.

We have determined the blocks formed by the roots of $Q_{m,n,r}(z)$ for all thirteen parameter conditions of m, n and r. The plots show that the blocks formed when two or more parameters are equal can be described by the blocks formed when parameters are non-equal. In other words, the results in Tables 3.12-3.15 describe the size and shape of blocks formed by the roots of $Q_{m,n,r}(z)$ for all thirteen parameter conditions. By introducing the terms a, b and c the size of blocks in Tables 3.12-3.15 can be simplified (as shown in Tables 3.22− 3.24). Let a denote the smallest parameter of $Q_{m,n,r}(z)$, let b denote the difference between the largest and second largest parameter and c denote the difference between the second largest and smallest parameter.

Block	block size when $m \geq r \geq n$	block size when $r \geq m \geq n$
A	a	a
B	$b-1$	b

TABLE 3.22: Size of blocks when $m \geq r \geq n$ or $r \geq m \geq n$.

Block	block size when $m \geq n \geq r$	block size when $r \geq n \geq m$
A	a	a
B	$b-1$	b
C	$c-1$	c
D	$(a+1)\times c$	$a \times c$
E	$c \times b$	$c \times b$

TABLE 3.23: Size of blocks when $m \geq n \geq r$ or $r \geq n \geq m$.

Block	block size when $n \geq r \geq m$	block size when $n \geq m \geq r$
A	a	a
B	$b-1$	b
C	c	$c-1$
D	$a \times c$	$(a+1)\times c$
E	$(c+1)\times b$	$(c-1)\times b$
F	$n \geq m+r$ block size is a $n < m+r$ block size is $b \times a$	$n \geq m+r$ block size is a $n < m+r$ block size is $b \times a$
G	$n \leq m+r+1$ block size is $b-1$ $n > m+r+1$ block size is $a \times (b-1)$	$n \leq m+r+1$ block size is b $n > m+r+1$ block size is $(a+1)\times b$

TABLE 3.24: Size of blocks when $n \geq r \geq m$ or $n \geq m \geq r$.

By introducing the terms

$$\gamma = \begin{cases} 0 & \text{when } r \geq m \\ 1 & \text{when } r < m, \end{cases} \tag{3.6}$$

$$\delta = \begin{cases} 0 & \text{when } r < m \\ 1 & \text{when } r \geq m, \end{cases} \tag{3.7}$$

$$\zeta = \begin{cases} -1 & \text{when } r < m \\ 1 & \text{when } r \geq m \ , \end{cases} \tag{3.8}$$

the results in Tables 3.22−3.24 can be further simplified to the results in Table 3.25.

Block	largest parameter	second largest parameter	smallest parameter
A	a	a	a
B	$b-\delta$	$b-\gamma$	$b-\gamma$
C	$c-\gamma$	$c-\gamma$	
D	$(a+\gamma)\times c$	$(a+\gamma)\times c$	
E	$(c+\zeta)\times b$	$c\times b$	
F	$n \geq m+r$ block size is a $n < m+r$ block size is $b\times a$		
G	$n \leq m+r+1$ block size is $b-\delta$ $n > m+r+1$ block size is $(a+\gamma)\times(b-\delta)$		

TABLE 3.25: Size of blocks formed by the roots of $Q_{m,n,r}(z)$ when n is the largest, second largest and smallest parameter. The term a denotes the smallest parameter, b denotes the difference between the largest and second largest parameter and c denotes the difference between the second largest and smallest parameter. The constants γ, δ and ζ are defined in (3.6)-(3.8).

3.2 The partition λ associated with $Q_{m,n,r}(z)$

Our aim is to determine the explicit form of the partition λ of $Q_{m,n,r}(z)$ and its conjugate partition λ^*. The motivation for studying the partitions is to explore how aspects of these partitions play a role in properties of $Q_{m,n,r}(z)$. Once we have the explicit form of λ we can find its conjugate partition λ^* using the Young diagram of λ. Towards the end of this chapter we determine the 2-core and 2-quotient of the partition λ of $Q_{m,n,r}(z)$. For convenience, we introduce the notation $\lambda_{m,n,r}(z)$ to denote the partitions associated with $Q_{m,n,r}(z)$, and and $\lambda^*_{m,n,r}(z)$ to denote the conjugate of and $\lambda_{m,n,r}(z)$.

3.2.1 The partition λ

We are interested in the partition λ of

$$Q_{m,n,r}(z) = c_{m,n,r}\mathcal{W}\Big(\big\{\mathrm{He}_{1+4j}(z)\big\}_{j=0}^{m-1}\,;\,\big\{\mathrm{He}_{2+4j}(z)\big\}_{j=0}^{n-1}\,;\,\big\{\mathrm{He}_{3+4j}(z)\big\}_{j=0}^{r-1}\Big). \tag{3.9}$$

The parts λ_j, in the partition λ of the Wronskian, $\mathcal{W}(f_{n_1}, f_{n_2}, \dots, f_{n_\ell})$ are defined as

$$\lambda_j = n_j + j - \ell. \tag{3.10}$$

By the definition of λ the associated degree vector of $\lambda_{m,n,r}$, $n_\lambda = (n_1, n_2, \dots, n_\ell)$, where $n_1, n_2, \dots, n_\ell$ are the degrees of the Hermite polynomials in (3.9), ordered from large to small.

Theorem 29. *When all parameters are equal*

$$\lambda_{n,n,n} = \left(\left\{(j)^3\right\}_{j=1}^{n}\right).$$

Proof. The 4-Okamoto polynomial

$$Q_{n,n,n}(z) = c_{n,n,n}\mathcal{W}\Big(\big\{\mathrm{He}_{1+4j}(z)\big\}_{j=0}^{n-1}\,;\,\big\{\mathrm{He}_{2+4j}(z)\big\}_{j=0}^{n-1}\,;\,\big\{\mathrm{He}_{3+4j}(z)\big\}_{j=0}^{n-1}\Big),$$

therefore, the associated degree vector of $\lambda_{n,n,n}$ is

$$n_\lambda = (4n-1, 4n-2, 4n-3, 4n-5, 4n-6, \dots, 3, 2, 1).$$

It follows from (3.10) that

$$\lambda_{n,n,n} = \big(n, n, n, n-1, n-1, n-1, \ldots, 1, 1, 1\big).$$

□

Theorem 30. *When $m > n$ the partition*

$$\lambda_{m,n,n} = \left(\left\{n + 3j - 2\right\}_{j=1}^{m-n}; \left\{(j)^3\right\}_{j=1}^{n}\right).$$

Proof. The 4-Okamoto polynomial $Q_{m,n,n}(z)$ is defined as

$$Q_{m,n,n}(z) = c_{m,n,n}\mathcal{W}\Big(\left\{\mathrm{He}_{1+4j}(z)\right\}_{j=0}^{m-1}; \left\{\mathrm{He}_{2+4j}(z)\right\}_{j=0}^{n-1}; \left\{\mathrm{He}_{3+4j}(z)\right\}_{j=0}^{n-1}\Big). \tag{3.11}$$

Therefore, when $m > n$ the associated degree vector of $\lambda_{m,n,n}$ with $m > n$ is

$$n_\lambda = \big(4m-3, 4m-7, \ldots, 4n+1, 4n-1, 4n-2, 4n-3, 4n-5, \ldots, 3, 2, 1\big),$$

and the partition

$$\lambda_{m,n,n} = \big(3m-2n-2, 3m-2n-5, \ldots, n+1, n, n, n, n-1, \ldots, 1, 1, 1\big).$$

□

Theorem 31. *When $n > m$ the partition*

$$\lambda_{m,n,n} = \left(\left\{\left(m + 2j\right)^2\right\}_{j=1}^{n-m}; \left\{(j)^3\right\}_{j=1}^{m}\right).$$

Proof. The polynomial $Q_{m,n,n}(z)$ is defined by (3.11). When the parameter $n > m$ the degree vector associated with $\lambda_{m,n,n}$ is

$$n_\lambda = \big(4n-1, 4n-2, 4n-5, 4n-6, \ldots, 4m+2, 4m-1, 4m-2, 4m-3, \ldots, 3, 2, 1\big).$$

It follows from (3.10) that when $n > m$ the partition

$$\lambda_{m,n,n} = \big(2n-m, 2n-m, 2n-m-2, 2n-m-2, \ldots, m+2, m+2, m, m, m, \ldots, 1, 1, 1\big).$$

$\square$

Theorem 32. *When $m > n > r$ the partition*

$$\lambda_{m,n,r} = \left(\left\{2n-r+3j-2\right\}_{j=1}^{m-n}; \left\{\big(r+2j-1\big)^2\right\}_{j=1}^{n-r}; \left\{(j)^3\right\}_{j=1}^{r}\right).$$

Proof. When $m > n > r$ the degree vector associated with $\lambda_{m,n,r}$ is

$$\begin{aligned} n_\lambda \;&=\; \big(4m-3, 4m-7, \ldots, 4n+1, 4n-2, 4n-3, 4n-6, 4n-7, \ldots, 4r+2,\\ &\qquad 4r+1, 4r-1, 4r-2, 4r-3, 4r-5, \ldots, 3, 2, 1\big). \end{aligned}$$

Therefore, when $m > n > r$ the partition

$$\begin{aligned} \lambda_{m,n,r} \;&=\; \big(3m-n-r-2, 3m-n-r-5, \ldots, 2n-r+1, 2n-r-1, 2n-r-1,\\ &\qquad 2n-r-3, 2n-3-r, \ldots, r+1, r+1, r, r, r, \ldots, 1, 1, 1\big). \end{aligned}$$

$\square$

Theorem 33. *The partition $\lambda_{m,n,r}(z)$ for all thirteen parameter conditions of m, n and r can be found in Table 3.26.*

Proof. Similar to the proof of Theorem 29-32. $\square$

case no.	condition	partition $\lambda_{m,n,r}$
1	$m > n > r$	$\left(\left\{2n-r+3j-2\right\}_{j=1}^{m-n};\left\{(r+2j-1)^2\right\}_{j=1}^{n-r};\left\{(j)^3\right\}_{j=1}^{r}\right)$
2	$n > m = r$	$\left(\left\{r+3j-1\right\}_{j=1}^{n-r};\left\{(j)^3\right\}_{j=1}^{r}\right)$
3	$m = n > r$	$\left(\left\{(r+2j-1)^2\right\}_{j=1}^{n-r};\left\{(j)^3\right\}_{j=1}^{r}\right)$
4	$n > r > m$	$\left(\left\{2r-m+3j-1\right\}_{j=1}^{n-r};\left\{(m+2j)^2\right\}_{j=1}^{r-m};\left\{(j)^3\right\}_{j=1}^{m}\right)$
5	$n > m > r$	$\left(\left\{2m-r+3j-1\right\}_{j=1}^{n-m};\left\{(r+2j-1)^2\right\}_{j=1}^{m-r};\left\{(j)^3\right\}_{j=1}^{r}\right)$
6	$m > n = r$	$\left(\left\{n+3j-2\right\}_{j=1}^{m-n};\left\{(j)^3\right\}_{j=1}^{n}\right)$
7	$m = n = r$	$\left(\left\{(j)^3\right\}_{j=1}^{n}\right)$
8	$n = r > m$	$\left(\left\{(m+2j)^2\right\}_{j=1}^{n-m};\left\{(j)^3\right\}_{j=1}^{m}\right)$
9	$r > n > m$	$\left(\left\{2n-m+3j\right\}_{j=1}^{r-n};\left\{(m+2j)^2\right\}_{j=1}^{n-m};\left\{(j)^3\right\}_{j=1}^{m}\right)$
10	$m > r > n$	$\left(\left\{2r-n+3j-2\right\}_{j=1}^{m-r};\left\{n+j\right\}_{j=1}^{2r-2n};\left\{(j)^3\right\}_{j=1}^{n}\right)$
11	$r > m > n$	$\left(\left\{2m-n+3j\right\}_{j=1}^{r-m};\left\{n+j\right\}_{j=1}^{2m-2n};\left\{(j)^3\right\}_{j=1}^{n}\right)$
12	$r > n = m$	$\left(\left\{n+3j\right\}_{j=1}^{r-n};\left\{(j)^3\right\}_{j=1}^{n}\right)$
13	$m = r > n$	$\left(\left\{n+j\right\}_{j=1}^{2m-2n};\left\{(j)^3\right\}_{j=1}^{n}\right)$

TABLE 3.26: The partition $\lambda_{m,n,r}$ for all thirteen parameter conditions of m, n and r.

The partitions in Table 3.26 are unordered, since the upper limit of each sequence in Table 3.26 gives the largest term of the sequence, and the lower limit i.e. $j = 1$ gives the smallest term of each sequence. A comparison of the results in Table 3.26 shows that all partitions contain "triple" terms, i.e. of the form $(x)^3$, where x is a positive integer. Similarly, all partitions in Table 3.26 contain "single" terms, i.e. of the form x, and only some contain "double" terms, i.e. of the form $(x)^2$. A comparison of the sequences in Table 3.26 shows that the upper limit of each sequence can be described by the relative size of m, n and r. Similarly, each sequence in Table 3.26 can be expressed in terms of the relative size of m, n and r. Let a denote the smallest parameter, let b denote the difference between the largest and second largest parameter, and c denotes the difference between the second largest and smallest parameter, out of m, n and r. The results in Table 3.26 can be simplified to Table 3.27.

case no.	condition	partition $\lambda_{m,n,r}$
1	$m > n > r$	$\left(\left\{2c+a-2+3j\right\}_{j=1}^{b}; \left\{(a-1+2j)^2\right\}_{j=1}^{c}; \left\{(j)^3\right\}_{j=1}^{a}\right)$
2	$n > m = r$	$\left(\left\{a-1+3j\right\}_{j=1}^{b}; \left\{(j)^3\right\}_{j=1}^{a}\right)$
3	$m = n > r$	$\left(\left\{(a-1+2j)^2\right\}_{j=1}^{c}; \left\{(j)^3\right\}_{j=1}^{a}\right)$
4	$n > r > m$	$\left(\left\{2c+a-1+3j\right\}_{j=1}^{b}; \left\{(a+2j)^2\right\}_{j=1}^{c}; \left\{(j)^3\right\}_{j=1}^{a}\right)$
5	$n > m > r$	$\left(\left\{2c+a-1+3j\right\}_{j=1}^{b}; \left\{(a-1+2j)^2\right\}_{j=1}^{c}; \left\{(j)^3\right\}_{j=1}^{a}\right)$
6	$m > n = r$	$\left(\left\{a-2+3j\right\}_{j=1}^{b}; \left\{(j)^3\right\}_{j=1}^{a}\right)$
7	$m = n = r$	$\left(\left\{(j)^3\right\}_{j=1}^{a}\right)$
8	$n = r > m$	$\left(\left\{(a+2j)^2\right\}_{j=1}^{c}; \left\{(j)^3\right\}_{j=1}^{a}\right)$
9	$r > n > m$	$\left(\left\{2c+a+3j\right\}_{j=1}^{b}; \left\{(a+2j)^2\right\}_{j=1}^{c}; \left\{(j)^3\right\}_{j=1}^{a}\right)$
10	$m > r > n$	$\left(\left\{2c+a-2+3j\right\}_{j=1}^{b}; \left\{a+j\right\}_{j=1}^{2c}; \left\{(j)^3\right\}_{j=1}^{a}\right)$
11	$r > m > n$	$\left(\left\{2c+a+3j\right\}_{j=1}^{b}; \left\{a+j\right\}_{j=1}^{2c}; \left\{(j)^3\right\}_{j=1}^{a}\right)$
12	$r > n = m$	$\left(\left\{a+3j\right\}_{j=1}^{b}; \left\{(j)^3\right\}_{j=1}^{a}\right)$
13	$m = r > n$	$\left(\left\{a+j\right\}_{j=1}^{2c}; \left\{(j)^3\right\}_{j=1}^{a}\right)$

TABLE 3.27: The partition $\lambda_{m,n,r}$ for all thirteen parameter conditions of m, n and r. The term a denotes the smallest parameter, b denotes the difference between the largest and second largest parameter, and c denotes the difference between the second largest and smallest parameter out of m, n and r.

A comparison of the partitions in Table 3.27 shows that that $\lambda_{m,n,r}$ when two or more parameters are equal is consistent with the partition $\lambda_{m,n,r}$ when no parameters are equal. For example, if we consider the partition $\lambda_{m,n,r}$ for cases 1, 3, and 6. It is clear to see that the the partition for case 3 can be obtained from the partition for case 1 by setting $b = 0$. Similarly, the case 6 partition can be obtained from the case 1 partition by setting $c = 0$. The case 6 partition can also be obtained from the case 9 partition by setting $c = 0$. In other words, $\lambda_{m,n,r}(z)$ when two or more parameters are equal parameters can be obtained from $\lambda_{m,n,r}(z)$ where no parameters are equal, by setting the term b and or c to equal zero. This means the partitions in Table 3.27 for cases 1,4,5,9,10 and 11, covers all thirteen parameter conditions of $\lambda_{m,n,r}$. Therefore, we will focus on these six cases of $\lambda_{m,n,r}$. A comparison of the partitions $\lambda_{m,n,r}$ when parameters are not equal, shows that when n is the smallest parameter (i.e. cases 10 and 11) $\lambda_{m,n,r}$ does not contain any double terms and instead, contain two sequences of single terms and one sequence of triple terms. However, when parameters are not equal and n is not the smallest parameter (i.e. cases 1,4,5 and 9) $\lambda_{m,n,r}$ contains a sequence of single, double and triple terms. By introducing the terms $\widetilde{\beta}$ and $\widetilde{\gamma}$ defined in (3.12) and (3.13), the partitions in in Table 3.27 can be further simplified to Theorem 34.

Theorem 34. *Let a denote the smallest parameter, b denote the difference between the largest and second largest parameter, and c denote the difference between the second largest and smallest parameter out of m, n and r. When n is the smallest parameter the partition*

$$\lambda_{m,n,r} = \left(\left\{a + 2c - \widetilde{\beta} + 3j\right\}_{j=1}^{b}; \left\{a + j\right\}_{j=1}^{2c}; \left\{(j)^3\right\}_{j=1}^{a}\right),$$

and when n is not the smallest parameter

$$\lambda_{m,n,r} = \left(\left\{a + 2c - \widetilde{\beta} + 3j\right\}_{j=1}^{b}; \left\{\left(a - \widetilde{\gamma} + 2j\right)^2\right\}_{j=1}^{c}; \left\{(j)^3\right\}_{j=1}^{a}\right).$$

Where the term

$$\widetilde{\beta} = \begin{cases} 0 & \textit{when } r \textit{ is the largest parameter,} \\ 1 & \textit{when } n \textit{ is the largest parameter,} \\ 2 & \textit{when } m \textit{ is the largest parameter,} \end{cases} \tag{3.12}$$

and

$$\widetilde{\gamma} = \begin{cases} 0 & \textit{when } r > m, \\ 1 & \textit{when } m > r. \end{cases} \tag{3.13}$$

We have determined the explicit form of the partition $\lambda_{m,n,r}$ for all thirteen parameter conditions of m, n and r. Our aim is to now determine the explicit form the conjugate partition $\lambda^*_{m,n,r}$ using the Young diagram of $\lambda_{m,n,r}$.

We first discuss the Young diagram of $\lambda_{m,n,r}$. Earlier we discussed that $\lambda_{m,n,r}$ consists of single, double and or triple terms (see Table 3.26). This means the Young diagrams of $\lambda_{m,n,r}$ will consist of single rows, i.e. consecutive rows that are different in length, double rows, i.e. two consecutive rows of the same length, and triple rows i.e. three consecutive rows of the same length. Table 3.26 tells us that the Young diagram of $\lambda_{m,n,r}$ for all parameter conditions will contain a sets of triple rows i.e. $3a$ rows that form a total of a triple rows. The partitions $\lambda_{m,n,r}$ in Table 3.26 tell us that when two parameters are equal, the Young diagram of $\lambda_{m,n,r}$ consists of single and triple rows or double and triple rows. The partition $\lambda_{n,n,n}$ in Table 3.26 tells us that the Young diagram of $\lambda_{n,n,n}$ consists of a sets of triple rows. Earlier we discussed that $\lambda_{m,n,r}$ where two or more parameters are equal can be obtained from $\lambda_{m,n,r}$ where no parameters are equal. Therefore, we will be focusing on the partitions $\lambda_{m,n,r}$ where parameters are not equal.

Remark 9. When parameters are not equal and n is not the smallest parameter

$$\lambda_{m,n,r} = \left(\left\{ a + 2c - \widetilde{\beta} + 3j \right\}_{j=1}^{b}; \left\{ \left(a - \widetilde{\gamma} + 2j\right)^2 \right\}_{j=1}^{c}; \left\{ (j)^3 \right\}_{j=1}^{a} \right), \tag{3.14}$$

where $\widetilde{\beta}$ and $\widetilde{\gamma}$ are defined in (3.12) and (3.13). When this is the case, the Young diagram of $\lambda_{m,n,r}$ consists of single, double and triple rows. It follows from (3.14) that the Young diagram of $\lambda_{m,n,r}(z)$ consists of b single rows, c sets of double rows, i.e. $2c$ rows that form c double rows, and a sets of triple rows, i.e. $3a$ rows that form a triple row. Row b of the Young diagram of $\lambda_{m,n,r}$ (defined in (3.14)) is simply the shortest single row of the diagram and row $b+2c-1$ and $b+2c$ together form the shortest double row of the Young diagram.

Figure 3.20 shows examples of Young diagrams of $\lambda_{m,n,r}$ given by (3.14). The Young diagrams in Figure 3.20 all consist of three single rows, two sets of double rows and one set of triple rows. This tells us that $b=3$, $c=2$ and $a=1$ for each $\lambda_{m,n,r}$ in Figure 3.20.

Remark 10. When parameters are not equal and n is the smallest parameter

$$\lambda_{m,n,r} = \left(\left\{ a + 2c - \widetilde{\beta} + 3j \right\}_{j=1}^{b}; \left\{ a + j \right\}_{j=1}^{2c}; \left\{ (j)^3 \right\}_{j=1}^{a} \right), \tag{3.15}$$

where $\widetilde{\beta}$ and $\widetilde{\gamma}$ are defined in (3.12) and (3.13). When this is the case the Young diagram of $\lambda_{m,n,r}$ consists of single and triple rows and does not consist of any double rows. It follows from (3.15) that the Young diagram of $\lambda_{m,n,r}(z)$ consists of b single rows where consecutive rows decrease in length by three and $2c$ single rows where consecutive rows decrease in length by two. The Young diagram also consists of a sets of triple rows. Row b of the Young diagram of $\lambda_{m,n,r}$ (defined in (3.15) is the shortest single row such that row b is shorter than row $b-1$ by three boxes. Row $b+2c$ is simply the shortest single row of the Young diagram of $\lambda_{m,n,r}$ defined in (3.15).

Figure 3.21 shows examples of Young diagrams of $\lambda_{m,n,r}$ given by (3.15). Both Young diagrams in Figure 3.21 consist of three single rows where consecutive rows decrease in length by three, four single rows where consecutive rows decrease in length by one, and one set of triple rows. This tells us that $b=3$, $c=2$ and $a=1$ for both $\lambda_{m,n,r}$ in Figure 3.21.

$m > n > r$ $\quad$ $n > r > m$

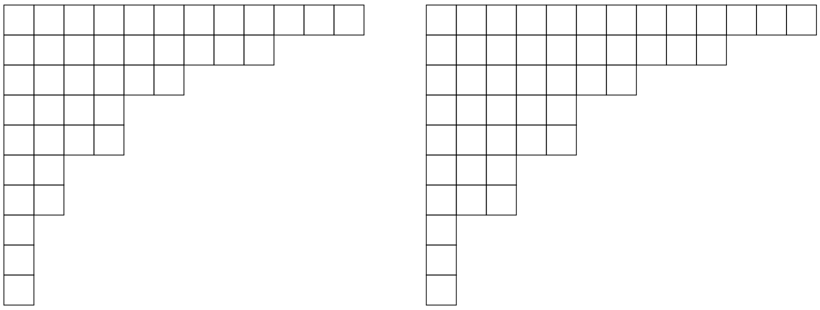

$\lambda_{6,3,1} = (12, 9, 6, 4^2, 2^2, 1^3)$ $\quad$ $\lambda_{1,6,3} = (13, 10, 7, 5^2, 3^2, 1^3)$

$n > m > r$ $\quad$ $r > n > m$

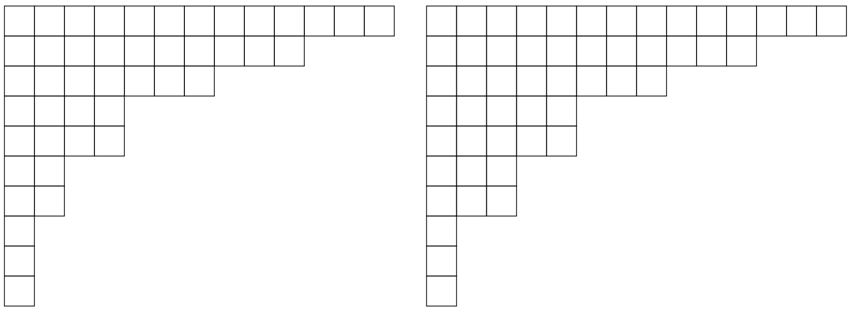

$\lambda_{3,6,1} = (13, 10, 7, 4^2, 2^2, 1^3)$ $\quad$ $\lambda_{1,3,6} = (14, 11, 8, 5^2, 3^2, 1^3)$

FIGURE 3.20: Examples of $\lambda_{m,n,r}$ and the Young diagram of $\lambda_{m,n,r}$. The parameters m, n and r are not equal and n is not the smallest parameter.

It follows from (3.15) in Remark 10 that the difference between row b and $b+1$ of the Young diagram of $\lambda_{m,n,r}(z)$ is one when $m > r > n$, and three when $r > m > n$. The difference between row $b + 2c$ and row $b + 2c + 1$ is one for both cases. This tells us that if a Young diagram consists of single and triple rows with no double rows we can determine whether the parameter condition of $\lambda_{m,n,r}$ is $m > r > n$ or $r > m > n$ by looking at the difference in length between row b and row $b+1$. Table 3.28 outlines the difference in length between row b and row $b + 1$ when $m > r > n$ and when $r > m > n$.

Figure 3.23 shows the Young diagrams in Figure 3.21 with coloured boxes to

$m > r > n$ $\qquad\qquad$ $r > m > n$

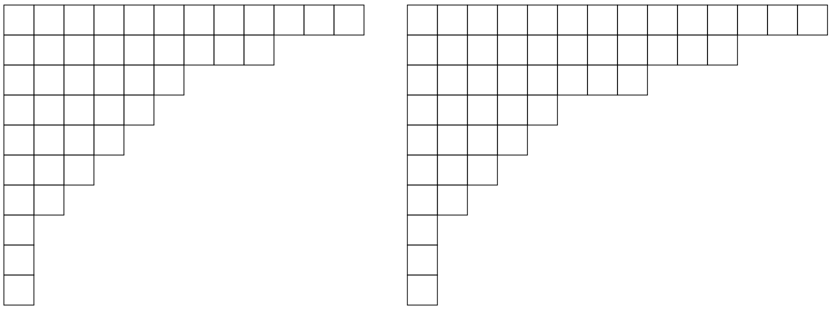

$\lambda_{6,1,3} = (12, 9, 6, 5, 4, 3, 2, 1^3)$ $\quad$ $\lambda_{3,1,6} = (14, 11, 8, 5, 4, 3, 2, 1^3)$

FIGURE 3.21: Examples of $\lambda_{m,n,r}$ and the Young diagram of $\lambda_{m,n,r}$. The parameters m, n and r are not equal and n is the smallest parameter.

case no	parameter condition	row b and $b + 1$
10	$m > r > n$	1
11	$r > m > n$	3

TABLE 3.28: Difference in length between row b and $b+1$ of the Young diagram of $\lambda_{m,n,r}$ when $m > r > n$ or $r > m > n$. When parameters are not equal and n is the smallest parameter, row b is the shortest single row such that row b is shorter than row $b - 1$ by three boxes.

highlight the difference in length between row b and row $b + 1$. Figure 3.23 shows the general form of the Young diagram of $\lambda_{m,n,r}$ when $m > r > n$ and when $r > m > n$.

It follows from Remark 9 that when parameters are not equal and n is not the smallest parameter, the difference in length between row b and $b + 1$ of the Young diagram of $\lambda_{m,n,r}$ defined in (3.14) is either two or three. Similarly, the difference between row $b + 2c$ and $b + 2c + 1$ of the Young diagram is either one or two. The results in Table 3.29 show that the combination of differences between row b and $b+1$ and row $b+2c$ and $b+2c+1$ is different for each of the four parameter cases in Table 3.29. Therefore, if the Young diagram of $\lambda_{m,n,r}(z)$ consists of single, double and triple rows Table 3.29 can be used as a criteria to determine the parameter condition of m, n and r.

$m > r > n$ $\qquad$ $r > m > n$

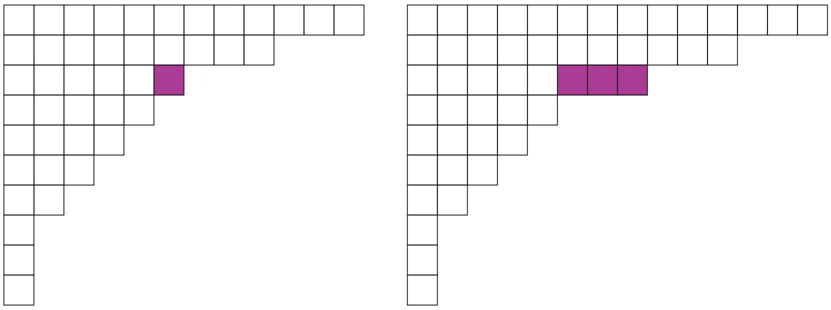

$\lambda_{6,1,3} = (12, 9, 6, 5, 4, 3, 2, 1^3)$ $\quad$ $\lambda_{3,1,6} = (14, 11, 8, 5, 4, 3, 2, 1^3)$

FIGURE 3.22: The Young diagrams in Figure 3.21 with coloured boxes. Row b of each diagram contains purple coloured boxes to highlight the difference in length between row b and row $b+1$. Row b of the Young digram when $m > r > n$ or $r > m > n$ is the shortest single row such that row b is shorter than row $b-1$ by three boxes.

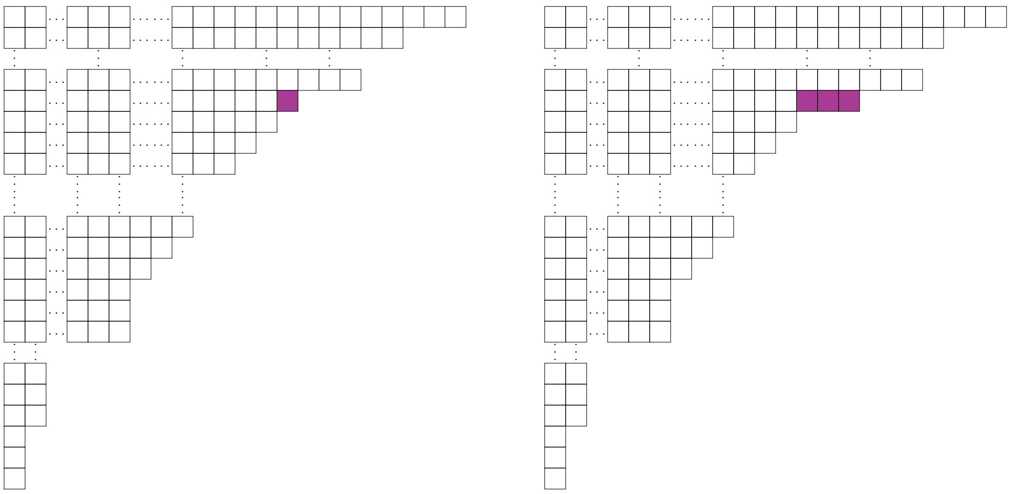

(A) $m > r > n$ $\qquad$ (B) $r > m > n$

FIGURE 3.23: The Young diagram of $\lambda_{m,n,r}$ when $m > r > n$ and $r > m > n$. Row b of both diagrams is the shortest single row such that row b is shorter than row $b-1$ by three boxes. The purple coloured boxes in row b highlight the difference in length between row b and row $b+1$.

Figure 3.24 shows the Young diagrams in 3.20 with the addition of coloured boxes to highlight the difference in length between between row b and $b+1$ and row $b+2c$ and $b+2c+1$. Figure 3.25 shows the general form of the Young diagram of $\lambda_{m,n,r}$ when $m > n > r$, $n > r > m$, $n > m > r$ and $r > n > m$.

case no	condition	row b and $b+1$	row $b+2c$ and $b+2c+1$
1	$m > n > r$	2	1
4	$n > r > m$	2	2
5	$n > m > r$	3	1
9	$r > n > m$	3	2

TABLE 3.29: Difference in length between row b and $b+1$ and row $b+2c$ and $b+2c+1$ of the Young diagram of $\lambda_{m,n,r}$. When parameters are not equal and n is not the smallest parameter, row b is simply the shortest single row of the diagram and row $b+2c-1$ and row $b+2c$ together form the shortest double row of the Young diagram.

To summarise, if the Young diagram of $\lambda_{m,n,r}(z)$ consists of single, double and triple rows, it follows from Remark 9 that the parameters m, n and r are not equal and n is not the smallest parameter. When this is the case, Table 3.29 can be used as a criteria to determine the parameter condition of m, n and r. If the Young diagram of $\lambda_{m,n,r}(z)$ consists of single rows where consecutive rows decrease in length by three and single rows where consecutive rows decrease in length by one and the Young diagram also consists of triple rows, it follows from Remark 10 that the parameters are not equal and n is the smallest parameter. This means the parameter condition of $\lambda_{m,n,r}(z)$ is either $m > r > n$ or $r > m > n$. We can distinguish between the two parameters cases using Table 3.28 as a criteria. The terms a, b and c can be found by determining the number of single, double and triple rows in the Young diagram of $\lambda_{m,n,r}$. We will discuss examples later in this chapter. To recap, the term a denotes the smallest parameter out of m, n and r, b denotes the difference between the largest and second largest parameter and c denotes the difference between the second largest and smallest parameter out of m, n and r.

3.2.2 The conjugate of λ

We have determined the explicit form of the partition $\lambda_{m,n,r}$ and the general form of the Young diagram of $\lambda_{m,n,r}$. Our aim is to now determine the explicit form of

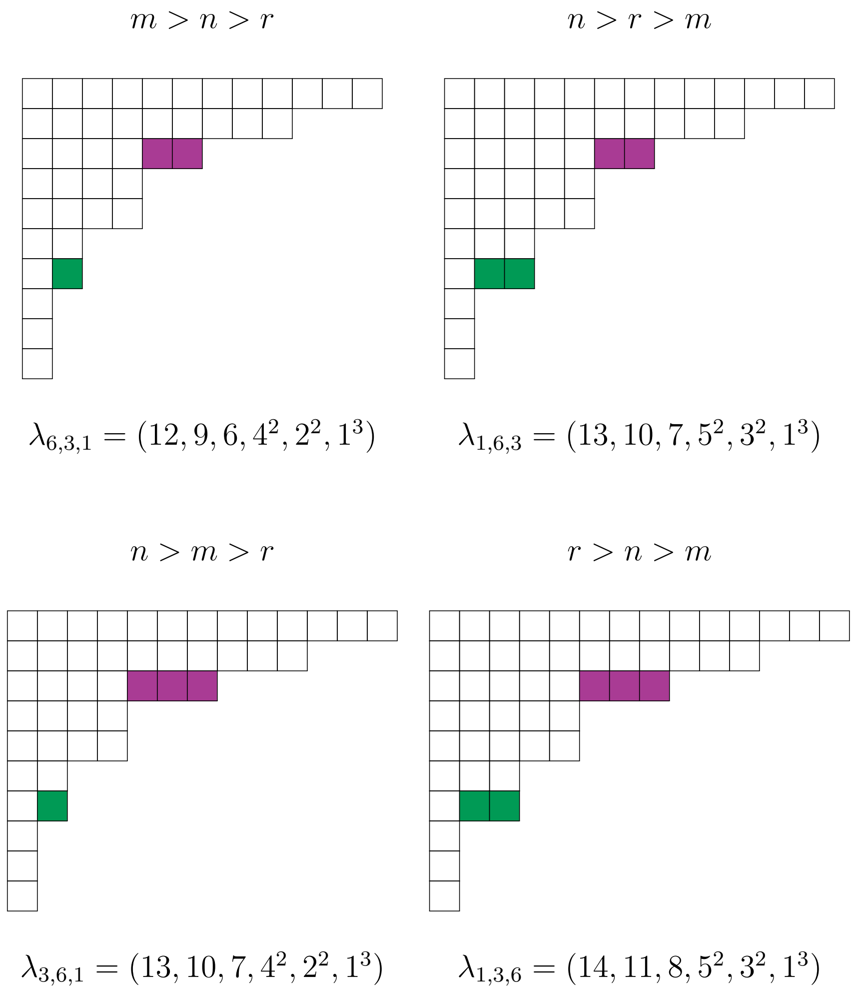

FIGURE 3.24: The Young diagrams in Figure 3.20 with coloured boxes. Row b of all four Young diagrams is the shortest single row of the diagram. The purple coloured boxes in row b highlight the difference in length between row b and row $b+1$. Row $b+2c-1$ and $b+2c$ together form the shortest double row of the Young diagram. Row $b+2c$ contains green coloured boxes to highlight the difference in length between row $b+2c$ and row $b+2c+1$.

the conjugate partition of $\lambda_{m,n,r}$.

Theorem 35. *When $r > n > m$ the conjugate partition of $\lambda_{m,n,r}$ is*

$$\lambda^*_{m,n,r} = \left(\left\{m + n - 3j + r + 3\right\}_{j=1}^{m}; \left\{(r - n + 2j)^2\right\}_{j=1}^{n-m}; \left\{(j)^3\right\}_{j=1}^{r-n}\right).$$

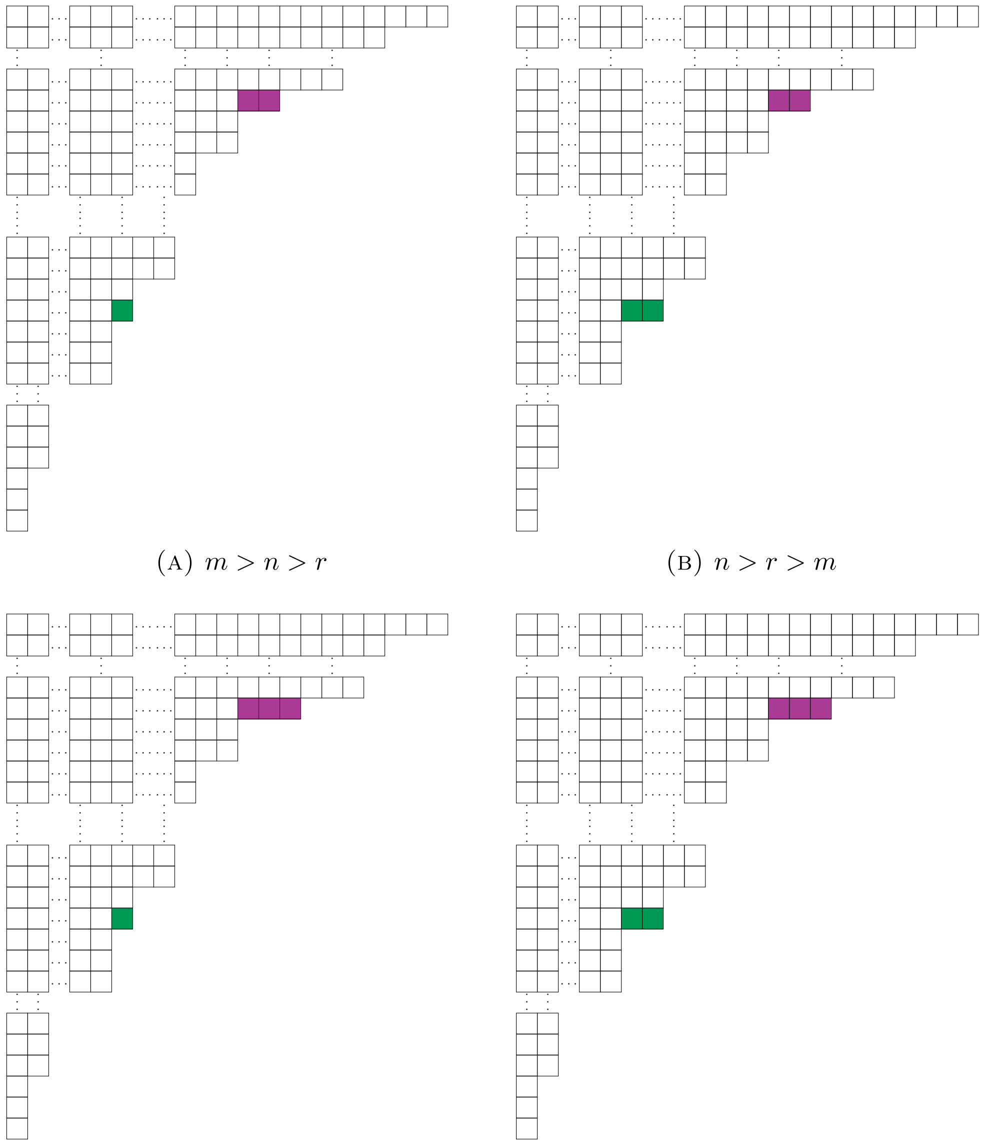

(A) $m > n > r$

(B) $n > r > m$

(C) $n > m > r$

(D) $r > n > m$

FIGURE 3.25: The Young diagram of $\lambda_{m,n,r}$ when $m > n > r$, $n > r > m$, $n > m > r$ and $r > n > m$. Row b is the shortest single row of the diagram and contains purple coloured boxes to highlight the difference in length between row b and row $b+1$. Row $b+2c-1$ and $b+2c$ together form the shortest double row of the Young diagram. Row $b+2c$ contains green coloured boxes to highlight the difference in length between row $b+2c$ and row $b+2c+1$.

Proof. The partition $\lambda_{m,n,r}$ when $r > n > m$ is

$$\lambda_{m,n,r} = \left(\left\{ 2n - m + 3j \right\}_{j=1}^{r-n}; \left\{ (m+2j)^2 \right\}_{j=1}^{n-m}; \left\{ (j)^3 \right\}_{j=1}^{m} \right).$$

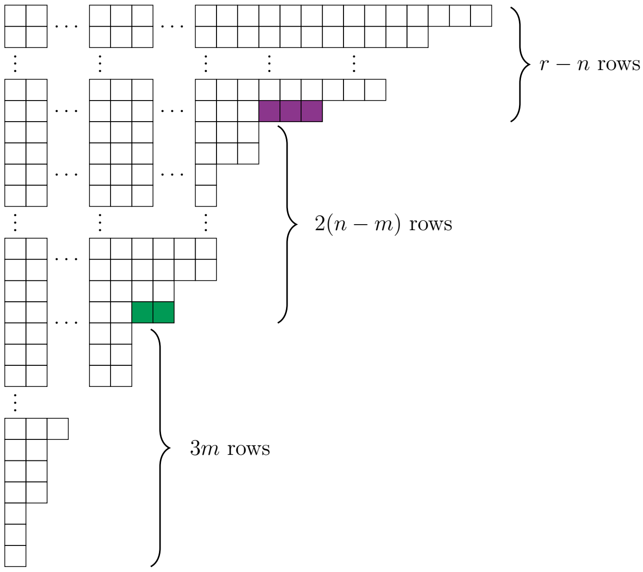

FIGURE 3.26: The Young diagram of $\lambda_{m,n,r}$ when $r > n > m$ shown in Figure 3.25. The brackets indicate the number of rows in the Young diagram.

Figure 3.26 shows the general Young diagram of $\lambda_{m,n,r}$ when $r > n > m$. Row b is the shortest single row of the diagram and is of length $2n - m + 3$. The purple coloured boxes in row b highlight the difference in length between row b and $b+1$. Row $b + 2c$ in Figure 3.26 is of length $m + 2$. The green coloured boxes in row $b + 2c$ highlight the difference in length between row $b + 2c$ and $b + 2c + 1$. Since the Young diagram of $\lambda_{m,n,r}$ consists of rows of length $2n - m + 3$ and $m + 2$, the Young diagram of $\lambda^*_{m,n,r}$ will consist of columns of length $2n - m + 3$ and $m + 2$ (as shown in Figure 3.27). The boxes outlined in purple and green in the Young diagram of $\lambda^*_{m,n,r}$ shown in Figure 3.27 indicate the position of the purple and green boxes in the Young diagram of $\lambda_{m,n,r}$ in Figure 3.26.

Since, the first column of the Young diagram of $\lambda_{m,n,r}$ in Figure 3.26 is of length $m + n + r$, it means the first row of the Young diagram of $\lambda^*_{m,n,r}$ is of length $m+n+r$. Figure 3.27 shows that the two rows containing a box outlined in green, are both of the same length i.e. both rows form a double row. Figure 3.27 shows

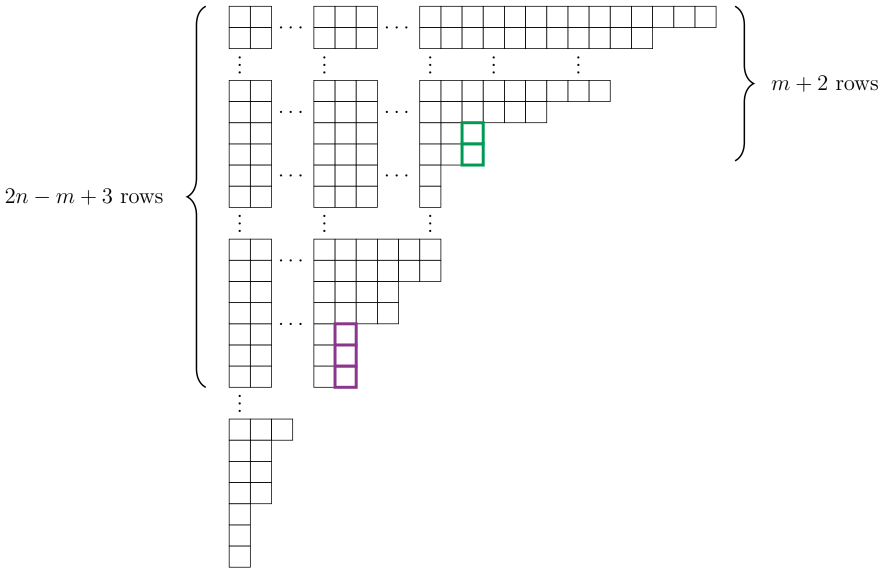

FIGURE 3.27: The Young diagram of $\lambda^*_{m,n,r}$ when $r > n > m$ with brackets indicating the number of rows.

that the Young diagram of $\lambda^*_{m,n,r}$ when $r > n > m$ consists of m single rows. The longest single row in Figure 3.27 is of length $m+n+r$ and consecutive single rows decrease in length by three. Therefore, the single rows in Figure 3.27 are of length

$$m + n - 3j + r + 3, \quad j = 1, 2, \ldots, m. \tag{3.16}$$

The first row of the Young diagram of $\lambda_{m,n,r}$ in Figure 3.26 is of length $3r-m-n$. This means the first column of the Young diagram of $\lambda^*_{m,n,r}$ in Figure 3.27 is of length $3r-m-n$. Therefore, the $3(r-n-1)$ rows below the three rows containing the boxes outlined in purple in Figure 3.27). Figure 3.27) shows that the three rows that contain the boxes outlined in purple are of the same length, i.e. all three rows form a triple row. Therefore, the Young diagram in Figure 3.27 consists of $3(r-n)$ rows that form triple rows. Figure 3.27 shows that the longest row to form a triple row is of length $r-n$ and the shortest row is of length one. Figure 3.27 shows the rows that form triple rows are of length

$$(j)^3, \quad j = 1, 2, \ldots, r - n.$$

So far, we have found that Figure 3.27 consists of m single row and $3(r-n)$ rows that form triple rows. Therefore, the remaining $2(n-m)$ rows must form double rows. We know that the rows in Figure 3.27 that contain the boxes outlined in purple are of length $r-n$. Figure 3.27 shows a difference of two boxes between the longest triple row and shortest double row. This tells us that the shortest row that form a double row is of length $r-n+2$. We know that there are $n-m$ double rows and that consecutive double rows decrease in length by two. It follows from Figure 3.27 that rows that form double rows in the Young diagram of $\lambda^*_{m,n,r}$ when $r>n>m$ are of length

$$(r-n+2j)^2, \quad j=1,2,\ldots,n-m.$$

□

Theorem 36. *When $m>r>n$ the conjugate partition of $\lambda_{m,n,r}$ is*

$$\lambda^*_{m,n,r} = \left(\left\{m+n-3j+r+3\right\}_{j=1}^{n+1};\left\{(m-r+j-1)\right\}_{j=1}^{2(r-n)};\left\{(j)^3\right\}_{j=1}^{m-r-1}\right).$$

Proof. The partition $\lambda_{m,n,r}$ when $m>r>n$ is

$$\lambda_{m,n,r} = \left(\left\{2r-n+3j-2\right\}_{j=1}^{m-r};\left\{n+j\right\}_{j=1}^{2(r-n)};\left\{(j)^3\right\}_{j=1}^{n}\right).$$

Figure 3.28 shows the general Young diagram of $\lambda_{m,n,r}$ when $m>r>n$. The Young diagram does not contain any double rows. Instead, the Young diagram in Figure 3.28 consists of $m-r$ single rows, where consecutive rows decrease in length by three, $2(r-n)$ single rows, where consecutive rows decrease in length by one, and $3n$ rows that form triple rows. Row b of the Young diagram in Figure 3.28 is of length $2r-n+1$ and contains the purple coloured box. Row $b+2c$ of the Young diagram is of length $n+1$ and contains the green coloured box.

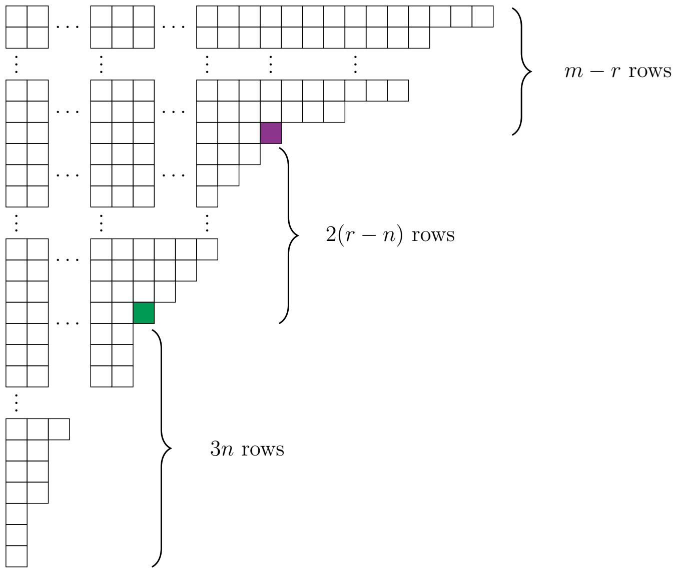

FIGURE 3.28: The Young diagram of $\lambda_{m,n,r}$ when $m > r > n$ shown in Figure 3.25. The brackets indicate the number of rows in the Young diagram.

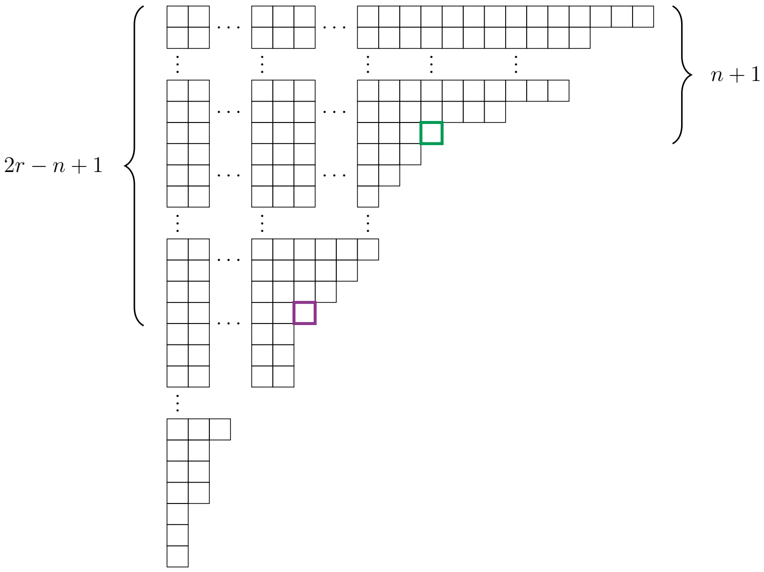

FIGURE 3.29: Young diagram of $\lambda^*_{m,n,r}$ when $m > r > n$ with brackets indicating the number of rows.

Figure 3.29 shows the Young diagram of $\lambda^*_{m,n,r}$ when $m > r > n$. Figure 3.29 shows that there are $n + 1$ single rows where consecutive rows decrease in length by three. The longest single row is of length $m+r+n$. Therefore, the single rows in Figure 3.29 where consecutive rows decrease in length by three are of length

$$m + n - 3j + r + 3, \quad j = 1, 2, \ldots, n + 1.$$

We know that the first column of the Young diagram $\lambda^*_{m,n,r}$ in Figure 3.29 is of length $3m - r - n - 2$. Hence, there must be $3(m - r - 1)$ rows below the row containing the box outlined in purple in Figure 3.29. Figure 3.29 shows that all the rows below the row containing the box outlined in purple form triple rows. Figure 3.29 shows that the rows that form triple rows are of length

$$(j)^3, \quad j = 1, 2, \ldots, m - r - 1.$$

So far, we know that the Young diagram in Figure 3.29 consists of $n + 1$ single rows, where consecutive rows decrease in length by three and $3(m - r - 1)$ rows that form triple rows. Therefore, the remaining $2(r-n)$ rows are single rows where consecutive rows decrease in length by one. The shortest row of this form is of length $m-r$. Therefore, the single rows where consecutive rows decrease in length by one are of length

$$m - r + j - 1, \quad j = 1, 2, \ldots, 2(r - n).$$

□

Theorem 37. *The conjugate partition of $\lambda_{n,n,n}$ is*

$$\lambda^*_{n,n,n} = \left(\left\{ 3n - 3j + 3 \right\}_{j=1}^{n} \right).$$

Proof. The partition

$$\lambda_{n,n,n} = \left(\left\{ (j)^3 \right\}_{j=1}^{n} \right).$$

Figure 3.30 shows the general Young diagram of the partition $\lambda_{n,n,n}$. The first column of the Young diagram in Figure 3.30 is of length $3n$, the second column is

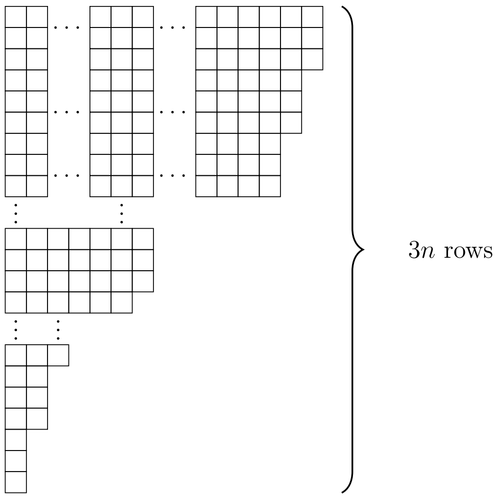

FIGURE 3.30: The Young diagram of $\lambda_{n,n,n}$. The bracket indicates the number of rows in the Young diagram.

of length $3n-3$ and so on. Therefore, the conjugate partition of $\lambda_{n,n,n}$ is

$$\lambda^*_{n,n,n} = \big(3n, 3n-3, 3n-6, \ldots, 3\big).$$

$\square$

Theorem 38. *The conjugate partition $\lambda^*_{m,n,r}$ of $\lambda_{m,m,r}$ for all thirteen parameter conditions of m, n and r are consistent with the results found in Table 3.30.*

Proof. Similar to the proof of Theorem 35−37. $\square$

The partitions in Table 3.30 can be expressed by the terms a, b and c. Where a denotes the smallest parameter, b denotes the difference between the largest and second largest parameter, and c denotes the difference between the second largest and smallest parameter. The partitions in Table 3.30 will be used later on in this chapter.

condition	$\lambda^*_{m,n,r}$
$m \geq n \geq r$	$\left(\left\{m+n-3j+r+3\right\}_{j=1}^{r+1}; \left\{\left(m-n+2j-2\right)^2\right\}_{j=1}^{n-r}; \left\{(j)^3\right\}_{j=1}^{m-n-1}\right)$
$n \geq r \geq m$	$\left(\left\{m+n-3j+r+3\right\}_{j=1}^{m}; \left\{\left(n-r-2j+2\right)^2\right\}_{j=1}^{r-m+1}; \left\{(j)^3\right\}_{j=1}^{n-r-1}\right)$
$n \geq m \geq r$	$\left(\left\{m+n-3j+r+3\right\}_{j=1}^{r+1}; \left\{\left(n-m+2j\right)^2\right\}_{j=1}^{m-r-1}; \left\{(j)^3\right\}_{j=1}^{n-m}\right)$
$r \geq n \geq m$	$\left(\left\{m+n-3j+r+3\right\}_{j=1}^{m}; \left\{\left(r-n+2j\right)^2\right\}_{j=1}^{n-m}; \left\{(j)^3\right\}_{j=1}^{r-n}\right)$
$m \geq r \geq n$	$\left(\left\{m+n-3j+r+3\right\}_{j=1}^{n+1}; \left\{\left(m-r+j-1\right)\right\}_{j=1}^{2(r-n)}; \left\{(j)^3\right\}_{j=1}^{m-r-1}\right)$
$r \geq m \geq n$	$\left(\left\{m+n-3j+r+3\right\}_{j=1}^{n}; \left\{\left(r-m+j\right)\right\}_{j=1}^{2(m-n)}; \left\{(j)^3\right\}_{j=1}^{r-m}\right)$

TABLE 3.30: The conjugate partition $\lambda^*_{m,n,r}$ of $\lambda_{m,n,r}$ for all parameter conditions of m, n and r.

3.2.3 The 2-core of λ

The explicit form of the partition $\lambda_{m,n,r}$ for all thirteen parameter conditions of m, n and r can be found in Table 3.26. The Maya diagram diagram of $\lambda_{m,n,r}$ can be found by placing beads and empty beads along the border of the Young diagram of $\lambda_{m,n,r}$. The Maya diagram of $\lambda_{m,n,r}$ will consist of empty beads in position $0 + 4j$ and beads in position $1 + 4j$, $2 + 4j$ and $3 + 4j$. Arranging the Maya digram of $\lambda_{m,n,r}$ from left to right onto a four runners gives the abacus display in Figure 3.31. Figure 3.31 shows that the first runner contains no beads, the second runner contains m beads, the third runner contains n beads and the fourth runner contains r beads.

Figure 3.31 shows that every bead in the 4-runner abacus display $\lambda_{m,n,r}$ has a bead directly above it. If an empty bead appeared above a bead in Figure 3.31 it tells us that $\lambda_{m,n,r}$ contains rim 4-hooks. Since, no beads appear above any of the beads it Figure 3.31, it shows that $\lambda_{m,n,r}$ does not contain any rim 4-hooks. Therefore, $\lambda_{m,n,r}$ is a 4-core partition for all parameters of m, n and r.

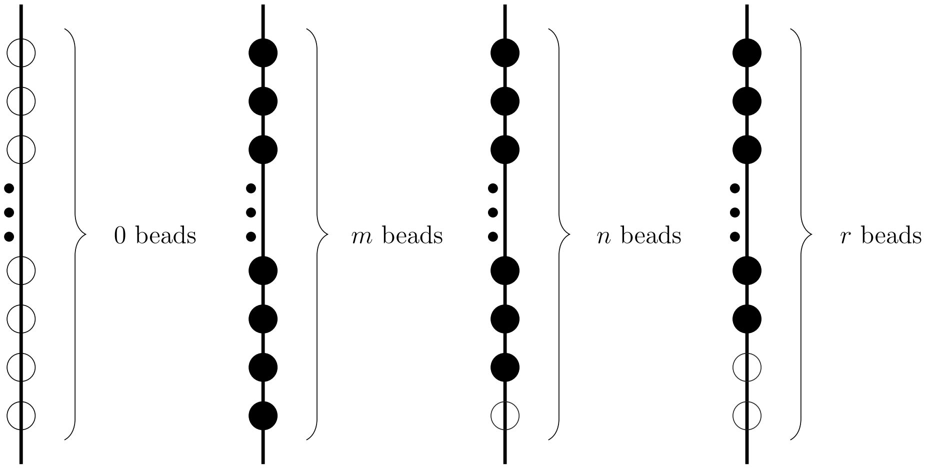

FIGURE 3.31: The 4-runner abacus display of $\lambda_{m,n,r}$.

Our aim is to determine the 2-core and 2-quotient of $\lambda_{m,n,r}$. Figure 3.32 shows the 2-runner abacus display of $\lambda_{m,n,r}$. Figure 3.32 is the result of arranging all beads and empty beads in Figure 3.31 onto two runners.

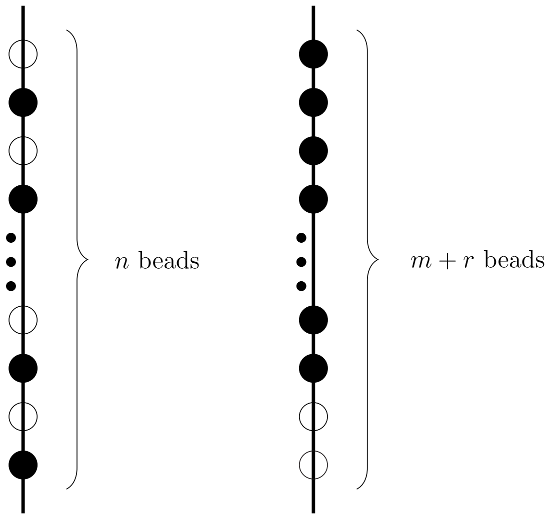

FIGURE 3.32: The 2-runner abacus display of $\lambda_{m,n,r}$.

Theorem 39. *The 2-core of $\lambda_{m,n,r}$ when $n < m+r$ is*

$$\delta = \big(m+r-n,\, m+r-n-1,\, m+r-n-2, \ldots, 3, 2, 1\big).$$

Proof. Figure 3.33 is the result of pushing all beads in Figure 3.32 up as far as they will go. Figure 3.33 tells us that the Young diagram of the 2-core δ when $n < m+r$ is of the form shown in Figure 3.34. The Young diagram in Figure 3.34 tells us that when $n < m+r$ the partition is

$$\delta = \big(m + r - n,\, m + r - n - 1, \dots, 3, 2, 1\big).$$

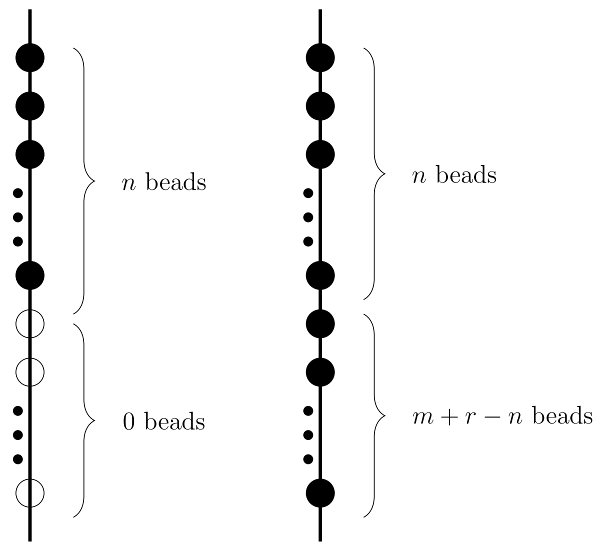

FIGURE 3.33: The 2-runner abacus display of the 2-core of $\lambda_{m,n,r}$ when $n < m+r$.

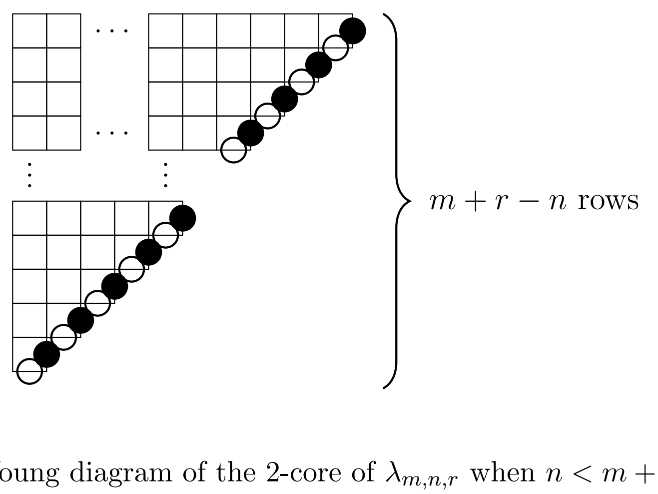

FIGURE 3.34: The Young diagram of the 2-core of $\lambda_{m,n,r}$ when $n < m+r$.

□

Theorem 40. *The 2-core of $\lambda_{m,n,r}$ when $n = m + r$ is the empty set.*

Proof. If both runners in Figure 3.32 consist of the same number of beads, once all beads have been pushed up as far as they can go, only empty beads follow after the last bead of each runner. □

Theorem 41. *The 2-core of $\lambda_{m,n,r}$ when $n > m + r$ is*

$$\delta = \big(n - m - r - 1,\, n - m - r - 2, n - m - r - 3, \ldots, 3, 2, 1\big).$$

Proof. Figure 3.32 shows that the first runner of the 2-runner abacus display of $\lambda_{m,n,r}$ consists of n beads and the second runner consists of $m + r$ beads. When $n > m + r$ the first runner will contain more beads than the second runner. Therefore, the 2-quotients that are obtained will not be ordered when $n > m + r$. In Remark 4 it explains how to ensure that the 2-quotient (μ, ν) obtained from the 2-runner abacus display of a partition is ordered. The display in Figure 3.35 is the results of adding an additional bead to the start of Figure 3.32 and rearranging beads and empty beads between the two runners. The orange bead in Figure 3.35 is the additional bead that has been added.

The abacus display in Figure 3.36 is of the 2-core of $\lambda_{m,n,r}$ when $n > m + r$. A comparison between Figures 3.33 and 3.36 shows that the Young diagram of the 2-core of $\lambda_{m,n,r}$ when $n > m + r$ is of the form shown in Figure 3.34 but with $n - m - r - 1$ rows instead of $m + r - n$ rows. Therefore, when $n > m + r$ the 2-core of $\lambda_{m,n,r}$ is

$$\gamma = \big(n - m - r - 1,\, n - m - r - 2, n - m - r - 3, \ldots, 3, 2, 1\big).$$

□

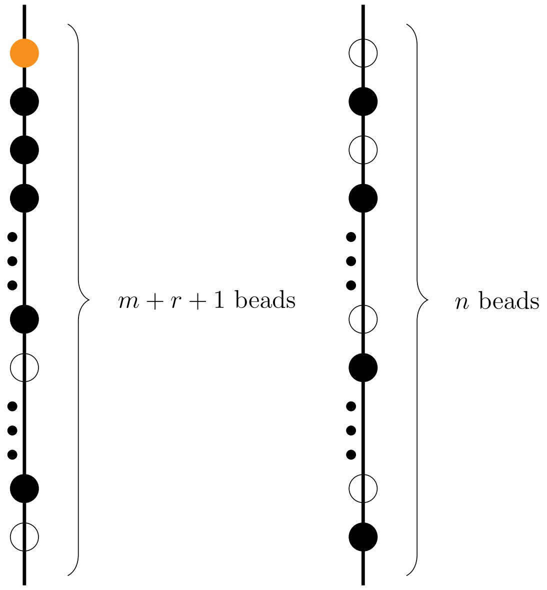

FIGURE 3.35: The 2-runner abacus display of $\lambda_{m,n,r}$ with an additional bead (coloured orange) to ensure the second runner contains at least as many beads as the first runner of the abacus display.

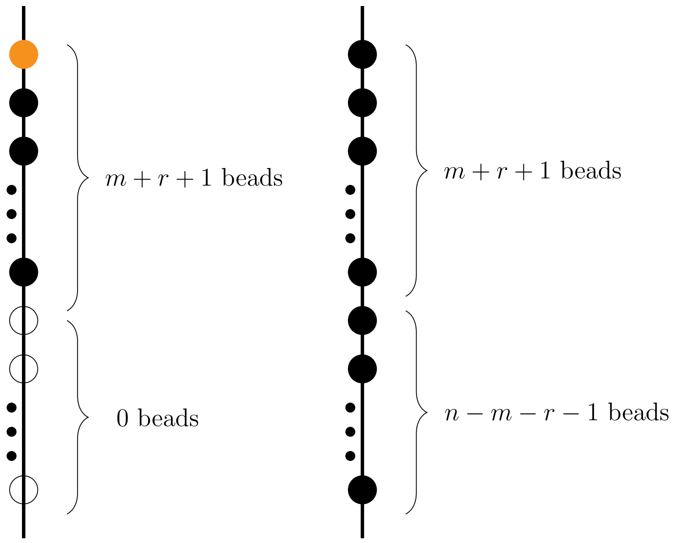

FIGURE 3.36: The 2-runner abacus display of the 2-core $\lambda_{m,n,r}$ when $n > m + r$.

3.2.4 The 2-quotient of λ

Our aim is to now determine the 2-quotient of $\lambda_{m,n,r}$. Interestingly, we find that whether $n > m+r$ or $n \leq m+r$ affects the 2-core and the 2-quotient of $\lambda_{m,n,r}$. The same conditions on n and $m + r$ appear when we investigated the blocks formed by the roots of $Q_{m,n,r}(z)$.

Theorem 42. *The 2-quotient* (μ, ν) *of* $\lambda_{m,n,r}$ *when* $n \leq m + r$ *is*

$$\begin{aligned} \big((n, n-1, n-2, \dots, 1),\ (r-m, r-m-1, \dots, 1)\big) &\quad \textit{when} \quad r > m, \\ \big((n, n-1, n-2, \dots, 1),\ (m-r-1, m-r-2, \dots, 1)\big) &\quad \textit{when} \quad r < m, \\ \big((n, n-1, n-2, \dots, 1),\ \emptyset\big) &\quad \textit{when} \quad r = m. \end{aligned}$$

Proof. The abacus display in Figure 3.32 tells us that the partition μ in the 2-quotient of $\lambda_{m,n,r}$ when $n \leq m + r$ is

$$\mu = (n, n-1, n-2, \dots, 1).$$

Figure 3.32 shows that the number of beads in the second runner depends on the parameters m and r. Figure 3.37 shows how the second runner in Figure 3.32 looks when $r > m$, $r = m$ and $r < m$. Figure 3.37 shows that when $r > m$ a total of $r - m$ beads need to be pushed up to form the second runner of the abacus display of the 2-core. The j th bead that requires pushing up, needs to be pushed up by j places. This means when $r > m$ and $n \leq m + r$, the partition ν is

$$\nu = (r-m, r-m-1, \dots, 3, 2, 1).$$

Figure 3.37 shows that when $r < m$, the number of beads that require pushing up is $m - r - 1$, and the j th bead that requires pushing, needs to be pushed up by j places. This tells us that when $r < m$ and $n \leq m + r$, the partition ν is

$$\nu = (m-r-1, m-r-2, \dots, 3, 2, 1).$$

Lastly, Figure 3.37 shows that when $r = m$ the number of beads that need to be pushed up to form the second runner of the abacus display of the 2-core is zero. Therefore, when $r = m$ and $n \leq m + r$, the partition ν is the empty set. □

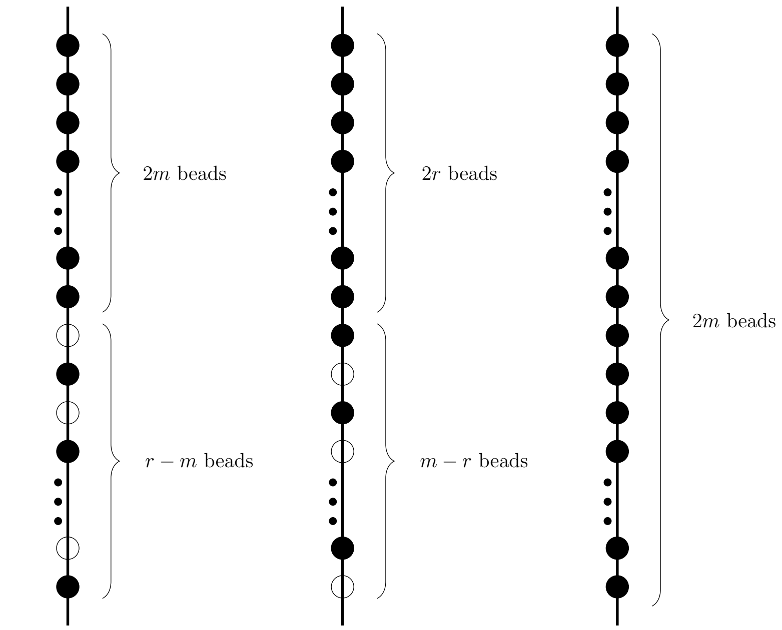

(A) $r > m$ (B) $r < m$ (C) $r = m$

FIGURE 3.37: The second runner of 2-runner abacus display of $\lambda_{m,n,r}$ (shown in Figure 3.32) when $r > m$, $r < m$ and $r = m$.

Theorem 43. *The 2-quotient (μ, ν) of $\lambda_{m,n,r}$ when $n > m + r$ is*

$$\begin{aligned} \big((r-m, r-m-1, \ldots, 1), (n, n-1, n-2, \ldots, 1)\big) &\quad \textit{when} \quad r > m, \\ \big((m-r-1, m-r-2, \ldots, 1)\,(n, n-1, n-2, \ldots, 1)\big) &\quad \textit{when} \quad r < m, \\ \big(\emptyset\ , (n, n-1, n-2, \ldots, 1)\big) &\quad \textit{when} \quad r = m. \end{aligned}$$

Proof. The second runner in Figure 3.35 tells us that the partition

$$\nu = (n, n-1, n-2, \ldots, 1),$$

when $n > m + r$. Figure 3.35 shows that the number of beads in the first runner depend on the parameters m and r. Therefore, the relative size of parameters m and r needs to be considered in order to find the partition μ. Figure 3.38 shows how the first runner of Figure 3.35 looks when $r > m$, $r < m$ and $r = m$. A comparison between Figures 3.38 and 3.37 shows that the partition obtained from each sub-figure is the same for both figures.

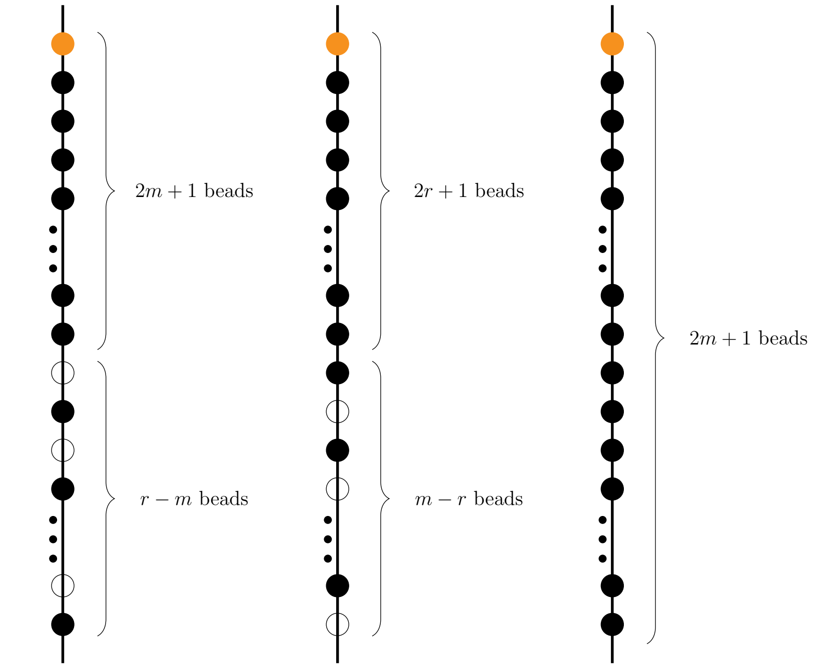

(A) $r > m$ (B) $r < m$ (C) $r = m$

FIGURE 3.38: The first runner of 2-runner abacus display of $\lambda_{m,n,r}$ (shown in Figure 3.35) when $r > m$, $r < m$ and $r = m$.

□

3.3 The $R_{m,n,r}(z)$ polynomials

It follows from (2.11) that the 4-Okamoto polynomial

$$Q_{m,n,r}(z) = \mathrm{i}^d \, Q_{s,t,u}(-\mathrm{i}z), \tag{3.17}$$

where d is defined in (3.3) and s, t and u are non-negative integers such that $\lambda^*_{m,n,r} = \lambda_{s,t,u}$. For convenience, we introduce the polynomial $R_{m,n,r}(z)$ defined in the following definition.

Definition 30. Define $R_{m,n,r}(z)$ as

$$R_{m,n,r}(z) = \mathrm{i}^d\, c_{m,n,r} \mathcal{W}\Big(\big\{ \mathrm{He}_{1+4j}(-\mathrm{i}z) \big\}_{j=0}^{m-1} ;\ \big\{ \mathrm{He}_{2+4j}(-\mathrm{i}z) \big\}_{j=0}^{n-1} ;\ \big\{ \mathrm{He}_{3+4j}(-\mathrm{i}z) \big\}_{j=0}^{r-1} \Big),$$

where $c_{m,n,r}$ is defined in (3.2) and d is defined in (3.3).

It follows from (3.17) that there exists non-negative integers s, t and u such that

$$Q_{m,n,r}(z) = R_{s,t,u}(z).$$

Our aim is to find the polynomials $R_{s,t,u}(z)$ using the partition $\lambda^*_{m,n,r}$. The motivation for studying the $R_{s,t,u}(z)$ polynomials is to check our findings on the blocks formed by the roots of $Q_{m,n,r}(z)$. We do this by confirming that there is a 90 degree rotation between the blocks formed by $Q_{m,n,r}(z)$ and $Q_{s,t,u}(z)$. Figure 3.5 shows an illustration of the blocks $A - G$ formed by the roots of $Q_{m,n,r}(z)$. Figure 3.39 shows how the blocks in Figure 3.5 look after a 90 degree rotation.

Our aim is to find the polynomials $R_{s,t,u}(z)$ equal to $Q_{m,n,r}(z)$. We can find the parameters s, t and u using the partition $\lambda^*_{m,n,r}$ associated with $R_{s,t,u}(z)$. Remarks 9 and 10 can be used to determine if parameters s, t and u are equal and whether t is the smallest parameter or not by looking at the number of single, double or triple terms in $\lambda^*_{m,n,r}$. The parameters s, t and u can be determined by looking at the number of single, double or triple terms in $\lambda^*_{m,n,r}$. To recap the term a of $R_{s,t,u}(z)$ denotes the smallest parameter out of s, t and u, the term b denotes the difference between the largest and second largest parameter and the term c denotes the difference between the second largest and smallest parameter out of s, t and u. The largest parameter out of s, t and u is the term $a + b + c$, the second largest parameter is $a + c$ and the smallest parameter is a. We can find the parameter condition of $R_{s,t,u}(z)$ by looking at the difference in length between

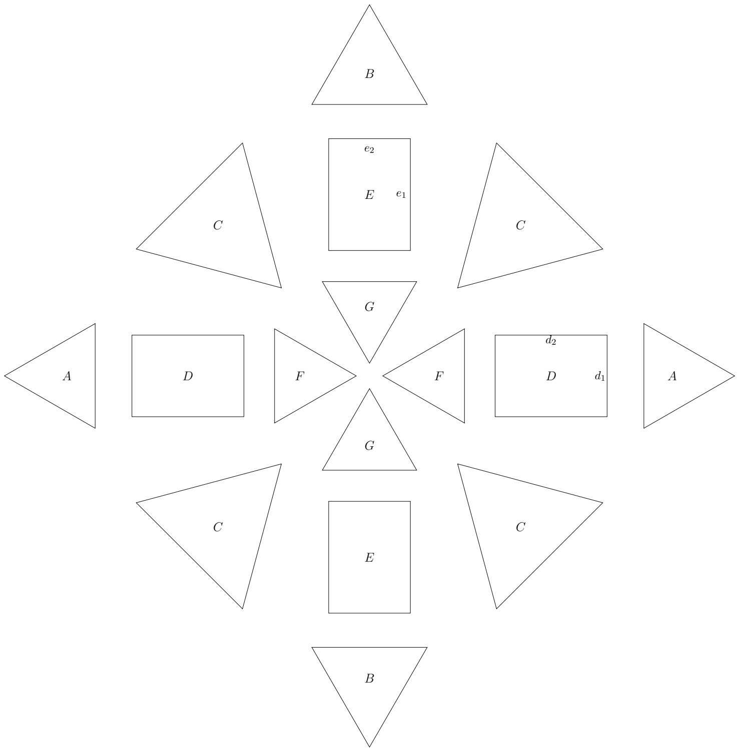

FIGURE 3.39: A 90 degree rotation of the blocks formed by roots of $Q_{m,n,r}(z)$ shown in Figure 3.5.

row b and row $b+1$ and row $b+2c$ and row $b+2c+1$ of the Young diagram of $\lambda^*_{m,n,r}$ associated with $R_{s,t,u}(z)$. The results in Tables 3.29 and 3.28 can be used as a criteria to determine the parameter condition of $R_{s,t,u}(z)$. The parameter condition of $R_{s,t,u}(z)$ and $Q_{s,t,u}(z)$ are the same. Therefore, by considering the parameter condition of $R_{s,t,u}(z)$ we can determine the blocks formed by the roots of $Q_{s,t,u}(z)$ using the results in Tables 3.22-3.24. Once we have determined the blocks formed by the roots of $Q_{s,t,u}(z)$ we can check if there is a 90 degree rotation between the blocks formed by the roots of $Q_{m,n,r}(z)$ and $Q_{s,t,u}(z)$.

Theorem 44. *When $r > n > m$ the polynomials $Q_{m,n,r}(z)$ and $R_{r-n,\,r-m,\,r}(z)$ are equal.*

Proof. When $r > n > m$ the conjugate partition of $\lambda_{m,n,r}$ is

$$\lambda^*_{m,n,r} = \left(\left\{m+n-3j+r+3\right\}_{j=1}^{m}; \left\{(r-n+2j)^2\right\}_{j=1}^{n-m}; \left\{(j)^3\right\}_{j=1}^{r-n}\right).$$

Since $\lambda^*_{m,n,r}$ when $r > n > m$ contains single, double and triple terms it follows from Remark 9 that the parameters of associated polynomial $R_{s,t,u}(z)$ are not equal and the parameter t is not the smallest parameter. This means $R_{s,t,u}(z)$ is either a case 1,4,5 or 9 polynomial. The Young diagram of $\lambda^*_{m,n,r}$ when $r > n > m$ can be found in Figure 3.40. The Young diagram in Figure 3.40 consists of m single rows, $2(n-m)$ rows that form a double row, and $3(r-n)$ rows that form a triple row. Therefore, the term $b = m$, $c = n-m$ and $a = r-n$ of $R_{s,t,u}(z)$ when $r > n > m$. This tells us that the parameters of $R_{s,t,u}(z)$ are $r-n$, $r-m$ and r.

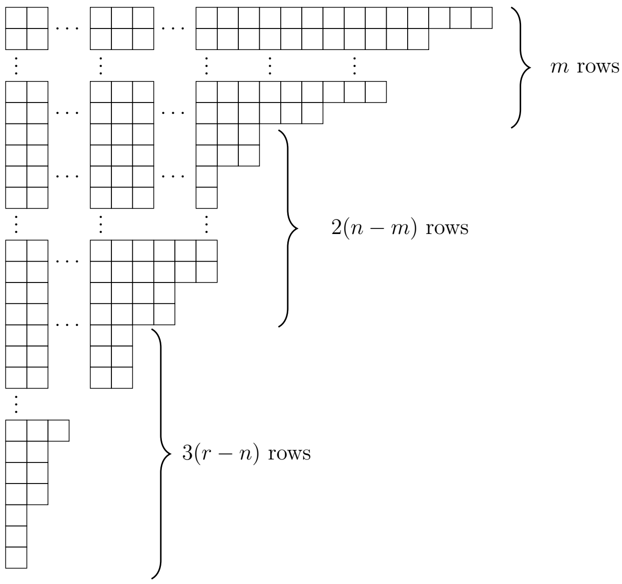

FIGURE 3.40: The Young diagram of $\lambda^*_{m,n,r}$ when $r > n > m$. The brackets indicate the number of rows in the diagram.

Figure 3.40 shows that the difference between row b and row $b+1$ is three, and the difference between row $b+2c$, i.e. the shortest row that forms a double row, and $b+2c+1$ is two. According to Table 3.29 $R_{s,t,u}(z)$ must be a case 9 polynomial i.e $u > t > s$. Therefore, the polynomial in Figure 3.40 is associated with $R_{r-n,\, r-m,\, r}(z)$.

□

Suppose we want to check the results in Table 3.31. We have proven that when $r > n > m$ i.e. when $Q_{m,n,r}(z)$ is a case 9 polynomial, it is equal to $R_{r-n,r-m,r}(z)$, which happens to also be a case 9 polynomial. Therefore, $Q_{r-n,r-m,r}(z)$ is a case 9 polynomial. It follows from Table 3.31 that the roots of $Q_{r-n,r-m,r}(z)$ form the blocks found in Table 3.32. A comparison of the results in Tables 3.31 and 3.32 show a 90 degree rotation between the blocks formed by $Q_{m,n,r}(z)$ and $Q_{r-n,r-m,r}(z)$ when $r > n > m$. This confirms that the results in Table 3.31 hold true.

Block	$Q_{m,n,r}(z)$ with $r > n > m$
A	m-triangle
B	$(r-n)$-triangle
C	$(n-m)$-triangle
D	$m \times (n-m)$ rectangle
E	$(n-m) \times (r-n)$ rectangle

TABLE 3.31: Blocks formed by the roots of $Q_{m,n,r}(z)$ when $r > n > m$.

Block	$Q_{r-n,r-m,r}(z)$ with $r > n > m$
A	$(r-n)$-triangle
B	m-triangle
C	$(n-m)$-triangle
D	$(r-n) \times (n-m)$ rectangle
E	$(n-m) \times m$ rectangle

TABLE 3.32: Blocks formed by the roots of $Q_{r-n,r-m,r}(z)$ when $r > n > m$.

Theorem 45. *When $m > r > n$ the polynomials $Q_{m,n,r}(z)$ and $R_{m,\,m-r-1,\,m-n-1}(z)$ are equal.*

Proof. When $m > r > n$ the conjugate partition of $\lambda_{m,n,r}$ is

$$\lambda^*_{m,n,r} = \left(\left\{m+n-3j+r+3\right\}_{j=1}^{n+1}; \left\{(m-r+j-1)\right\}_{j=1}^{2(r-n)}; \left\{(j)^3\right\}_{j=1}^{m-r-1}\right).$$

Figure 3.41 shows the Young diagram of $\lambda^*_{m,n,r}$ when $m > r > n$. The Young diagram in Figure 3.41 consists of single and triple row and no double rows. It follows from Remark 10 that the parameters of the associated polynomial $R_{s,t,u}(z)$ are not equal and that t is the smallest parameter. This means $R_{s,t,u}(z)$ is either a case 10 or 11 polynomial. Figure 3.41 tells us that the term $b = n+1$, $c = r-n$ and

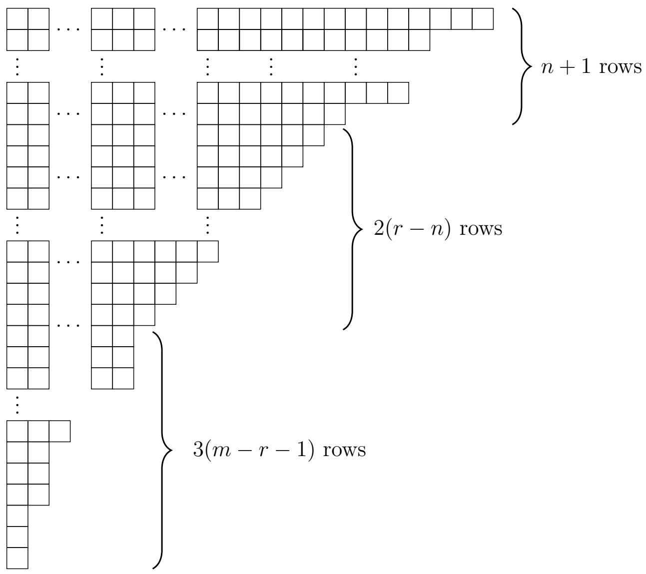

FIGURE 3.41: The Young diagram of $\lambda^*_{m,n,r}$ when $m > r > n$. The brackets indicate the number of rows in the diagram.

$a = m - r - 1$ of $R_{s,t,u}(z)$. Therefore, the parameters of $R_{s,t,u}(z)$ when $m > r > n$ are $m - r - 1$, $m - n - 1$ and m. Figure 3.41 shows that the difference between row b and row $b + 1$ is one. It follows from Table 3.12 that $R_{s,t,u}(z)$ is a case 10 polynomial i.e. $s > u > t$. Therefore, when $m > r > n$ the polynomials $Q_{m,n,r}(z)$ and $R_{m,m-r-1,m-n-1}(z)$ are equal. □

Theorem 46. *When $n > r > m$ the polynomials $Q_{m,n,r}(z)$ and $R_{n-m,\,n,\,n-r-1}(z)$ are equal.*

Proof. When $n > r > m$ the conjugate partition of $\lambda_{m,n,r}$ is

$$\lambda^*_{m,n,r} = \left(\left\{m + n - 3j + r + 3\right\}_{j=1}^{m}; \left\{\left(n - r - 2j + 2\right)^2\right\}_{j=1}^{r-m+1}; \left\{(j)^3\right\}_{j=1}^{n-r-1}\right).$$

Figure 3.42 shows the Young diagram of $\lambda^*_{m,n,r}$ when $n > r > m$. The Young diagram in Figure 3.42 consists of single, double and triple rows. It follows from Remark 9 that the parameters of the associated polynomial $R_{s,t,u}(z)$ are not equal and that t is not the smallest parameter. This means $R_{s,t,u}(z)$ is either a case 1,4,5 or 9 polynomial. Figure 3.42 tells us that the term $b = m$, $c = r - m + 1$ and

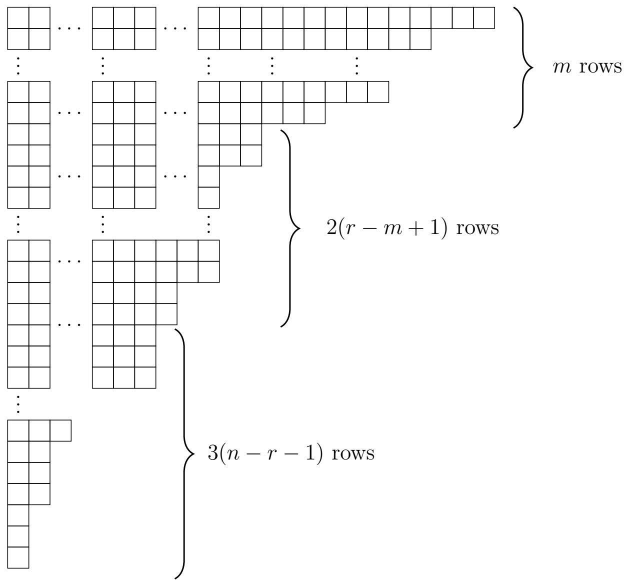

FIGURE 3.42: The Young diagram of $\lambda^*_{m,n,r}$ when $n > r > m$. The brackets indicate the number of rows in the diagram.

$a = n - r - 1$ of the associated $R_{s,t,u}(z)$. Therefore, the parameters of $R_{s,t,u}(z)$ when $n > r > m$, are $n-r-1$, $n-m$ and n. Figure 3.42 shows that the difference between row b and row $b+1$ is three and the difference between row $b+2c$ and $b+2c+1$ is one. It follows from Table 3.29 that $R_{s,t,u}(z)$ is a case 5 polynomial i.e. $t > s > u$. Therefore, when $n > r > m$ the polynomials $Q_{m,n,r}(z)$ and $R_{n-m,\,n,\,n-r-1}(z)$ are equal. $\square$

Theorem 46 tells us that when $Q_{m,n,r}(z)$ is a case 4 polynomial, i.e. $n > r > m$ it is equal to $R_{n-m,\,n,\,n-r-1}(z)$ which happens to be a case 5 polynomial. Therefore, $R_{n-m,\,n,\,n-r-1}(z)$ is a case 5 polynomial, The blocks formed by the roots of $Q_{m,n,r}(z)$ when $Q_{m,n,r}(z)$ is a case 4 polynomial can be found in Table 3.33. The blocks formed when $Q_{m,n,r}(z)$ is a case 5 polynomial i.e. $n > m > r$ can be found Table 3.34. It follows from Table 3.34 that the roots of $Q_{n-m,\,n,\,n-r-1}(z)$ form the blocks shown in Table 3.35. A comparison of the blocks in Tables 3.33 and 3.35 shows a 90 degree rotation, as expected.

Theorem 47. *The polynomials $R_{s,t,u}(z)$ equal to $Q_{m,n,r}(z)$ for each of the thirteen parameter conditions of m, n and r can be found in Tables 3.36 and 3.37.*

Block	$Q_{m,n,r}(z)$ when $n > r > m$
A	m-triangle
B	$(n-r-1)$-triangle
C	$(r-m)$-triangle
D	$m \times (r-m)$ rectangle
E	$(r-m+1) \times (n-r)$ rectangle
F	m-triangle when $n \geq m+r$
	$(n-r) \times m$ trapezoid when $n < m+r$
G	$(n-r-1)$-triangle when $n \leq m+r+1$
	$m \times (n-r-1)$ trapezoid when $n > m+r+1$

TABLE 3.33: Blocks formed by the roots of $Q_{m,n,r}(z)$ when $n > r > m$.

Block	$Q_{m,n,r}(z)$ when $n > m > r$
A	r-triangle
B	$(n-m)$-triangle
C	$(m-r-1)$-triangle
D	$(r+1) \times (m-r)$ rectangle
E	$(m-r-1) \times (n-m)$ rectangle
F	r-triangle when $n \geq m+r$
	$(n-m) \times r$ trapezoid when $n < m+r$
G	$(n-m)$-triangle when $n \leq m+r+1$
	$(r+1) \times (n-m)$ trapezoid when $n > m+r+1$

TABLE 3.34: Blocks formed by the roots of $Q_{m,n,r}(z)$ when $n > m > r$.

Block	$Q_{n-m,\,n,\,n-r-1}(z)$ when $n > r > m$
A	$(n-r-1)$-triangle
B	m-triangle
C	$(r-m)$-triangle
D	$(n-r) \times (r-m+1)$ rectangle
E	$(r-m) \times m$ rectangle
F	$(n-r-1)$-triangle when $n \geq m+r$
	$m \times (n-r-1)$ trapezoid when $n < m+r$
G	m-triangle when $n \leq m+r+1$
	$(n-r) \times m$ trapezoid when $n > m+r+1$

TABLE 3.35: Blocks formed by the roots of $Q_{n-m,\,n,\,n-r-1}(z)$ when $n > r > m$.

3.4 The discriminant of $Q_{m,n,r}(z)$

In Chapter 1, we discussed the discriminant of Yablonskii–Vorob'ev polynomials $Q_n(z)$. Examples of the discriminant of $Q_n(z)$ can be found in Table 1.3. The

case no.	parameter condition of $Q_{m,n,r}(z)$	equivalent polynomial of $R_{s,t,u}(z)$	parameter condition of $R_{s,t,u}(z)$	case no.
1	$m > n > r$	$R_{m,\,m-r-1,\,m-n-1}(z)$	$s > t > u$	1
4	$n > r > m$	$R_{n-m,\,n,\,n-r-1}(z)$	$t > s > u$	5
5	$n > m > r$	$R_{n-m,\,n,\,n-r-1}(z)$	$t > u > s$	4
9	$r > n > m$	$R_{r-n,\,r-m,\,r}(z)$	$u > t > s$	9
10	$m > r > n$	$R_{m,\,m-r-1,\,m-n-1}(z)$	$s > u > t$	10
11	$r > m > n$	$R_{r-n,\,r-m,\,r}(z)$	$u > s > t$	11

TABLE 3.36: Polynomials $R_{s,t,u}(z)$ that are equal to $Q_{m,n,r}(z)$ when m, n and r are not equal.

case no.	parameter condition of $Q_{m,n,r}(z)$	equivalent polynomial of $R_{s,t,u}(z)$	parameter condition of $R_{s,t,u}(z)$	case no.
2	$n > m = r$	$R_{n-m,\,n,\,n-r-1}(z)$	$t > s > u$	5
3	$m = n > r$	$R_{0,\,n,\,n-r-1}(z)$	$t > u > s$	4
6	$m > n = r$	$R_{m,\,m-n-1,\,m-n-1}(z)$	$s > t = u$	6
7	$m = n = r$	$R_{0,\,0,\,n}(z)$	$u > s = t$	12
8	$n = r > m$	$R_{0,\,r-m,\,r}(z)$	$u > t > s$	9
12	$r > n = m$	$R_{r-n,\,r-n,\,r}(z)$	$u > s = t$	12
13	$m = r > n$	$R_{r-n,\,0,\,r}(z)$	$u > s > t$	11

TABLE 3.37: Polynomials $R_{s,t,u}(z)$ that are equal to $Q_{m,n,r}(z)$ when two or more parameters of out of m, n and r are equal.

general form the of the discriminant of $Q_n(z)$ polynomials is given in Theorem 3. This theorem is due to Roberts [74]. The general form the of the discriminant of generalised Hermite and generalised Okamoto polynomials can also be found in [74]. A generalisation of the discriminant of 4-Okamoto polynomials is not obvious from results found by Roberts on the discriminate of generalised Okamoto polynomials. This motivates us to investigate the discriminate of 4-Okamoto polynomials. We start our investigation by considering 4-Okamoto polynomials with equal parameters. Let $\mathrm{Dis}(Q_{n,n,n}(z))$ be the discriminant of

$$\frac{Q_{n,n,n}(z)}{z^k},$$

where

$$k = \frac{n(n+1)}{2},$$

is the multiplicity of the roots of $Q_{n,n,n}(z)$ at the origin. Table 3.38 shows the prime factors of the $\mathrm{Dis}(Q_{n,n,n}(z))$ for $n = 1, \ldots, 8$. The results in Table 3.38 were found using Maple. Table 3.38 shows that the prime factors of the $\mathrm{Dis}(Q_{n,n,n}(z))$ include the prime 2 and primes of the form $(4x-1)$ and $(4x+1)$. A comparison of the discriminants in Table 3.38 shows that the $\mathrm{Dis}(Q_{n,n,n}(z))$ is negative for certain values of n. Further examples show that the $\mathrm{Dis}(Q_{n,n,n}(z)) < 0$ when $n = 1 \bmod 4$ or $n = 2 \bmod 4$. A comparison of the results in Table 3.38 show that the powers of 2 are of the form

$$\frac{n^2(n+1)^2}{2}.$$

$$\begin{aligned}
\mathrm{Dis}(Q_{1,1,1}(z)) &= -(2)^2(3) \\
\mathrm{Dis}(Q_{2,2,2}(z)) &= -(2)^{18}(3)^9(5)(7)^3 \\
\mathrm{Dis}(Q_{3,3,3}(z)) &= (2)^{72}(3)^{35}(5)^{13}(7)^{10}(11)^5 \\
\mathrm{Dis}(Q_{4,4,4}(z)) &= (2)^{200}(3)^{88}(5)^{52}(7)^{32}(11)^{18}(13)^5 \\
\mathrm{Dis}(Q_{5,5,5}(z)) &= -(2)^{450}(3)^{203}(5)^{123}(7)^{82}(11)^{35}(13)^{18}(17)^7(19)^9 \\
\mathrm{Dis}(Q_{6,6,6}(z)) &= -(2)^{882}(3)^{419}(5)^{222}(7)^{169}(11)^{75}(13)^{35}(17)^{26}(19)^{34}(23)^{11} \\
\mathrm{Dis}(Q_{7,7,7}(z)) &= (2)^{1568}(3)^{778}(5)^{367}(7)^{300}(11)^{159}(13)^{79}(17)^{53}(19)^{71}(23)^{42} \\
\mathrm{Dis}(Q_{8,8,8}(z)) &= (2)^{2592}(3)^{1336}(5)^{603}(7)^{471}(11)^{287}(13)^{175}(17)^{84}(19)^{116}(23)^{89}(29)^{13}(31)^{15}
\end{aligned}$$

TABLE 3.38: Prime factors of the $\mathrm{Dis}(Q_{n,n,n}(z))$ for $n = 1 \ldots 8$.

Our aim is to find the general form of the $\mathrm{Dis}(Q_{n,n,n}(z))$. The discriminants in Table 3.38 show that the "last" prime factor, i.e. the one furthest to the right is of the form $(4n-1)$ to some power, when for $n = 1, 2, 3, 5, 6, 8$. When $n = 4$ and $n = 7$ the term $(4n-1)$ are integers that are not prime, therefore, they are "missing" from Table 3.38. The results in Table 3.38 suggest that the $\mathrm{Dis}(Q_{n,n,n}(z))$ for all values of n involve an integer factor of the form $(4n-1)$ to some power. The results in Table 3.38 show that the second to last prime factor of the $\mathrm{Dis}(Q_{n,n,n}(z))$ is of the form $(4n-3)$ to some power for certain values of n, and the third to last prime factor is of the form $(4n-5)$ to some power for certain values of n, and so on. This suggests the j th to last integer factor of $\mathrm{Dis}(Q_{n,n,n}(z))$ is of the form $(4n-2j+1)$ to some power. Table 3.38 shows that the $\mathrm{Dis}(Q_{n,n,n}(z))$ for $n = 1$ and $n = 2$ involves $2n$ small primes. This includes the prime 2 and $2n-1$ odd prime. The number of primes involved in the the $\mathrm{Dis}(Q_{n,n,n}(z))$ in Table 3.38 suggest that the $\mathrm{Dis}(Q_{n,n,n}(z))$ can be written as $2n$ integers to some power, where integers can be prime or not prime. So far, we know that integer factor of the absolute value of the $\mathrm{Dis}(Q_{n,n,n}(z))$ is

$$| \mathrm{Dis}(Q_{n,n,n}(z)) |= 2^{\frac{n^2(n+1)^2}{2}} \prod_{j=1}^{2n-1} (4n-2j+1)^{\mathcal{G}_n(j)}, \tag{3.18}$$

where $\mathcal{G}_n(j)$ is to be determined.

$$\mathrm{Dis}(Q_{1,1,1}(z)) = -(2)^2(3)$$

$$\mathrm{Dis}(Q_{2,2,2}(z)) = -(2)^{18}(3)^9(5)(7)^3$$

$$\mathrm{Dis}(Q_{3,3,3}(z)) = (2)^{72}(3)^{35}(5)^{13}(7)^{10}(11)^5$$

$$\mathrm{Dis}(Q_{4,4,4}(z)) = (2)^{200}(3)^{88}(5)^{52}(7)^{32}(11)^{18}(13)^5$$

$$\mathrm{Dis}(Q_{5,5,5}(z)) = -(2)^{450}(3)^{203}(5)^{123}(7)^{82}(11)^{35}(13)^{18}(17)^7(19)^9$$

$$\mathrm{Dis}(Q_{6,6,6}(z)) = -(2)^{882}(3)^{419}(5)^{222}(7)^{169}(11)^{75}(13)^{35}(17)^{26}(19)^{34}(23)^{11}$$

$$\mathrm{Dis}(Q_{7,7,7}(z)) = (2)^{1568}(3)^{778}(5)^{367}(7)^{300}(11)^{159}(13)^{79}(17)^{53}(19)^{71}(23)^{42}$$

$$\mathrm{Dis}(Q_{8,8,8}(z)) = (2)^{2592}(3)^{1336}(5)^{603}(7)^{471}(11)^{287}(13)^{175}(17)^{84}(19)^{116}(23)^{89}(29)^{13}(31)^{15}$$

Table 3.39: Prime factors of the $\mathrm{Dis}(Q_{n,n,n}(z))$ for $n = 1 \dots 8$. Terms of the form $4n-1$, $4n-3$, $4n-5$, $4n-7$ and $4n-9$ to some power, have been coloured red, blue, purple, green and orange, respectively.

The discriminants in Table 3.39 show that when $j = 1$ and $n \geq 1$ the terms (in red) are of the form

$$(4n-1)^{2n-1}.$$

When $j = 2$ and $n \geq 2$ the terms (in blue) in Table 3.39 are of the form

$$(4n-3)^{2n-3},$$

when $j = 3$ and $n \geq 3$ terms (in purple) are of the

$$(4n-5)^{8n-14},$$

when $j = 4$ and $n \geq 4$ the terms (in green) are of the form

$$(4n-7)^{8n-22},$$

and when $j = 5$ and $n \geq 5$ the terms (in orange) are of the form

$$(4n-9)^{18n-55}.$$

Further example show that when $j = 6$ and $n \geq 6$ terms are of the form

$$(4n-11)^{18n-73},$$

and when $j = 7$ and $n \geq 7$ terms are of the form

$$(4n-13)^{32n-140}.$$

The results above tells us that when $n \geq j$ terms of the form $(4n - 2j + 1)$ are to the power of

$$2n\left(\frac{j}{2}\right)^2 - \frac{4j^3 + 2j}{12}, \tag{3.19}$$

when j is even and

$$2n\left(\frac{j+1}{2}\right)^2 - \frac{4j^3 + 6j^2 + 2j}{12}, \tag{3.20}$$

when j is odd. Therefore, the $\mathrm{Dis}(Q_{n,n,n}(z))$ involves two separte products, one for $n \geq j$ and one for $n < j$. This means the integer factor of the $\text{Dis}(Q_{n,n,n}(z))$ is of the form

$$| \text{Dis}(Q_{n,n,n}(z)) |= 2^{\frac{n^2(n+1)^2}{2}} \prod_{j=n+1}^{2n-1} (4n-2j+1)^{\mathcal{F}_n(j)} \prod_{j=1}^{n} (4n-2j+1)^{\widetilde{\mathcal{G}}_n(j)}, \quad (3.21)$$

where $\mathcal{F}_n(j)$ is to be determined. It follows from (3.19) and (3.20) that

$$\widetilde{\mathcal{G}}_n(j) = 2n\left(\left\lceil \frac{j}{2} \right\rceil\right)^2 - \frac{4j^3+3j^2-3j^2(-1)^j+2j}{12}. \quad (3.22)$$

Our aim is to now determine $\mathcal{F}_n(j)$. We know that when $n \geq j$ terms are of the form

$$\prod_{j=1}^{n} (4n-2j+1)^{\widetilde{\mathcal{G}}(n)}, \quad (3.23)$$

where $\widetilde{\mathcal{G}}(n)$ is defined in (3.22). We can use (3.23) to find "missing terms", i.e. integers that are not prime that are to the power of another integer. We can find missing terms by dividing the prime factors of the $\text{Dis}(Q_{n,n,n}(z))$ by the terms obtained from (3.23). For example, Table 3.38 shows that the prime factors of the

$$\text{Dis}(Q_{3,3,3}(z)) = (2)^{72}(3)^{35}(5)^{13}(7)^{10}(11)^5. \quad (3.24)$$

According to (3.23) the $\text{Dis}(Q_{3,3,3}(z))$ includes the term $(9)^3$. If we divide (3.24) by $(9)^3$ we get

$$(2)^{72}(3)^{29}(5)^{13}(7)^{10}(11)^5.$$

This tells us that the $\text{Dis}(Q_{3,3,3}(z))$ is

$$\text{Dis}(Q_{3,3,3}(z)) = (2)^{72}(3)^{29}(5)^{13}(7)^{10}(9)^3(11)^5.$$

If we continue this process of dividing the prime factors of the $\text{Dis}(Q_{n,n,n}(z)$ by terms obtained from (3.23) we find the results in Table 3.40. The highlighted terms in Table 3.40 are the terms obtained from (3.23) when $j = n$. The terms in Table 3.40 where $j \geq n$ do not contain any missing terms. The terms in Table

3.40 where $j < n$ do contain missing terms. For example, according to (3.21) when $n \geq 5$ the $\mathrm{Dis}(Q_{n,n,n}(z))$ includes terms of the form $(9)^{\mathcal{F}_n(j)}$. Our aim is to now determine $\mathcal{F}_n(j)$.

$$\begin{aligned}
\mathrm{Dis}(Q_{1,1,1}(z)) &= -(2)^2(3)\\
\mathrm{Dis}(Q_{2,2,2}(z)) &= -(2)^{18}(3)^9(5)(7)^3\\
\mathrm{Dis}(Q_{3,3,3}(z)) &= (2)^{72}(3)^{29}(5)^{13}(7)^{10}(9)^3(11)^5\\
\mathrm{Dis}(Q_{4,4,4}(z)) &= (2)^{200}(3)^{61}(5)^{45}(7)^{32}(9)^{10}(11)^{18}(13)^5(15)^7\\
\mathrm{Dis}(Q_{5,5,5}(z)) &= -(2)^{450}(3)^{177}(5)^{97}(7)^{82}(11)^{35}(13)^{18}(17)^7(15)^{26}(19)^9\\
\mathrm{Dis}(Q_{6,6,6}(z)) &= -(2)^{882}(3)^{357}(5)^{169}(7)^{160}(11)^{75}(13)^{35}(15)^{53}(17)^{26}(19)^{34}(21)^9(23)^{11}\\
\mathrm{Dis}(Q_{7,7,7}(z)) &= (2)^{1568}(3)^{621}(5)^{261}(7)^{266}(11)^{159}(13)^{79}(15)^{84}(17)^{53}(19)^{71}(21)^{34}(23)^{42}\\
&\quad (25)^{11}(27)^{13}
\end{aligned}$$

TABLE 3.40: Prime factors of the $\mathrm{Dis}(Q_{n,n,n}(z))$ for $n = 1\ldots7$ including with all terms of the form of (3.23). The terms highlighted in yellow are the terms obtained form (3.23) when $j = n$.

Table 3.40 shows that when $n = 2, 3, 4$, the powers of 3 are equal to

$$6n^2 - 10n + 5.$$

Similarly, Table 3.40 shows that when $n \geq 3$, the powers of 5 are of equal to

$$10n^2 - 38n + 37$$

and when $n \geq 4$, the power of 7 are equal to

$$14n^2 - 76n + 112.$$

Let us assume that the powers of 3 for $n \geq 2$ are of the form

$$6n^2 - 10n + 5.$$

We can find the missing terms of the form $(9)^{\mathcal{F}_n(j)}$ by diving the results in Table 3.40 for $n \geq 5$ by

$$(3)^{6n^2-10n+5}.$$

For example, Table 3.40 shows that the

$$\mathrm{Dis}(Q_{5,5,5}(z)) = -(2)^{450}(3)^{177}(5)^{97}(7)^{82}(11)^{35}(13)^{18}(17)^{7}(15)^{26}(19)^{9}.$$

Dividing this result by $(3)^{6(3)^2-10(3)+5}$ i.e. by $(3)^{105}$ gives

$$-(2)^{450}(3)^{72}(5)^{97}(7)^{82}(11)^{35}(13)^{18}(17)^{7}(15)^{26}(19)^{9},$$

which is equivalent to

$$-(2)^{450}(9)^{36}(5)^{97}(7)^{82}(11)^{35}(13)^{18}(17)^{7}(15)^{26}(19)^{9}.$$

Therefore, we find that the

$$\mathrm{Dis}(Q_{5,5,5}(z)) = -(2)^{450}(3)^{105}(5)^{97}(7)^{82}(9)^{36}(11)^{35}(13)^{18}(17)^{7}(15)^{26}(19)^{9}.$$

Continuing this process of finding missing terms of the form $(9)^{\mathcal{F}_n(j)}$ where $n \geq 5$ gives the results in Table 3.41. The results in this Table 3.41 do not contain any missing terms.

The general form of $\mathcal{F}_n(j)$ is unclear from the results in Table 3.41. For convenience, we now write the product

$$\prod_{j=n+1}^{2n-1} (4n - 2j + 1)^{\mathcal{F}_n(j)} \tag{3.25}$$

as

$$\prod_{j=1}^{n-1} (2n - 2j + 1)^{\widetilde{\mathcal{F}}_n(j)}. \tag{3.26}$$

$$\mathrm{Dis}(Q_{1,1,1}(z)) = -(2)^2(3)$$

$$\mathrm{Dis}(Q_{2,2,2}(z)) = -(2)^{18}(3)^9(5)(7)^3$$

$$\mathrm{Dis}(Q_{3,3,3}(z)) = (2)^{72}(3)^{29}(5)^{13}(7)^{10}(9)^3(11)^5$$

$$\mathrm{Dis}(Q_{4,4,4}(z)) = (2)^{200}(3)^{61}(5)^{45}(7)^{32}(9)^{10}(11)^{18}(13)^5(15)^7$$

$$\mathrm{Dis}(Q_{5,5,5}(z)) = -(2)^{450}(3)^{105}(5)^{97}(7)^{82}(9)^{36}(11)^{35}(13)^{18}(17)^7(15)^{26}(19)^9$$

$$\mathrm{Dis}(Q_{6,6,6}(z)) = -(2)^{882}(3)^{161}(5)^{169}(7)^{160}(9)^{98}(11)^{75}(13)^{35}(15)^{53}(17)^{26}(19)^{34}(21)^9(23)^{11}$$

$$\mathrm{Dis}(Q_{7,7,7}(z)) = (2)^{1568}(3)^{229}(5)^{261}(7)^{266}(9)^{196}(11)^{159}(13)^{79}(15)^{84}(17)^{53}(19)^{71}(21)^{34}(23)^{42}(25)^{11}(27)^{13}$$

TABLE 3.41: Factors of the $\mathrm{Dis}(Q_{n,n,n}(z))$ for $n = 1 \ldots 7$ with no missing terms. The terms highlighted in yellow are the terms obtained from (3.23) when $j = n$.

Table 3.42 gives examples of terms of the form of (3.26).

n	$j = 1$	$j = 2$	$j = 3$
2	$(3)^9$	–	–
3	$(5)^{13}$	$(3)^{29}$	–
4	$(7)^{32}$	$(5)^{45}$	$(3)^{61}$
5	$(9)^{36}$	$(7)^{82}$	$(5)^{97}$
6	$(11)^{75}$	$(9)^{98}$	$(7)^{160}$
7	$(13)^{79}$	$(11)^{159}$	$(9)^{196}$
8	$(15)^{146}$	$(13)^{175}$	$(11)^{287}$
9	$(17)^{150}$	$(15)^{268}$	$(13)^{323}$
10	$(19)^{253}$	$(17)^{284}$	$(15)^{450}$

TABLE 3.42: Terms of the form of (3.26) in the $\mathrm{Dis}(Q_{n,n,n}(z))$ for $n = 1 \ldots 10$ with $j = 1$, $j = 2$ and $j = 3$.

The results in Table 3.42 show that when $j = 1$ and $n = 2t$, where t is a non-negative integer,

$$\widetilde{\mathcal{F}}_{2t}(1) = \frac{4}{3}t^3 + 2t^2 + \frac{23}{3}t - 2,$$

and when $n = 2t + 1$,

$$\widetilde{\mathcal{F}}_{2t+1}(1) = \frac{4}{3}t^3 + 2t^2 + \frac{23}{3}t + 2.$$

This tells us that when n is even

$$\widetilde{\mathcal{F}}_n(1) = \frac{4}{3}\left(\frac{n}{2}\right)^3 + 2\left(\frac{n}{2}\right)^2 + \frac{23}{3}\left(\frac{n}{2}\right) - 2, \tag{3.27}$$

and when n is odd

$$\widetilde{\mathcal{F}}_n(1) = \frac{4}{3}\left(\frac{n-1}{2}\right)^3 + 2\left(\frac{n-1}{2}\right)^2 + \frac{23}{3}\left(\frac{n-1}{2}\right) + 2. \tag{3.28}$$

Table 3.42 shows that

$$\widetilde{\mathcal{F}}_{2t+1}(2) = \frac{4}{3}t^3 + 4t^2 + \frac{95}{3}t - 8,$$

and

$$\widetilde{\mathcal{F}}_{2t+2}(2) = \frac{4}{3}t^3 + 4t^2 + \frac{95}{3}t + 8.$$

Therefore, when n is even

$$\widetilde{\mathcal{F}}_n(2) = \frac{4}{3}\left(\frac{n-2}{2}\right)^3 + 4\left(\frac{n-2}{2}\right)^2 + \frac{95}{3}\left(\frac{n-2}{2}\right) + 8, \tag{3.29}$$

and when n is odd

$$\widetilde{\mathcal{F}}_n(2) = \frac{4}{3}\left(\frac{n-1}{2}\right)^3 + 4\left(\frac{n-1}{2}\right)^2 + \frac{95}{3}\left(\frac{n-1}{2}\right) - 8. \tag{3.30}$$

Similarly, the results in Table 3.42 show that

$$\widetilde{\mathcal{F}}_{2t+2}(3) = \frac{4}{3}t^3 + 6t^2 + \frac{215}{3}t - 18,$$

and

$$\widetilde{\mathcal{F}}_{2t+3}(3) = \frac{4}{3}t^3 + 6t^2 + \frac{215}{3}t + 18.$$

This tells us that when n is even

$$\widetilde{\mathcal{F}}_n(3) = \frac{4}{3}\left(\frac{n-2}{2}\right)^3 + 6\left(\frac{n-2}{2}\right)^2 + \frac{215}{3}\left(\frac{n-2}{2}\right) - 18, \tag{3.31}$$

and when n is odd

$$\widetilde{\mathcal{F}}_n(3) = \frac{4}{3}\left(\frac{n-3}{2}\right)^3 + 6\left(\frac{n-3}{2}\right)^2 + \frac{215}{3}\left(\frac{n-2}{2}\right) + 18. \tag{3.32}$$

A comparison of the polynomials of the form $\widetilde{\mathcal{F}}_{2t+\alpha}(j)$, where α is a positive integer, shows that the coefficient of t^2 is $2j$, and the coefficient of t^0 is either $2j^2$ or $-2j^2$. The polynomials that we have seen so far, show that the coefficient of t^0 is $2j^2$ when $n+j$ is even, and $-2j^2$ when $n+j$ is odd. A comparison of the terms in (3.27)-(3.32) shows that the terms inside the parenthesis are of the form

$$\left\lceil \frac{n-j}{2} \right\rceil.$$

The results in (3.27)-(3.32) and examples with large values of n and j show that

$$\widetilde{\mathcal{F}}_n(j) = \frac{4}{3}\left(\left\lceil\frac{n-j}{2}\right\rceil\right)^3 + 2j\left(\left\lceil\frac{n-j}{2}\right\rceil\right)^2 + \frac{24j^2-1}{3}\left(\left\lceil\frac{n-j}{2}\right\rceil\right) + 2(-1)^{n+j}j^2.$$

Conjecture 1. Let $\mathrm{Dis}(Q_{n,n,n}(z))$ be the discriminant of

$$\frac{Q_{n,n,n}(z)}{z^k},$$

where

$$k = \frac{n(n+1)}{2},$$

is the multiplicity of the roots of $Q_{n,n,n}(z)$ at the origin. Then the $\mathrm{Dis}(Q_{n,n,n}(z))$ is given by

$$|\ \mathrm{Dis}(Q_{n,n,n}(z))\ | = 2^{\frac{n^2(n+1)^2}{2}} \prod_{j=1}^{n-1}(2n-2j+1)^{\widetilde{\mathcal{F}}_n(j)} \prod_{j=1}^{n}(4n-2j+1)^{\widetilde{\mathcal{G}}_n(j)}$$

where

$$\widetilde{\mathcal{F}}_n(j) = \frac{4}{3}\left(\left\lceil\frac{n-j}{2}\right\rceil\right)^3 + 2j\left(\left\lceil\frac{n-j}{2}\right\rceil\right)^2 + \frac{24j^2-1}{3}\left(\left\lceil\frac{n-j}{2}\right\rceil\right) + 2(-1)^{n+j}j^2,$$

and

$$\widetilde{\mathcal{G}}_n(j) = 2n\left(\left\lceil\frac{j}{2}\right\rceil\right)^2 - \frac{4j^3+3j^2-3j^2(-1)^j+2j}{12}.$$

The $\mathrm{Dis}(Q_{n,n,n}(z)) < 0$ if and only if $n = 1 \bmod 4$ or $n = 2 \bmod 4$.

Conjecture 1 has been checked for $n = 1, \ldots, 25$. A problem that remain open is to find the discriminant of 4-Okamoto polynomials for all parameter conditions of m, n and r.

Chapter 4

Conclusion

The aim of this thesis was to explore properties of the generalised Okamoto polynomials and the 4-Okamoto polynomials. I found that the structures formed by the roots of generalised Okamoto polynomials and 4-Okamoto polynomials depend on the relative size of the parameters of the polynomial.

In Chapter 1, we discussed that Veselov [79] conjectured that all Wronskians of Hermite polynomials arise in connection to rational solutions of one of the A_N-Painlevé system. Filipuk and Clarkson [33] investigated rational solutions of the A_4-Painlevé system and found that some rational solutions of the system can be expressed in terms of the 5-Okamoto polynomials. Figure 4.1, as well as other plots, show that the roots of the 5-Okamoto polynomial $Q_{m,n,r,s}(z)$ form A blocks, i.e. equilateral triangle blocks that lie on the imaginary axis, of size a. Where a denotes the smallest parameter of the polynomial. We saw that the roots of the generalised Okamoto polynomials $Q_{m,n}(z)$ and the roots of the 4-Okamoto polynomials $Q_{m,n,r}(z)$ also form A blocks of size a.

Figure 4.1 shows that similar to the blocks formed by the roots of 4-Okamoto polynomials, the roots of the 5-Okamoto polynomial also form B blocks, i.e. equilateral triangle blocks that lie on the real axis and C blocks, i.e. equilateral triangle blocks that lie in each quadrant of the complex plane. The size of the B and C

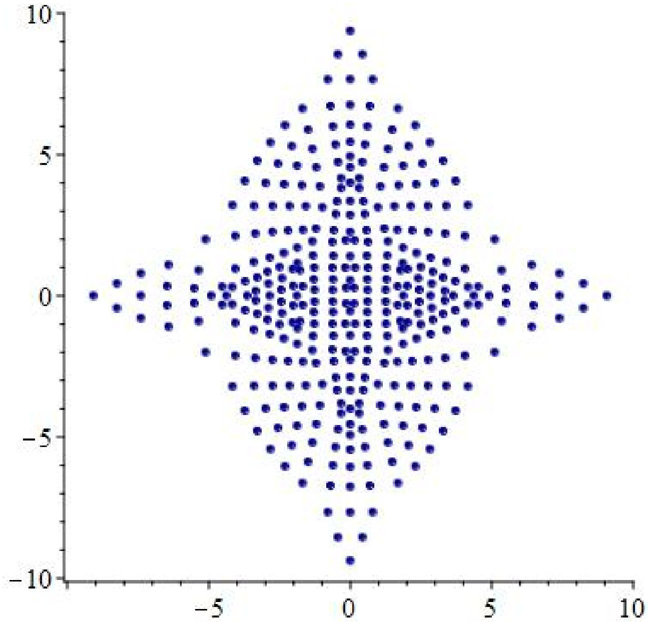

FIGURE 4.1: Plot of the roots of $Q_{3,9,10,14}(z)$.

blocks in Figure 4.1 suggests that the relative size of m, n, r and s has an affect on the size of blocks formed by the roots of 5-Okamoto polynomials. The other blocks that can be seen in Figure 4.1 are more complicated than the blocks formed by the roots of 4-Okamoto polynomials. A problem that remains open is to determine the blocks formed by the roots of 5-Okamoto polynomials.

In this thesis, I studied the families of partitions associated with the generalised Okamoto polynomials and the 4-Okamoto polynomials. I found that the partitions associated with $Q_{m,n}(z)$ are 3-core partitions and partitions associated with $Q_{m,n,r}(z)$ are 4-core partitions. It follows from the Wronskian definition of the 5-Okamoto polynomials $Q_{m,n,r,s}(z)$ (defined in Definition 6) that the family of partitions associated with the 5-Okamoto polynomials are 5-core partitions. By the definition of $Q_{m,n,r,s}(z)$ the partition λ associated with 5-Okamoto polynomials $Q_{n,n,n,n}(z)$ is

$$\lambda = \left(\left\{ (j)^4 \right\}_{j=1}^{n} \right).$$

Veselov's [79] conjecture motivates us to investigate properties of the Wronskian of Hermite polynomials. Let us define the N-Okamoto polynomials as the

$$\mathcal{W}\Big(\big\{\mathrm{He}_{1+Nj}(z)\big\}_{j=0}^{m_1-1};\ \big\{\mathrm{He}_{2+Nj}(z)\big\}_{j=0}^{m_2-1};\ldots;\big\{\mathrm{He}_{N-1+Nj}(z)\big\}_{j=0}^{m_{N-1}-1}\Big). \quad (4.1)$$

It follows from (4.1) that the family of partitions λ associated with N-Okamoto polynomials are N-core partitions. The partition λ associated with N-Okamoto polynomials with parameters equal to m is

$$\lambda = \left(\left\{(j)^{N-1}\right\}_{j=1}^{m}\right).$$

The conjugate of this partition is

$$\lambda^* = \left(\left\{(N-1)m-(N-1)j+N-1\right\}_{j=1}^{m}\right).$$

An interesting task for the future would be to investigate properties of the N-Okamoto polynomials. For example, the blocks formed by the roots of N-Okamoto polynomial in the complex plane and the discriminant of N-Okamoto polynomial.

In this thesis, I determined the general form of the discriminant of 4-Okamoto polynomials with equal parameters. A problem that remains open is to find the discriminant of 4-Okamoto polynomials for all parameter conditions of m, n and r.

Another interesting open problem is how the 4-Okamoto polynomials relate to rational solutions of the Painlevé equations.

Bibliography

[1] M. J. Ablowitz and P. A. Clarkson, Solitons, Nonlinear Evolution Equations and Inverse Scattering, *London Mathematical Society Lecture Note Series* **149** (1991).

[2] V. E. Adler, Nonlinear chains and Painlevé equations, *Physica* **D37** (1994) 335-351.

[3] T. Amdeberhan, Discriminants of Umemura polynomials associated to Painlevé III, *Phys. Lett. A* **354** (2006) 410–413.

[4] L. K. Bass, J. J. C. Nimmo, C. Rogers and W. K. Schief, Electrical structures of interfaces. A Painlevé II model, *Proc. Roy. Soc. London Ser. A* **466** (2010) 2117–2136.

[5] A. P. Bassom, P. A. Clarkson and A. C. Hicks, Bäcklund transformations and solution hierarchies for the fourth Painlevé equation, *Stud. Appl. Math.* **95** (1995) 1-71.

[6] D. Bermúdez and D. J. Fernández, Complex solutions to the Painlevé IV equation through supersymmetric quantum mechanics, *AIP Conf. Proc* **1420** (2012) 47-51.

[7] M. Bertola and T. Bothner, Zeros of large degree Vorob'ev-Yablonski polynomials via a Hankel determinant identity, *International Mathematics Research Notices* **19** (2015) 9330–9399.

[8] P. Bracken, P. P. Goldstein and A. M. Grundland, On vortex solutions and links between the Weierstrass system and the complex sine-Gordon equation, *J. Nonl. Math. Phys.* **10** (2003) 464–486.

[9] E. Brèzin and S. Hikami, Characteristic polynomials of random matrices, *Commun. Math. Phys.* **214** (2000) 111–135.

[10] N. Bonneux, Asymptotic behavior of Wronskian polynomials that are factorized via p-cores and p-quotients, *Mathematical Physics, Analysis and Geometry* **23** (2020), 36 pp.

[11] N. Bonneux, C. Dunning and M. Stevens, Coefficients of Wronskian Hermite polynomials, *Studies in Applied Mathematics* **144** (2020) 245-288.

[12] T. Bothner, P. D. Miller and Y. Sheng, Rational solutions of the Painlevé-III equation, *Stud. Appl. Math.* **141** (2018) 626-679.

[13] T. Bothner and P. D. Miller, Rational solutions of the Painlevé-III equation: large parameter asymptotics, *Constr. Approx.* **51** (2020) 123-224.

[14] R. J. Buckingham, Large-Degree Asymptotics of Rational Painlevé-IV Functions Associated to Generalized Hermite Polynomials, *International Mathematics Research Notices* **18** (2020) 5534–5577.

[15] R. J. Buckingham and P. D. Miller, Large-degree asymptotics of rational Painlevé II functions: noncritical behaviour, *Nonlinearity* **27** (2014) 2489-2578.

[16] R. J. Buckingham and P. D. Miller, Large-degree asymptotics of rational Painlevé-II functions: critical behaviour, *Nonlinearity* **28** (2015) 1539-1596.

[17] R. J. Buckingham and P. D. Miller, Large-degree asymptotics of rational Painlevé-IV solutions by the isomonodromy method, arXiv:2008.00600 (2020).

[18] R. J. Buckingham and P. D. Miller, On the algebraic solutions of the Painlevé-III (D7) equation, arXiv:2202.04217 (2022).

[19] F. Bureau, Painlevé Transcendents, their Asymptotics and Physical Applications, *NATO ASI Series B: Physics* **278** (1993) 103–123.

[20] H. Chen, M. Chen, G. Blower and Y. Chen, Single-user MIMO system, Painlevé transcendents, and double scaling, *J. Math. Phys.* **58** (2017) 123502.

[21] P. A. Clarkson, Painlevé equations — nonlinear special functions, *J. Comp. Appl. Math.* **153** (2003) 127–140.

[22] P. A. Clarkson, The fourth Painlevé equation and associated special polynomials, *J. Math. Phys.* **44** (2003) 5350-5374.

[23] P. A. Clarkson, The third Painlevé equation and associated special polynomials, *J. Phys. A* **36** (2003) 9507–9532.

[24] P. A. Clarkson, Special polynomials associated with rational solutions of the fifth Painlevé equation, *J. Comp. Appl. Math.* **178** (2005) 111-129.

[25] P. A. Clarkson, Painlevé equations – nonlinear special functions, in: Orthogonal Polynomials and Special Functions: Computation and Application [F. Màrcellan and W. Van Assche, Editors], *Lect. Notes Math.,* **1883** (2006) 331–411.

[26] P. A. Clarkson, Special polynomials associated with rational solutions of the defocusing non-linear Schrödinger equation and the fourth Painlevé equation, *Europ. J. Appl. Math.* **17** (2006) 293–322.

[27] P. A. Clarkson, Vortices and polynomials, *Stud. Appl. Math.* **123** (2009) 37–62.

[28] P. A. Clarkson and E. L. Mansfield, The second Painlevé equation, its hierarchy and associated special polynomials, *Nonlinearity* **16** (2003) R1–R26.

[29] P. A. Clarkson, D. Gómez-Ullate, Y. Grandati and R. Milson, Rational solutions of higher order Painlevé systems I, *Stud. Appl. Math.* **144** (2020) 357–385.

[30] A. J. Durán, Exceptional Charlier and Hermite orthogonal polynomials, *Journal of Approximation Theory* **182** (2014) 29–58.

[31] K. Dysthe, H. E. Krogstad and P. Müller, Oceanic rogue waves,*Annu. Rev. Fluid Mech.* **40** (1991) 287.

[32] G. Felder, A. D. Hemery, A. P. Veselov, Zeros of Wronskians of Hermite polynomials and Young diagrams, *Physica D: Nonlinear Phenomena* **241** (2012) 2131-2137.

[33] G. V. Filipuk and P. A. Clarkson, The symmetric fourth Painlevé hierarchy and associated special polynomials, *Stud. Appl. Math.* **121** (2008) 157–188.

[34] A. S. Fokas and M. J. Ablowitz, On a unified approach to transformations and elementary solutions of Painlevé equations, *J. Math. Phys.* **23** (1982) 2033–2042.

[35] S. Fukutani, K. Okamoto and H. Umemura, Special polynomials and the Hirota bilinear relations of the second and the fourth Painlevé equations, *Nagoya Math. J* **159** (2000) 179-200.

[36] B. Gambier, Sur les équations différentielles du second ordre et du premier degré dont l'intégrale générale est á points critiques fixés, *Acta Math.* **33** (1909) 1-55.

[37] V. I. Gromak, Solutions of Painlevé's fifth equation, *Differential Equations* **12** (1976) 519–521.

[38] V. I. Gromak, Theory of the fourth Painlevé equation, *Differential Equations* **23** (1987) 506–513.

[39] V. I. Gromak, I. Laine and S. Shimomura, Painlevé Differential Equations in the Complex Plane, *Studies in Math.* **28** (2002).

[40] D. Gómez-Ullate, Y. Grandati and R. Milson, Rational extensions of the quantum harmonic oscillator and exceptional Hermite polynomials, *Journal of Physics A: Mathematical and Theoretical* **47** (2014) Paper No. 015203, 27 pp.

[41] D. Gómez-Ullate, Y. Grandati and R. Milson, Complete classification of rational solutions of A_{2n}-Painlevé systems, *Adv. Math.* **385** (2021) Paper No. 107770, 51 pp.

[42] K. Iwasaki, H. Kimura, S. Shimomura and M. Yoshida, From Gauss to Painlevé: A Modern Theory of Special Functions, *Aspects of Mathematics* **16** (1889).

[43] G. James, Some combinatorial results involving Young diagrams, *Mathematical Proceedings of the Cambridge Philosophical Society* **83** (1978) 1-10.

[44] M. Jimbo and T. Miwa, Monodromy preserving deformations of linear ordinary differential equations with rational coefficients. II, *Physica* **D2** (1981) 407–448.

[45] K. Kajiwara, On a q-difference Painlevé III equation: II. Rational solutions, *J. Nonl. Math. Phys.* **10** (2003) 282–303.

[46] K. Kajiwara and Y. Ohta, Determinantal structure of the rational solutions for the Painlevé II equation, *J. Math. Phys.* **37** (1996) 4393–4704.

[47] K. Kajiwara and Y. Ohta, Determinantal structure of the rational solutions for the Painlevé IV equation, *J. Phys. A* **31** (1998) 2431-2446.

[48] K. Kajiwara and T. Masuda, On the Umemura polynomials for the Painlevé III equation, *Phys. Lett. A* **260** (1999) 462–467.

[49] A. V. Kitaev, C. K. Law and J. B. McLeod, Rational solutions of the fifth Painlevé equation, *Diff. Int. Eqns.* **7** (1994) 967-1000.

[50] D. E. Littlewood and A. C. Aitken, Modular representations of symmetric groups, *Proceedings of the Royal Society of London. Series A. Mathematical and Physical Sciences* **209** (1951).

[51] N. A. Lukashevich, Theory of the fourth Painlevé equations, *Differential Equations* **3** (1967) 395–399.

[52] N. A. Lukashevich, The second Painlevé equation, *Differential Equations* **6** (1971) 853-854.

[53] I. G. Macdonald, Symmetric Functions and Hall Polynomials, *Oxford Mathematical Monographs,* Oxford University Press, Oxford, Second edition (1995).

[54] I. Marquette and C. Quesne, Connection between quantum systems involving the fourth Painlevé transcendent and k-step rational extensions of the harmonic oscillator related to Hermite exceptional orthogonal polynomial, *J. Math. Phys.* **57** (2016) 52101.

[55] D. Masoero and P. Roffelsen, Poles of Painlevé IV rationals and their distribution, *Symmetry Integrability Geom. Methods Appl.* **14** (2018) Paper No. 002, 49 pp.

[56] D. Masoero and P. Roffelsen, Roots of generalised Hermite polynomials when both parameters are large, *Nonlinearity* **34** (2021) 1663-1732.

[57] T. Masuda, Classical transcendental solutions of the Painlevé equations and their degeneration, *Tohoku Math. J.* **56** (2004) 467–490.

[58] T. Masuda, Rational solutions of the Noumi and Yamada system of type $A_4^{(1)}$, *J. Math. Phys.* **53** (2012) 023504.

[59] T. Masuda, Y. Ohta and K. Kajiwara, A determinant formula for a class of rational solutions of Painlevé V equation, *Nagoya Math. J.* **168** (2002) 1-25.

[60] K. Matsuda, Rational solutions of the A_4 Painlevé equation, *Proc. Jpn. Acad.* **81** (2005) 85–88.

[61] M. Mazzocco, Rational solutions of the Painlevé VI equation, *Journal of Physics A: Mathematical and General* **34** (2001) 2281–2294.

[62] Y. Murata, Rational solutions of the second and the fourth Painlevé equations, *Funkcial. Ekvac.* **28** (1985) 1–32.

[63] M. Noumi, Notes on Umemura polynomials, *Annales de la Faculté des sciences de Toulouse: Mathématiques*, Serie 6, **29** (2020) 1091-1118.

[64] M. Noumi and Y. Yamada, Umemura polynomials for the Painlevé V equation, *Phys. Lett.* **247** (1998) 65-69.

[65] M. Noumi and Y. Yamada, Affine Weyl groups, discrete dynamical systems and Painlevé equations, *Comm. Math. Phys.* **199** (1998) 281-295.

[66] M. Noumi and Y. Yamada, Higher Order Painlevé Equations of Type $A_\ell^{(1)}$, *Funkcialaj Ekvacioj* **41** (1998) 483–503.

[67] M. Noumi and Y. Yamada, Symmetries in the fourth Painlevé equation and Okamoto polynomials, *Nagoya Math. J.* **153** (1999) 53-86.

[68] S. Odake and S. Sasaki, Infinitely many shape invariant potentials and new orthogonal polynomials, *Physics Letters B* **679** (2009) 414–417.

[69] K. Okamoto, Polynomial Hamiltonians associated with Painlevé equations. I, *Proc. Japan Acad. Ser. A Math. Sci.* **56** (1980) 264–268.

[70] K. Okamoto, Polynomial Hamiltonians associated with Painlevé equations. II, *Proc. Japan Acad. Ser. A Math. Sci.* **56** (1980) 367-371.

[71] K. Okamoto, Studies on the Painlevé equations III. Second and fourth Painlevé equations, PII and PIV, *Math. Ann.* **275** (1986) 221–255.

[72] K. Okamoto, Studies on the Painlevé equations I. Sixth Painlevé equation PVI, *Ann. Mat. Pura Appl.* **146** (1987) 337–381.

[73] E. Picard, Mémoire sur la théorie des fonctions algébrigues de deux variables, *J. de Math* **5** (1889) 135-318.

[74] D. P. Roberts, Discriminants of some Painlevé polynomials, *Number Theory for the Millennium* **III** (2003) 205–221.

[75] C. Rogers and P. A. Clarkson, Ermakov-Painlevé II reduction in cold plasma physics. Application of a Bäcklund transformation, *J. Nonlinear Math. Phys.* **25** (2018) 247–261.

[76] M. Taneda, Remarks on the Yablonskii–Vorob'ev polynomials, *Nagoya Math. J.* **159** (2000) 87–111.

[77] H. Umemura, On rational solutions of the second Painlevé equation, *Diff. Eqns.* **1** (1965) 58-59.

[78] H. Umemura, Special polynomials associated with the Painlevé equations I, *Annales de la Faculté des sciences de Toulouse : Mathématiques* **29** (2020) 1063-1089.

[79] A. P. Veselov, On Stieltjes relations, Painlevé-IV hierarchy and complex monodromy, *J. Phys. A* **34** (2001) 3511-3519.

[80] A. P. Veselov and A. B. Shabat, A dressing chain and the spectral theory of the Schrödinger operator, *Funct. Anal. Appl.* **27** (1993) 1-21.

[81] A. P. Vorob'ev, On rational solutions of the second Painlevé equation, *Diff. Eqns.* **1** (1965) 58-59.

[82] M. Wildon, Counting partitions on the abacus, *Ramanujan J.* **17** (2008) 355–367.

[83] A. I. Yablonskii, On rational solutions of the second Painlevé equation, *Vesti Akad. Navuk. BSSR Ser. Fiz. Tkh. Nauk.* **3** (1959) 30-35.

[84] B. Yang and J. Yang, Universal rogue wave patterns associated with the Yablonskii–Vorob'ev polynomial hierarchy, *Physica D: Nonlinear Phenomena* **425** (2021) 132850.